IRE
Transactions
on ANTENNAS and PROPAGATION

Paul Weaver

VOLUME AP-3 JULY 1955 NUMBER 3
Published Quarterly

PUBLISHED BY THE
ofessional Group on Antennas and Propagation

IRE TRANSACTIONS PGAP IS A QUARTERLY PUBLICATION DEVOTED TO EXPERIMENTAL AND THEORETICAL PAPERS ON ANTENNAS AND WIRELESS PROPAGATION OF ELECTROMAGNETIC WAVES

MANUSCRIPTS should be submitted to John B. Smyth, Editor, U. S. Navy Electronics Laboratory, San Diego, California. Manuscripts should be original typewritten copy, double spaced, plus one carbon copy. References should appear as footnotes and include author's name, title, journal, volume, initial and final page numbers, and date. Each paper must have an abstract of not more than 200 words. News items concerning PGAP members and group activities should be sent to the News Editor, Mr. H. A. Finke, Polytechnic Research and Development Company, 55 Johnson Street, Brooklyn, New York.

ILLUSTRATIONS should be submitted as follows: All line drawings (graphs, charts, block diagrams, cutaways, etc.) should be inked uniformly and ready for reproduction. If commercially printed grids are used in graph drawings, author should be sure printer's ink is of a color that will reproduce. All half-tone illustrations (photographs, wash, airbrush, or pencil renderings, etc.) should be clean and ready to reproduce. Photographs should be glossy prints. Call-outs or labels should be marked on a registered tissue overlay, not on the illustration itself. No illustration should be larger than 8 x 10 inches.

Copies can be purchased from
THE INSTITUTE OF RADIO ENGINEERS
1 East 79 St., New York 21, N.Y.

PRICE PER COPY: members of the Professional Group on Antennas and Propagation, $2.05; members of the IRE, $3.10; nonmembers, $6.15.

ANNUAL SUBSCRIPTION PRICE: IRE members, $8.50; Colleges and public libraries, $10.00; nonmembers, $17.00.

Entered as second-class matter, at the post office at Menasha, Wisconsin, under the act of August 24, 1912. Acceptance for mailing at a special rate of postage is provided for in the act of February 28, 1925, embodied in Paragraph 4, Section 412, P. L. & R., authorized October 26, 1927.

Proceedings or Transactions?

J. R. PIERCE

J. R. Pierce, Editor of the PROCEEDINGS, has suggested that certain views regarding publications in the TRANSACTIONS or PROCEEDINGS be presented to the membership. It is felt best to present these ideas for comment as prepared by him in their original form.

Questions frequently arise—in Editorial Board discussions and among the reviewers of PROCEEDINGS papers—as to what should be published in the PROCEEDINGS and what should be published in the various TRANSACTIONS. This statement will not settle the matter, but it does clarify the present situation and suggest future possibilities.

One aspect of the present situation is that of twenty-three Professional Groups of the Institute, twenty-one publish TRANSACTIONS while only ten of the twenty-one TRANSACTIONS appear regularly. Thus, in some fields of interest the PROCEEDINGS is the Institute's only facility for publication, and in some it is the only regularly published facility. As long as this situation persists, there must be a certain seeming inconsistency in the publication policies of the PROCEEDINGS. In some fields the PROCEEDINGS will endeavor to publish all papers worthy of publication, and in other fields it will publish only a selected few of these papers. It is to be hoped, of course, that neither TRANSACTIONS nor PROCEEDINGS will publish papers which are not worthy of publication.

We hope that this inequity of coverage by the PROCEEDINGS is a temporary matter. While it continues, the PROCEEDINGS will have to cover some fields in more detail than is perhaps desirable and it may publish too little in the fields of the most active and effective Professional Groups. The remedy is obviously a continued expansion and improvement in the TRANSACTIONS, and effective liaison between the editors of TRANSACTIONS and the PROCEEDINGS.

Let us now consider the specific case in which a field is covered both by an active Professional Group with a fine TRANSACTIONS which appears regularly, and by the PROCEEDINGS. Among all papers worthy of publication, which should go to the PROCEEDINGS and which to the TRANSACTIONS? Above all, whatever the decision should be, papers should get into the right journal as promptly as possible. While an initial mistake might in some measure be remedied by republishing in the PROCEEDINGS a paper which appeared first in the TRANSACTIONS, this is bad, and papers will be reprinted only under the most unusual circumstances. A technical journal is most valuable and most interesting to its readers when its contents are fresh and new. What about simultaneous publication in the PROCEEDINGS and in the TRANSACTIONS? This is pointless, for the PROCEEDINGS reaches all members of the IRE. The problem, then, is to get the papers into the right journal the first time, and promptly.

It is not easy to lay down rules which will cover all papers. There is certainly a place in the PROCEEDINGS for review papers which summarize recent progress in a field, and for tutorial papers which teach new concepts and techniques of analysis. The PROCEEDINGS asks experts to write such papers.

Most of the material in the PROCEEDINGS is submitted unsolicited. In trying to lay down rules for reviewing papers, the Editorial Board has said that to appear in the PROCEEDINGS papers should be important enough to be of general interest (to a reasonable fraction of the Institute's 40,000 members). This has been further interpreted by saying that papers should represent either a contribution of permanent value, or sound work on a topic of great current interest.

In being more specific than this, one can only describe and comment on particular types of papers.

A paper submitted to the TRANSACTIONS or the PROCEEDINGS may constitute a sort of review or tutorial paper if it presents a rational approach to a new field quite clearly or completely, so that one unfamiliar or only slightly familiar with the field can use it. Such a paper may or may not contain important new information. If it is really good, it will be suitable for the PROCEEDINGS.

A paper may describe an important new invention or device. If this device has considerable present or potential importance, and if it has real novelty, the membership of the Institute should know about it promptly in a paper of length adequate to explain it clearly. Perhaps the author will want to treat at length many important details which are of interest largely to specialists; he should do so in the TRANSACTIONS. The PROCEEDINGS paper should, however, be a real technical paper and not a news item; it should be technically sound and complete enough so that a more detailed discussion can be based on it and can refer to it.

A new experimental result, or new theory, should be treated much as is a new invention or device.

Many papers are concerned with calculations of great importance, about, for example, vacuum tubes, networks, antennas, or solid-state devices. If a calculation exhibits a new and important principle which casts new light on important problems, it is suitable for the PROCEEDINGS. If it merely solves a particular difficult problem by ingenious but special methods, it will usually be of interest only to specialists. In such a case, the result, if it is important, can be conveyed to the general IRE membership through the abstracts of TRANSACTIONS papers which appear in the PROCEEDINGS, or through a letter to appear as Correspondence.

In all cases, we should ask, "Should people outside a particular Professional Group be told about the contents of the paper? Why should they be told? How much should they be told to make the telling a real technical communication and not a news note?"

Where should an author send his paper? If he believes that he has something to say to the entire IRE membership, he should send it directly to the PROCEEDINGS. If he is addressing only experts in his field, he should send it to the TRANSACTIONS. To assure the promptest publication the author should make the right choice.

Sometimes the author makes the wrong choice. It is up to the reviewers to be alert about this, and to recommend to the PROCEEDINGS or TRANSACTIONS a paper which they feel has been misdirected. This makes some sort of liaison desirable. Several Professional Groups have named one or more of their members to act as one of the three PROCEEDINGS reviewers on all papers in the field of their Group. This makes available at the time of the review for the PROCEEDINGS the opinion of a representative of the Professional Group.

The relationship between the TRANSACTIONS and PROCEEDINGS must evolve. During this evolution, it is important that at each stage both the TRANSACTIONS and PROCEEDINGS publish promptly interesting and worthwhile material. The material must be worthwhile in each case, and perhaps the chief distinction must be between what is interesting to a large and heterogeneous group and what is interesting to a specialized segment.

news and views

PGAP News

The PGAP panel on scatter propagation at the 1955 IRE Convention was unusually successful. Our use of this means of discussion has elicited so much favorable comment that we intend to pursue the panel technique at greater length in the future and plans are already afoot to do this at the 1956 IRE Convention.

Symposium on Electromagnetic Wave Theory—A very excellent technical program with an international flavor, sponsored by Commission VI of URSI and the University of Michigan was held at Ann Arbor, June 20 through June 25.

Arrangements have been made to publish the full texts of all symposium papers in a supplement to one of the forthcoming issues of the PGAP Transactions. As a special service, this supplement will be distributed without charge to all paid-up members of PGAP and to new members who pay their annual assessment before July 1 of this year. Copies will be available to nonmembers at a nominal cost.

The Physical Society has announced that the "Report of the Conference on the Physics of the Ionosphere," held at the Cavendish Laboratory, Cambridge, September 6–9, 1954, is now available and for sale. This report should be a valuable reference and may be obtained by writing directly to the Physical Society, 1, Lowther Gardens, Prince Consort Road, London S.W.7.

Back Issues of Transactions—From time to time we receive requests for back issues of our Transactions to help complete the references in certain libraries. The following are listed:

U. S. Navy Electronics Laboratory, San Diego, Calif.—Att. J. B. Smyth: All back issues to date for an auxiliary NEL reference library.

Central Radio Propagation Library, Boulder Laboratories, Boulder, Colorado—Att. Mrs. Victoria S. Barker: Transactions, February 1952 and March 1952.

If any of the membership feel sufficiently philanthropic, will then please communicate directly with the persons listed above?

Delmar C. Ports, PGAP Chairman and Chief Engineer of Jansky & Bailey, Inc., has been elected to the Board of Directors and made a Vice-President of the Corporation. Mr. Ports also has been unanimously re-elected by the Administrative Committee to serve as PGAP Chairman for another term.

Chapter News

Philadelphia Chapter—Following a "Meet the Speaker" dinner at the Engineer's Club, Philadelphia, the second regularly-scheduled meeting of the Philadelphia Chapter of the IRE Professional Group on Antennas and Propagation was held February 16, 1955, at the Towne Building, University of Pennsylvania. This meeting was held as a joint meeting together with the Philadelphia Chapter of the IRE Professional Group on Microwave Theory and Techniques. The attendance at this meeting totaled twenty-five members and guests. The meeting was called to order at 8:15 P.M. by the chairman of the Professional Group on Antennas and Propagation, Charles Polk.

As there was no business before the group, Mr. Polk introduced the speaker of the evening, Bruce Rankin of the David Sarnoff Laboratories, RCA, Princeton, New Jersey. Mr. Rankin's subject was "Antenna Systems for UHF Television Boosters."

UHF television booster antenna systems are used to fill in holes in the primary transmitter pattern rather than to extend the coverage of the primary transmitter. A comparison between booster installations (rebroadcasting at same frequency) vs satellite installations (rebroadcasting at different frequency) was made. An actual case history of an experimental installation made at Vicksburg, Mississippi, to improve coverage from a UHF station at Jackson, Mississippi channel 25 was

discussed. Problems of relative gain, ghosts, and cross-coupling were discussed. Detailed descriptions of both the receiving antenna, the amplifier, and the transmitting antenna were given. A novel feedback system for the elimination of the ghost problem was of particular interest. Results of the test and evaluation program for this type of equipment indicated its success.

Following the presentation of this paper the meeting was thrown open to questions and discussions from the floor.

Washington, D. C.—The Washington, D. C. Chapter held its final meeting of the year on May 23. The chapter officers for 1955–56 were elected and are as follows:

Chairman	Coleman Goatley
Vice-Chairman	Clarence H. Stewart, II
Secretary	William W. Balwanz

An interesting and informative paper entitled "Behavior of Ferrites in Microwave Components," was presented by J. C. Cacheris of the Diamond Ordnance Fuse Laboratory.

Plans are being made for the coming year which should result in increased and broadened activities and a continuing chapter growth.

Calendar of Coming Events

AIEE Summer Meeting, New Orlean House, Swampscott, Mass., June 27–July 1.

AIEE Pacific General Meeting, Butte, Mont., Aug. 15–19.

British National Radio Show, Earls Court, London, England, Aug. 23–Sept. 3.

Western Electronic Show & Convention, San Francisco Civic Auditorium, San Francisco, Calif., Aug. 24–26.

German Radio, Television, Gramophone and Radiogram Exhibition, Dusseldorf, Germany, Aug. 26–Sept. 4.

10th Annual Conference and Exhibit sponsored by ISA, Shrine Exposition Hall and Auditorium, Los Angeles, Calif., Sept. 12–16.

Industrial Electronics Conference, sponsored by the AIEE and IRE, Detroit Rackam Memorial Auditorium, Detroit, Mich., Sept. 28–29.

The National Electronics Conference, Hotel Sherman, Chicago, Ill., Oct. 3–5.

(Deadline for submitted abstracts is June 8. Abstracts of papers should be submitted for consideration to Prof. Gunnar Hok, 3517 Elec. Eng. Bldg., University of Michigan, Ann Arbor, Mich.)

AIEE Fall General Meeting, Morrison Hotel, Chicago, Ill., Oct. 3–7.

AIEE Aircraft Electronic Equipment Conference, Los Angeles, Calif., Oct. 11–13.

IRE East Coast Conference on Aeronautical & Navigational Electronics, Lord Baltimore Hotel, Baltimore, Md. Oct. 31–Nov. 1.

World Symposium on Applied Solar Energy, Conducted under leadership of Stanford Research Institute, Phoenix, Ariz., Nov. 2–5.

Nuclear Congress and Atomic Exposition, sponsored by the Engineers Joint Council, Cleveland, Ohio, Dec. 12–17.

AIEE Winter General Meeting, Statler Hotel, New York, N. Y., Jan 30–Feb. 3, 1956.

contributions

Back-Scatter from Perfectly-Conducting Doubly-Trochoidal and Doubly-Sinusoidal Surfaces*

W. C. HOFFMAN†

Summary—**Expressions are developed by means of the "current-distribution" method for the far-zone energy back-scattered from large perfectly-conducting doubly-trochoidal and doubly-sinusoidal surfaces.**

Introduction

THE PRESENT study was carried out in the course of an investigation of the sizeable power scattered back from the sea surface in propagation via the ionosphere at high radio frequencies. The latter results are presented elsewhere.[1] The surface of the ocean is in fact a random surface,[2] and the author has constructed[3] a theoretical solution to the problem of scattering from such a surface. However, that theory requires a knowledge of the co-variance function of the sea surface and the statistical estimation of this function appears to be an oceanographic problem of considerable difficulty. Consequently, as a working approximation doubly-trochoidal and doubly-sinusoidal models have been assumed for the sea surface and back-scatter determined from each in the far-zone by means of the "current-distribution" method.

The doubly-trochoidal surface appears to be a likely description of the sea surface for several reasons. According to Stokes' results of 1847 the theoretical wave profile is a trochoid.[2] The doubly-trochoidal surface takes "cross-sea,"[2] i.e., the fact that ocean waves are short-crested, into account. Finally, according to Lysanov,[4] a trochoidal wave *profile* gives rise to considerably more back-scatter than a sinusoidal profile of the same amplitude and wavelength. However, for amplitudes small with respect to wavelength a trochoid approaches a sine curve, and at least in the application[1] there is no appreciable difference between back-scatter from a doubly-trochoidal sea surface and a doubly-sinusoidal one.

General Expressions for the Back-Scattered Field

Only the far-zone field of the scattered wave will be investigated. The far-zone scattered field may be determined by the "current-distribution" method of antenna theory.[5] This technique attempts in essence to approximate the current distribution over a perfectly-conducting reflecting surface. Its use assumes that: (a) there is no shielding of parts of the surface by other parts,[6] (b) there is no current over the shadow area of the reflector, and (c) the current distribution over the illuminated region of the surface is the same at each point as that of a plane wave incident on the infinite tangent plane there, that is

$$\boldsymbol{K} = 2\boldsymbol{n} \times \boldsymbol{H}_0 \qquad (1)$$

$\boldsymbol{n}$ being the unit vector normal to the surface, $\boldsymbol{K}$ the surface current density, and $\boldsymbol{H}_0$ the magnetic vector of the incident field. Thus the results will be restricted to perfectly-conducting surfaces of small curvature and to nongrazing incidence.

* Original manuscript received by the PGAP, July 28, 1954; revised manuscript received February 15, 1955. This work was done at the U. S. Navy Electronics Lab., San Diego, Calif.

† Rand Corp., Los Angeles, Calif.

[1] W. C. Hoffman, "A theoretical model for high-frequency back-scatter from the sea surface via the ionosphere," to appear in *Jour. Atmos. & Terres. Phys.*

[2] H. U. Sverdrup, M. W. Johnson, and R. H. Fleming, "The Oceans," Prentice Hall, Inc., New York, N. Y., ch. 14; 1946.

[3] W. C. Hoffman, "Scattering of electromagnetic waves from a random surface," to appear in *Quart. Appl. Math.*

[4] Y. P. Lysanov, "On the scattering of electromagnetic waves from a rough surface," *Doklady Akad. Nauk*, vol. 87, pp. 719–722; 1952.

[5] S. Silver, "Microwave Antenna Theory and Design," McGraw-Hill Book Co., Inc., New York, N.Y., secs. 5.7–5.8; 1949.

[6] This excludes the radar case, since it involves grazing incidence.

The "current-distribution" method is also the basis of the approach adopted by Brekhovskikh,[7] Isakovich,[8] and Lysanov[9] to the problem of scattering from rough surfaces. The present approach differs from that of Brekhovskikh and Lysanov in several respects, notably in taking account of edge effects and in the manner in which the surface integrals are evaluated.

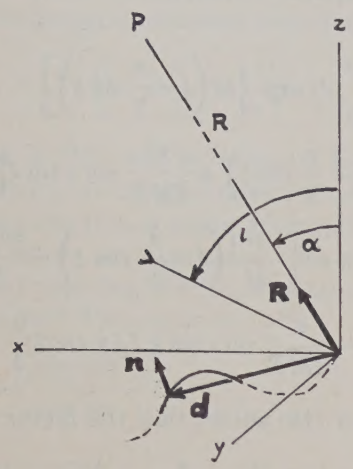

Fig. 1—Co-ordinate system for far-zone back-scattered field.

Let the co-ordinate system be chosen as shown in Fig. 1, with the origin at the center of the illuminated area and with the wave-normal of the incident wave in the xz-plane. Let d denote the vector from the origin to the surface element dS, and let $\boldsymbol{R}$ be a unit vector directed from the origin to the field point P, which is a distance R away from the origin. The scattered field in the far-zone is then given by[5]

$$\boldsymbol{E}_s(P) = -\frac{i\omega\mu}{2\pi}\frac{e^{-ikR}}{R}\int_\Sigma \{\boldsymbol{n}\times\boldsymbol{H}_0 - [(\boldsymbol{n}\times\boldsymbol{H}_0)\cdot\boldsymbol{R}]\boldsymbol{R}\}e^{ik\boldsymbol{d}\cdot\boldsymbol{R}}dS. \quad (2)$$

Let I denote the surface integral in (2). Referring to Fig. 1, one sees that

$$\boldsymbol{R} = \boldsymbol{i}\sin\alpha + \boldsymbol{k}\cos\alpha \quad (3)$$

and

$$\boldsymbol{d} = x\boldsymbol{i} + y\boldsymbol{j} + Z(x, y)\boldsymbol{k}. \quad (4)$$

The incident wave will be assumed to be plane, and the two polarizations considered separately. For a *vertically-polarized* plane wave,

$$\boldsymbol{H}_0 = \boldsymbol{j}(E_0/\eta)\exp\{i[\omega t + k(x\sin\iota + Z\cos\iota)]\}$$

incident upon the surface Σ, the surface integral $\mathfrak{I}$ in (2) becomes, omitting the harmonic time factor exp $(i\omega t)$,

$$\mathfrak{I} = (-\boldsymbol{i}\cos\alpha + k\sin\alpha)(E_0/\eta) \times \int_\Sigma (n_x\sin\alpha + n_z\cos\alpha)e^{ik[x(\sin\iota+\sin\alpha)+Z(x,y)(\cos\iota+\cos\alpha)]}\,dS. \quad (5)$$

Similarly in the case of an incident *horizontally-polarized* plane wave:

$$\boldsymbol{H}_0 = (\boldsymbol{i}\cos\iota - \boldsymbol{k}\sin\iota)(E_0/\eta)\cdot\exp\{i[\omega t + k(x\sin\iota + Z(x, y)\cos\iota)]\}$$

one obtains from (2)–(4) the expression

$$\mathfrak{I} = (E_0/\eta)\int_\Sigma \{n_y\sin(\iota-\alpha)(-\boldsymbol{i}\cos\alpha + k\sin\alpha) + (n_x\sin\iota + n_z\cos\iota)\boldsymbol{j}\} \times\exp\{ik[x(\sin\iota+\sin\alpha)+Z(x, y)(\cos\iota+\cos\alpha)]\}dS, \quad (6)$$

again dropping the exponential time factor exp $(i\omega t)$.

For the case of back-scatter the angle of incidence is the same as the angle of observation, that is $\iota=\alpha$, and expressions (5) and (6) reduce to

$$\mathfrak{I} = (E_0/\eta)\int_\Sigma (n_x\sin\iota + n_z\cos\iota)\cdot\exp\{2ik(x\sin\iota + Z\cos\iota)\}dS \times\begin{cases}(-\boldsymbol{i}\cos\iota + k\sin\iota), & \textit{vertical polarization};\\ \boldsymbol{j}, & \textit{horizontal polarization.}\end{cases} \quad (7)$$

The surface integral in (7) is a scalar quantity common to both polarizations. Denote this integral by J:

$$\mathcal{J} = \int_\Sigma (n_x\sin\iota + n_z\cos\iota)\exp\{2ik(x\sin\iota + Z\cos\iota)\}dS. \quad (8)$$

The expression for the back-scattered field then appears in the form:

$$\boldsymbol{E}_s(P) = -\frac{1}{2}ik\frac{e^{-ikR}}{R}J\begin{cases}(-\boldsymbol{i}\cos\iota + k\sin\iota)E_{0\parallel} \\ \quad \text{for vertical polarization;}\\ \boldsymbol{j}E_{0\perp} \text{ for horizontal polarization.}\end{cases} \quad (9)$$

The Back-Scattered Field from a Doubly-Trochoidal Surface

The parametric representation of a doubly-trochoidal surface with wavelength to wave-height ratios N and M in the x and y directions, respectively:

$$N = \Lambda/\delta \qquad M = \Lambda'/\delta \quad (10)$$

and parameters u and v is given by

$$x(u, v) = u - \tfrac{1}{2}\delta\sin Ku,$$
$$y(u, v) = v - \tfrac{1}{2}\delta\sin K'v;$$
$$Z(u, v) = -\tfrac{1}{2}\delta\cos Ku\cos K'v; \quad (11)$$

where

$$K = 2\pi/\Lambda \qquad K' = 2\pi/\Lambda'. \quad (12)$$

According to the geometric definition of a trochoid, Ku is the opening angle of the circle of radius $1/K$, $K'v$ that

[7] L. M. Brekhovskikh, "The diffraction of waves by a rough surface," Part I and II, *Zhurnal Eksperimental'noi Teorticheskoi Fiziki*, vol. 23, pp. 275–288, 289–304; 1952.

[8] M. A. Isakovich, "The scattering of waves from a statistically rough surface," *Zhurnal Eksperimental'noi Teorticheskoi Fiziki*, vol. 23, pp. 305–314; 1952.

[9] Lysanov, *loc. cit.*

for the circle of radius $1/K'$. From (10) and (12) we have

$$\tfrac{1}{2}\,\delta K = \pi/N \qquad \tfrac{1}{2}\,\delta K' = \pi/M. \tag{13}$$

According to the formulas from differential geometry for surface normal,

$$n_x = -\frac{\pi}{N}\sin Ku\cos K'v\left(1-\frac{\pi}{M}\cos K'v\right)/(EG-F^2)^{1/2};$$

$$n_z = \left(1-\frac{\pi}{N}\cos Ku\right)\left(1-\frac{\pi}{M}\cos K'v\right)/(EG-F^2)^{1/2}$$

and

$$dS = (EG - F^2)^{1/2}dudv.$$

Thus the surface integral (8) takes the form

$$J = \int_{-(l/2)}^{(l/2)}\int_{-(w/2)}^{(w/2)} \exp\left\{2ik\left(u\sin\iota - \frac{\delta}{2}\sin\iota\sin Ku - \frac{\delta}{2}\cos\iota\cos Ku\cos K'v\right)\right\}$$
$$\times\left\{\left(1-\frac{\pi}{M}\cos K'v\right)\left[\cos\iota\left(1-\frac{\pi}{N}\cos Ku\right) - \frac{\pi}{N}\sin\iota\sin Ku\cos K'v\right]\right\}dudv, \tag{14}$$

where l and w denote the length and width, respectively, of the area illuminated on the trochoidal surface. The change of variables $\xi = Ku$, $\eta = K'v$, and a use of the trigonometric identity $\cos^2\phi = \frac{1}{2}(1+\cos 2\phi)$ makes it possible to write (14) as the iterated integral

$$J = \frac{1}{KK'}\int_{-\pi(l/\Lambda)}^{\pi(l/\Lambda)} d\xi \exp\left\{i\beta\left(\xi - \frac{\pi}{N}\sin\xi\right)\right\}$$
$$\times\int_{-\pi(w/\Lambda')}^{\pi(w/\Lambda')} \exp\left\{-i\gamma\cos\xi\cos\eta\right\}$$
$$\cdot\left\{\left[\cos\iota\left(1-\frac{\pi}{N}\cos\xi\right)+\frac{\pi^2}{2MN}\sin\iota\sin\xi\right)\right]$$
$$-\pi\left[\frac{\cos\iota}{M}\left(1-\frac{\pi}{N}\cos\xi\right)+\frac{\sin\iota}{N}\sin\xi\right]\cos\eta$$
$$+\frac{\pi^2}{2MN}\sin\iota\sin\xi\cos 2\eta\Big\}\,d\eta, \tag{15}$$

where

$$\beta = 2\frac{\Lambda}{\lambda}\sin\iota; \qquad \gamma = k\delta\cos\iota = 2\frac{\Lambda}{\lambda}\frac{\pi}{N}\cos\iota. \tag{16}$$

Let $[X]$ denote the *nearest* integer to X and define

$$L = [l/\Lambda); \qquad W = [w/\Lambda'). \tag{17}$$

Since the inner integral in (15) is equal to $(1+0(1/W))$ times the same integrand integrated over $(-\pi W, \pi W)$, and since W is assumed large, there is no significant loss in accuracy in approximating the limits of integration $\pm\pi w/\Lambda'$ by $\pm\pi W$. The formula

$$\int_{-\pi W}^{\pi W}\exp\left\{-i\gamma\cos\xi\cos\eta\right\}\cos n\eta\,d\eta$$
$$= (-i)^n 2\pi W J_n(\gamma\cos\xi), \quad (n = 0, 1, \cdots)$$

can then be applied to reduce (15) to a single fold integral

$$J = \frac{2\pi W}{KK'}\int_{-\pi(l/\Lambda)}^{\pi(l/\Lambda)} d\xi\exp\left\{i\beta\left(\xi-\frac{\pi}{N}\sin\xi\right)\right\}$$
$$\times\left\{\left[\cos\iota\left(1-\frac{\pi}{N}\cos\xi\right)+\frac{\pi^2}{2MN}\sin\iota\sin\xi\right\}\right.$$
$$\times J_0(\gamma\cos\xi)+\pi i\left[\frac{\cos\iota}{M}\left(1-\frac{\pi}{N}\cos\xi\right)+\frac{\sin\iota}{N}\sin\xi\right]$$
$$\left.\times J_1(\gamma\cos\xi) - \frac{\pi^2}{2MN}\sin\iota\sin\xi\,J_2(\gamma\cos\xi)\right\}. \tag{18}$$

Examination of (18) shows that the factor

$$\left(1-\frac{\pi}{N}\cos\xi\right)$$

in the first and second terms of the integrand is related to the derivative of the argument of the exponential function. Integration by parts and a use of the recurrence relation $2J_\nu'(z) = J_{\nu-1}(z) - J_{\nu+1}(z)$ for Bessel functions reduces (18) to

$$J = \frac{\cot\iota}{2\pi}W\Lambda'\lambda\left\{\sin\left[\beta\left(\pi\frac{l}{\Lambda}-\frac{\pi}{N}\sin\pi\frac{l}{\Lambda}\right)\right]\right.$$
$$\times J_0\left(\gamma\cos\pi\frac{l}{\Lambda}\right)+\frac{\pi}{M}\cos\left[\beta\left(\pi\frac{l}{\Lambda}-\frac{\pi}{N}\sin\pi\frac{l}{\Lambda}\right)\right]$$
$$\left.\times J_1\left(\gamma\cos\pi\frac{l}{\Lambda}\right)\right\}+\frac{W\Lambda'\delta}{2\sin\iota}\int_{-\pi(l/\Lambda)}^{\pi(l/\Lambda)}$$
$$\cdot\exp\left\{i\beta\left(\xi-\frac{\pi}{N}\sin\xi\right)\right\}$$
$$\times\left\{\frac{\pi}{2M}[J_0(\gamma\cos\xi)-J_2(\gamma\cos\xi)]\right.$$
$$\left.+iJ_1(\gamma\cos\xi)\right\}\sin\xi d\xi. \tag{19}$$

Now consider the integral

$$\mathcal{J}_1 = \frac{\delta}{2\sin\iota}W\Lambda'\int_{-\pi L}^{\pi L}\exp\left\{i\beta\left(\xi-\frac{\pi}{N}\sin\xi\right)\right\}$$
$$\times\left\{\frac{\pi}{2M}[J_0(\gamma\cos\xi)-J_2(\gamma\cos\xi)]\right.$$
$$\left.+iJ_1(\gamma\cos\xi)\right\}\sin\xi\,d\xi,$$

which differs from that in (19) only in the limits of integration. In fact

$$\frac{\delta}{2\sin\iota} W\Lambda' \int_{-\pi(l/\Lambda)}^{\pi(l/\Lambda)} \exp\left\{i\beta\left(\xi-\frac{\pi}{N}\sin\xi\right)\right\} \times\left\{\frac{\pi}{2M}\left[J_0(\gamma\cos\xi)-J_2(\gamma\cos\xi)\right]+iJ_1(\gamma\cos\xi)\right\}\sin\xi d\xi = (1+0(1/L))\mathcal{J}_1,$$

and since L is assumed large, $\mathcal{J}_1$ is an excellent approximation to the integral extended over the interval

$$\left(-\pi\frac{l}{\Lambda},\ \pi\frac{l}{\Lambda}\right).$$

The integral in (19) will be replaced by $\mathcal{J}_1$, therefore, and $\mathcal{J}_1$ reduced to an integral over a single period of the surface. The reduction is easily accomplished by breaking up the range of integration into subintervals of length 2π and applying certain summation formulas for sine and cosine.[10] The result is

$$\mathcal{J}_1=\frac{\delta}{2\sin\iota} W\Lambda' \frac{\sin L\beta\pi}{\sin\beta\pi} e^{-i\beta\pi} \times\begin{cases} \displaystyle\int_0^{2\pi} e^{i\beta(\xi-(\pi/N)\sin\xi)}\left\{\frac{\pi}{2M}\left[J_0(\gamma\cos\xi)-J_2(\gamma\cos\xi)\right]\right. \\ \qquad \left.+iJ_1(\gamma\cos\xi)\right\}\sin\xi d\xi, \textit{ for } L \textit{ even}; \\ \displaystyle\int_0^{2\pi} e^{i\beta(\xi+(\pi/N)\sin\xi)}\left\{-\frac{\pi}{2M}\left[J_0(\gamma\cos\xi)-J_2(\gamma\cos\xi)\right]\right. \\ \qquad \left.+iJ_1(\gamma\cos\xi)\right\}\sin\xi d\xi, \textit{ for } L \textit{ odd}. \end{cases} \quad (21)$$

The final form of J for back-scatter from a doubly-trochoidal surface is then:

$$J=\frac{\cot\iota}{2\pi} W\Lambda'\lambda\left\{\sin\left[\beta\left(\pi\frac{l}{\Lambda}-\frac{\pi}{N}\sin\pi\frac{l}{\Lambda}\right)\right]\cdot J_0\left(\gamma\cos\pi\frac{l}{\Lambda}\right)+\frac{\pi}{M}\cos\left[\beta\left(\pi\frac{l}{\Lambda}-\frac{\pi}{N}\sin\pi\frac{l}{\Lambda}\right)\right]\cdot J_1\left(\gamma\cos\pi\frac{l}{\Lambda}\right)\right\}+\mathcal{J}_1, \quad (22)$$

where $\mathcal{J}_1$ is given by (21). Numerical integration appears to be the only feasible approach to the evaluation of $\mathcal{J}_1$. Due to the rapid oscillation of the complex exponential in the integrand of $\mathcal{J}_1$ it is necessary to employ a large number of subintervals in the numerical integration.

The Back-Scattered Field from a Doubly-Sinusoidal Surface

Let the doubly-sinusoidal surface be given by

$$Z(x, y) = -\tfrac{1}{2}\delta\cos Kx\cos K'y, \quad (23)$$

where δ is the wave-height and K and K' have the same meanings as for the doubly-trochoidal surface (12). Then

$$n_x = -\tfrac{1}{2}\delta K\sin Kx\cos K'y/(EG-F^2)^{1/2}$$
$$n_z = 1/(EG-F^2)^{1/2}$$

so that we have for the expression (8) in the case of the doubly-sinusoidal surface (23):

$$J=\int_{-l/2}^{l/2}\int_{-w/2}^{w/2}(-\tfrac{1}{2}\delta K\sin\iota\sin Kx\cos K'y+\cos\iota) \times\exp\left\{2ik\left(x\sin\iota-\frac{\delta}{2}\cos\iota\cos Kx\cos K'y\right)\right\}dxdy \quad (24)$$

l and w being the length and width, respectively, of the illuminated area. Changing variables to $\xi=Kx$, $\eta=K'y$, one obtains in place of (24)

$$J=\frac{1}{KK'}\int_{-\pi(l/\Lambda)}^{\pi(l/\Lambda)}\int_{-\pi(w/\Lambda')}^{\pi(w/\Lambda')}\exp\left\{i\beta\xi-i\gamma\cos\xi\cos\eta\right\} \times\left(\cos\iota-\frac{\pi}{N}\sin\iota\sin\xi\cos\eta\right)d\xi d\eta, \quad (25)$$

where β and γ are defined by (16). As in the case of the doubly-trochoidal surface, the relative error in replacing the innermost limits of integration by $\pm\pi W$, W being given by (17), is, for the range of γ corresponding to radio frequencies of 5–30 mc, of the order of $1/W$, and so is negligible. Thus

$$\int_{-\pi(w/\Lambda')}^{\pi(w/\Lambda')}\exp\left\{-i\gamma\cos\xi\cos\eta\right\}\cdot\left(\cos\iota-\frac{\pi}{N}\sin\iota\sin\xi\cos\eta\right)d\eta \cong\sum_{n=0}^{\infty}\epsilon_n(-i)^nJ_n(\gamma\cos\xi)\cdot\int_{-\pi W}^{\pi W}\left(\cos\iota-\frac{\pi}{N}\sin\iota\sin\xi\cos\eta\right)\cos n\eta d\eta = 2\pi W\left[\cos\iota J_0(\gamma\cos\xi)+i\frac{\pi}{N}\sin\iota J_1(\gamma\cos\xi)\sin\xi\right].$$

Then J becomes

$$J=\frac{2\pi W}{KK'}\int_{-\pi(l/\Lambda)}^{\pi(l/\Lambda)}e^{i\beta\xi}\left[\cos\iota J_0(\gamma\cos\xi)+i\frac{\pi}{N}\sin\iota J_1(\gamma\cos\xi)\sin\xi\right]d\xi. \quad (26)$$

Since

$$\frac{d}{dx}J_0(z\cos x)=zJ_1(z\cos x)\sin x,$$

an integration by parts reduces (26) to an integration over $J_0(\gamma\cos\xi)$ only:

[10] W. Magnus and F. Oberhettinger, "*Formeln und Sätze*," Springer, Berlin, Ger., 2nd ed., p. 217, 1948.

$$J = \frac{W\Lambda\Lambda'}{2\pi}\left\{-\frac{\lambda}{\Lambda}\tan\iota J_0\left(\gamma\cos\pi\frac{l}{\Lambda}\right)\sin\left(\beta\pi\frac{l}{\Lambda}\right) + \frac{1}{\cos\iota}\int_{-\pi(l/\Lambda)}^{\pi(l/\Lambda)} e^{i\beta\xi}J_0(\gamma\cos\xi)d\xi\right\}.$$

The remaining integral may be evaluated through an application of the formula[11]

$$J_0(z\cos\theta) = \sum_{n=0}^{\infty}\epsilon_n(-1)^n J_n{}^2\left(\frac{z}{2}\right)\cos 2n\theta,$$

and termwise integration. The result is

$$J = \frac{W\Lambda\Lambda'}{2\pi}\left\{-\frac{\lambda}{\Lambda}\tan\iota J_0\left(\gamma\cos\pi\frac{l}{\Lambda}\right)\sin\left(\beta\pi\frac{l}{\Lambda}\right) + \frac{2}{\cos\iota}\sum_{n=0}^{\infty}\epsilon_n(-1)^n\frac{J_n{}^2\left(\frac{\gamma}{2}\right)}{4n^2-\beta^2} \times\left[2n\sin\left(2n\pi\frac{l}{\Lambda}\right)\cos\left(\beta\pi\frac{l}{\Lambda}\right) - \beta\cos\left(2n\pi\frac{l}{\Lambda}\right)\sin\left(\beta\pi\frac{l}{\Lambda}\right)\right]\right\}. \quad (27)$$

The series in this expression converges quite rapidly for the values of γ encountered in connection with back-scatter from the sea surface—in fact, two or three terms are usually sufficient. The doubly-sinusoidal surface in that case at least leads to much more convenient computations than doubly-trochoidal surface.

The Back-Scattered Energy

To determine the energy back-scattered to the antenna we refer to (9) and write the far-zone scattered field for an elliptically polarized incident wave as:

$$\boldsymbol{E}_s(P) = -\frac{ik}{2\pi}\frac{e^{-ikR}}{R}J[(-\boldsymbol{i}\cos\iota + \boldsymbol{k}\sin\iota)E_{0\parallel} + jE_{0\perp}e^{i\psi}].$$

[11] Magnus and Oberhettinger, *op. cit.*, p. 31.

Then the Poynting vector $\boldsymbol{S}(P)$ is given by

$$\boldsymbol{S} = \frac{1}{2}(\boldsymbol{E}_s\cdot\boldsymbol{E}_s{}^*)\boldsymbol{R} = \frac{1}{2\eta}\frac{k^2}{(2\pi R)^2}|J|^2E_0{}^2\boldsymbol{R}. \quad (28)$$

Now[12]

$$E_0{}^2 = 2\eta S_0 = \eta\frac{P_0G}{3\pi R^2}, \quad (29)$$

where G is the gain over a dipole and P_0 is the average transmitted power. Then the average power received by an antenna with effective aperture $A_e=\lambda^2G/4\pi$, is, from (28) and (29),

$$P_r = SA_e = \frac{P_0G^2}{24\pi^2R^4}|J|^2. \quad (30)$$

In terms of voltage delivered to the terminals of an antenna of resistance Ω, the received energy is

$$,^2 = \frac{P_0G^2}{24\pi^2R^4}\Omega|J|^2. \quad (31)$$

Conclusion

Having expressions (22) and (27) one can determine the average power back-scattered in the far-zone by means of (30). For large surfaces which are actually doubly-trochoidal or doubly-sinusoidal and for radio wavelengths larger than the surface roughness these results are accurate within the limits of the Kirchhoff approximation. For the sea surface, the doubly-trochoidal or doubly-sinusoidal surfaces are only rough approximations (which, however, increase in validity as the wavelength of the incident radiation increases.) It follows that application of the formulas mentioned above to back-scatter from the sea can give only order of magnitude results. That good agreement with respect to order of magnitude is achieved is shown by the application[1] previously mentioned.

[12] D. E. Kerr, "Propagation of Short Radio Waves," McGraw-Hill Book Co., Inc., New York, N. Y., pp. 28–31; 1951.

On Nonuniform Dielectric Media*

R. B. BARRAR† AND R. M. REDHEFFER‡

Summary—A theory of nonuniform dielectric media should prove valuable to people engaged in the design of antenna housings or radomes and to those designing absorbers. Such a theory is herein developed. The problem of inhomogeneous media is treated first by means of differential equations and then as a limiting case of an array of panels. Various equivalences such as behavior of a panel at arbitrary incidence angle with that at normal incidence are also discussed.

I. Introduction

With the increasing use of microwaves, one often needs a dielectric sheet, or an array of sheets, with preassigned transmission properties. This problem occurs, for example, in the design of antenna housing or *radomes*, and in the design of absorbing surfaces. The same questions arise in the most commonly used methods of measuring dielectric constants. Here we summarize certain facts that seem relevant.

In Section II we derive differential equations of the transmission line type for the electric and magnetic fields in a panel. Then an impedance is defined and a differential equation is derived for it.[1] Both the reflection and transmission coefficients of the panel are shown to depend on the impedance. Various properties of the impedance are derived from its differential equation.

In Section III we consider equivalences, e.g., equivalences relating the behavior of a panel at arbitrary incidence to that at normal incidence, equivalences relating behavior with arbitrary permeability to that with permeability unity, and so on.

In Section IV we treat a continuously varying panel as the limiting case of an array of homogeneous panels, and in this way we derive further properties of the panel.

II. Differential Equations

The Transmission-Line Equations

Consider a slab of stratified dielectric with faces perpendicular to the x-axis and with electric constants $\epsilon(x)$ and $\mu(x)$ which may be complex. A plane wave propagating in the x-z plane, with $\vec{E}$ perpendicular to the plane of incidence, has field components H_x, E_y, H_z only, and the fields are independent of y. Assuming $e^{i\omega t}$ time dependence, Maxwell's equations read

$$-\frac{\partial E_y}{\partial z} = -i\omega\mu(x)H_x$$

$$\frac{\partial E_y}{\partial x} = -i\omega\mu(x)H_z$$

$$\frac{\partial H_x}{\partial z} - \frac{\partial H_z}{\partial x} = -i\omega\epsilon(x)E_y. \tag{1}$$

Assuming a z dependence exp $(-i\omega\sqrt{\epsilon_0\mu_0}\, z \sin\theta)$ to correspond to an incident wave in free space traveling at an angle θ with the x-axis, we can reduce (1) to

$$\frac{dE_y}{dx} = -i\omega\mu(x)H_z \tag{2a}$$

$$\frac{dH_z}{dx} = -i\omega\left[\epsilon(x) - \frac{\mu_0\epsilon_0 \sin^2\theta}{\mu(x)}\right]E_y. \tag{2b}$$

If we identify E_y with voltage and H_z with current, these are the equations of a nonuniform transmission line extending in the x-direction, with series impedance $i\omega\mu(x)$, and shunt admittance

$$i\omega\left[\epsilon(x) - \frac{\mu_0\epsilon_0 \sin^2\theta}{\mu(x)}\right]$$

per unit length. If we recall that E_y and H_z are continuous across the face of the slab, we also see that the boundary conditions of transmission line theory also carry over, hence we may freely borrow well-known results from this theory.[2] Thus if one defines

$$Z_{yz}(x) = \frac{E_y(x)}{H_z(x)}, \tag{3}$$

and if $\Gamma(x)$ is the reflection coefficient, defined by

$$\Gamma(x) = \frac{E_y^{\text{reflected}}(d)}{E_y^{\text{incident}}(d)} \tag{4}$$

(see Fig. 1, next page), one finds

$$\Gamma(x) = \frac{Z_{yz}(x) - Z_\theta}{Z_{yz}(x) + Z_\theta} \qquad Z_\theta = \sqrt{\frac{\mu_0}{\epsilon_0}}\sec\theta; \tag{5}$$

and if $T(x)$ is the transmission coefficient, (when the panel is backed by free space on both sides) defined by

$$T(d) = \frac{E_y^{\text{transmitted}}(0)}{E_y^{\text{incident}}(d)}, \tag{6}$$

* Original manuscript received by the PGAP, December 1, 1954.

† Hughes Res. and Dev. Labs., Culver City, Calif. This paper was written while the author was at McMillan Laboratory, Inc., Ipswich, Mass.

‡ University of California at Los Angeles, Los Angeles, Calif.

[1] Related papers are: J. R. Pierce, "A note on the transmission line equation in terms of impedance," *Bell Sys. Tech. Jour.*, vol. 22, pp. 263–265; July, 1943, L. R. Walker and N. Wax, "Non-uniform transmission lines and reflection coefficients," *Jour. Appl. Phys.*, vol. 17, pp. 1043–1045; December, 1946, R. M. Redheffer, "Novel Uses of Functional Equations," *Jour. Rat. Mech. Anal.*, vol. 3, pp. 271–279; March, 1954.

[2] For transmission line theory and its application to homogeneous panels see S. Ramo and J. F. Whinnery, "Fields and Waves in Modern Radio," 2nd Ed., John Wiley and Sons, Inc., New York, N. Y., ch. 7; 1953.

one finds

$$T(d) = \frac{E_y^{\text{slab}}(0)}{E_y^{\text{slab}}(d)} \frac{2Z_{yz}(d)}{Z_{yz}(d) + Z_\theta}. \tag{7}$$

The results for waves polarized with E parallel to the plane of incidence can be derived similarly. Here one has only H_y, E_x, and E_z components, and the principal equations become, (assuming a z dependence) exp $(-i\omega\sqrt{\mu_0\epsilon_0}\, z \sin\theta)$,

$$\frac{dH_y}{dx} = -i\omega\epsilon(x)E_z,$$

$$\frac{dE_z}{dx} = -i\omega\left[\mu(x) - \frac{\mu_0\epsilon_0 \sin^2\theta}{\epsilon(x)}\right]H_y, \tag{2'}$$

$$Z_{zy}(x) = -E_z(x)/H_y(x) \tag{3'}$$

$$\Gamma(x) = \frac{E_z^{\text{reflected}}(d)}{E_z^{\text{incident}}(d)} = \frac{Z_{zy}(x) - \tilde{Z}_\theta}{Z_{zy}(x) + \tilde{Z}_\theta};$$

$$\tilde{Z}_\theta = \sqrt{\frac{\mu_0}{\epsilon_0}} \cos\theta, \tag{4'}$$

$$T(d) = \frac{E_z^{\text{transmitted}}(0)}{E_z^{\text{incident}}(d)} = \frac{E_z^{\text{slab}}(0)}{E_z^{\text{slab}}(d)} \frac{2Z_{zy}(d)}{Z_{zy}(d) + \tilde{Z}_\theta}. \tag{5'}$$

The change in sign between (3′) and (3) can be justified in the following way. If $\vec{S}$ is the Poynting vector, then $\vec{S} = 1/2(\vec{E}\times\vec{H})$. Then in our notation for perpendicular polarization $S_x = 1/2E_yH_z^* = 1/2|E_y|^2/Z_{yz}^*(x)$; while for parallel polarization $S_x = -1/2E_zH_y^* = +1/2|E_z|^2/Z_{zy}^*(x)$. For normal incidence one would naturally want these two expresions to have the same sign, thus the change in sign in (3) and (3′).

In the remaining part of this paper we will treat only the case of perpendicular polarization. However, since all the results will be based on (2) to (7), it is clear that these results can also be obtained for the parallel polarization.

The Impedance Equation

We note first that $T(x)$ as well as $\Gamma(x)$ depends only on the variable function $Z(x)$. [In the following we abbreviate $Z_{yz}(x)$ by $Z(x)$]. To see this we use (3) and (2a) to obtain

$$E_y(x) = Z(x)H_z(x) = \frac{i\omega Z(x)}{\mu(x)} \frac{dE_y(x)}{dx}. \tag{8}$$

One may integrate (8) to obtain

$$E_y(d) = E_y(0) \exp\frac{-i}{\omega}\int_0^d \frac{\mu(x)dx}{Z(x)}. \tag{9}$$

Thus (7) becomes

$$T(d) = \frac{2Z(d)}{Z(d) + Z_\theta} \exp\frac{i}{\omega}\int_0^d \frac{\mu(x)dx}{Z(x)}. \tag{10}$$

We now derive the differential equation satisfied by $Z(x)$, and list some of its consequences. By (2) and (3) one obtains

$$\frac{dZ(x)}{dx} = \frac{dE_y(x)}{dx}\frac{1}{H_z(x)} - \frac{dH_z(x)}{dx}\frac{E_y(x)}{(H_z(x))^2}$$

$$= -i\omega\mu(x) + i\omega\left[\epsilon(x) - \frac{\mu_0\epsilon_0 \sin^2\theta}{\mu(x)}\right]\left(\frac{E_y(x)}{H_z(x)}\right)^2$$

$$= -i\omega\mu(x) + i\omega\left[\epsilon(x) - \frac{\mu_0\epsilon_0 \sin^2\theta}{\mu(x)}\right]Z^2(x). \tag{11}$$

This is a Ricatti equation.[3] Let us study it when $\mu(x) = \cos^2\theta = 1$. Then (11) becomes

$$\frac{dZ(x)}{dx} = i\omega[\epsilon(x)Z^2(x) - 1]. \tag{12}$$

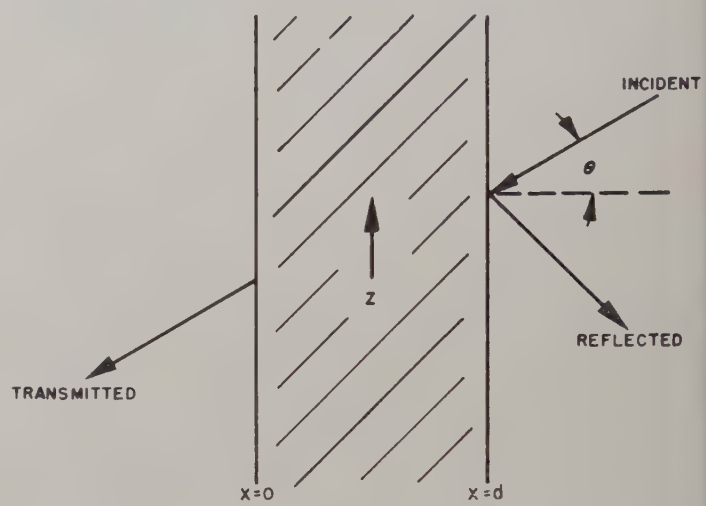

Fig. 1

Relations of the Solutions

Consider the three dimensional space generated by R, X, x; with $Z = R + iX$ and x the sample thickness. For each $\epsilon(x)$ and each terminating impedance, the behavior of the dielectric sheet is completely specified by a space curve in these co-ordinates. We shall now determine the whole system of curves from knowledge of a single curve.

If one knows a single solution of a Riccatti equation, all others are given by quadratures; however, in the case of (12) this integration would presuppose knowledge of $\epsilon(x)$. To avoid this, we work with $Y(x) = 1/Z(x)$. The equation for $Y(x)$ when $\mu(x) = \cos^2\theta = 1$ is

$$\frac{dY(x)}{dx} = i\omega[Y^2(x) - \epsilon(x)]. \tag{13}$$

Thus if $Y(x)$ is known, the general theory yields for any other solution $Y_1(x)$ the result

[3] For the theory of the Riccatti equation, see E. Kamke, "Differentialgleichungen Lösungsmethoden und Lösung, Band 1, Gewöhnliche Differentialgleichungen," 3. Auflage, reprinted by Chelsea Publishing Company, New York, N. Y., sec. A, 4.9; 1948.

$$\frac{1}{Y_1(x) - Y(x)}$$

$$= \left[\frac{1}{Y_1(0) - Y(0)} - i\omega \int_0^x \exp F dx\right] \exp(-F) \qquad (14a)$$

$$F = 2i\omega \int_0^x Y(x)dx, \qquad (14b)$$

or, in terms of $Z(x)$,

$$Z_1(x) = Z(x) + \left[C - i\omega \int_0^x \exp F dx\right]^{-1} \exp F \qquad (15)$$

with

$$\frac{1}{C} = \frac{1}{Z_1(0)} - \frac{1}{Z(0)} \qquad (16)$$

$$F = 2i\omega \int_0^x dx/Z(x). \qquad (17)$$

Thus each curve $Z_1(x)$ is determined by any other curve $Z(x)$ as asserted.

Discussion

These results are of course related to the underlying background of network theory. One cannot determine the imaginary part of a network impedance from knowledge of the real part at a particular frequency. Nor can one determine the complex impedance for one termination from that for another, at a particular frequency. (These determinations are impossible even if the network is lossless.) If the data be given, however, not for one frequency only, but for a whole interval of frequencies, then the determination can be made. It is just so in the present case, the role of the frequency being taken by the continuous variable x.

For constant values of x, ω and θ, the dielectric sheet is simply a fixed linear network, and hence it takes circles into circles. Corresponding to each complex value $Z(0)$ in the plane $x=0$ is a space curve in the space $R(x)$, $X(x)$, x. If $Z(0)$ is allowed to vary, so that it describes a curve on the plane $x=0$, then $Z(x)$ generates a surface. The result just quoted states that every cross section of that surface perpendicular to the x-axis is a circle, if the curve described by $Z(0)$ is a circle. Here we have the beginnings of a way to discuss the differential geometry of the surface. It can be shown that the radius and center of the circle both satisfy a first-order differential equation; further information is given by (15).

More generally one can form surfaces by regarding some of the quantities θ, ω, x, $R(0)$, $X(0)$, $R(x)$, $X(x)$ as parameters and taking the others as co-ordinate axes. Analysis of the differential geometry of these surfaces gives a solution to the problem of dielectric media. This approach will be discussed in a later article; for the present we note that the problem of frequency and angle dependence in general seems difficult, though perturbation theory gives results in particular cases.

Finally, we mention that a convenient check is given by the case $\sqrt{\epsilon} = h = \text{constant}$. Then (12) may be integrated at once to give

$$iZh = \tan(\omega x h + c), \qquad (18)$$

which is equivalent to the familiar expression

$$iZ(x)h = \frac{\tan \omega x h + hZ(0)}{1 - hZ(0) \tan \omega x h}. \qquad (19)$$

Moreover, substitution of (18) into (15) yields an expression of form (18) for Z, as it should no matter what values are given to the constants. The relations which follow can be similarly specialized.

Polar Co-ordinates

We define r, ϕ, a, b by

$$Z = re^{i(\phi - \pi/2)}, \qquad \epsilon = ae^{ib}. \qquad (20)$$

Substitution into (12) yields

$$\frac{rd\phi}{dr} = \frac{ar^2 \sin(b + \phi) - \sin\phi}{ar^2 \cos(b + \phi) + \cos\phi}, \qquad (21)$$

$$(dr/dx) - r(d\phi/dx)\cot(b+\phi) = \omega \sin(b+2\phi)\csc(b+\phi), \qquad (22)$$

after separating into real and imaginary parts and suitably combining the resulting relations.

Eq. (22) is a linear equation for r, the other quantities being regarded as known. In case the medium is lossless, so that $b=0$, the integrating factor is $\csc\phi$. Thus is obtained

$$(d/dx)(r \csc\phi) = 2\omega \cot\phi, \qquad (b = 0), \qquad (23)$$

which enables us to express r in terms of ϕ. Hence the polar equation is known when either r or ϕ is known as a function of x. An interesting complement to (23) is

$$(d/dx)(r \sin\phi) = \omega a r^2 \sin 2\phi, \quad (b = 0). \qquad (24)$$

We have also

$$\frac{d(r \sin\phi)}{d(r \csc\phi)} = a(r \sin\phi)^2, \qquad (b = 0) \qquad (25)$$

$$\frac{d[(\csc\phi)/r]}{d[(\csc\phi)r]} = -a. \qquad (b = 0). \qquad (26)$$

Realizability

Suppose a curve in the complex Z-plane is given. Can this curve be realized exactly as the impedance curve for a dielectric medium at normal incidence? Can it be so realized by a lossless medium? The answer to these questions is implicit in (21). For, the left side represents $\tan\psi$, where ψ is the angle between the tangent to the curve and the radius vector at any given point. The right side lies between limits depending on ϵ alone, at a given point (r, ϕ).

If we suppose

$$1 \leqq a \leqq A < \infty \qquad 0 \geqq b \geqq B > -\pi/2 \qquad (27)$$

as the conditions for physical realizability, then the

right-hand side of (21) attains its extreme values on the boundary of the region (27), not at an interior point. Hence the problem of physical realizability is reduced to an investigation of media with constant parameters. The choices $a=1$, $a=A$, $b=0$, $b=B$ determine arcs of circles through each point (r, ϕ). A prescribed curve $r=r(\phi)$ is realizable subject to (27) if and only if the tangent to $r=r(\phi)$ at each point lies between the tangents to an appropriate pair of these circles. [It should be observed that (22) can be satisfied automatically by using this equation to set up the correspondence between ϵ and x.]

For the important case of zero loss, $b=0$, (21) is

$$r d\phi/dr = \tan \psi = \tan \phi(ar^2 - 1)/(ar^2 + 1).$$

Eq. (26) may be integrated for constant a, so that the two families of circles determining physical realizability are now

$$x^2 + y^2 = cy - 1/A, \quad x^2 + y^2 = cy - 1, \qquad c \text{ a parameter.} \tag{28}$$

A curve in the Z-plane is realizable by a lossless dielectric having $1 \leqq \epsilon \leqq A$ if and only if its tangent at each point lies between the tangents of the two circles (28) through that point.

Some Examples

If one differentiates (2a) and then uses (2b), one obtains the following equation for E_y:

$$\frac{d}{dx}\left(\frac{1}{\mu(x)}\frac{dE_y}{dx}\right) + \omega^2\left[\epsilon(x) - \frac{\mu_0\epsilon_0 \sin^2\theta}{\mu(x)}\right]E_y = 0. \tag{29}$$

Since for perpendicular polarization there are only E_y, H_z, H_x components and $\vec{H} = i/\omega\mu \text{ curl } \vec{E}$, it follows that once one solves (29) the field is completely determined.

If one considers the important physical case of $\mu(x) = \bar{\mu} = \text{constant}$, (29) reduces to

$$\frac{d^2E_y}{dx^2} + k^2(me - s^2)E_y = 0 \tag{30a}$$

with

$$s = \sin\theta \tag{30b}$$

$$e = \epsilon(x)/\epsilon_0 \tag{30c}$$

$$m = \bar{\mu}/\mu_0 \tag{30d}$$

$$k^2 = \omega^2\epsilon_0\mu_0. \tag{30e}$$

Besides the usual case of $e=$ constant, there are several other cases where (30) has as its solution well-known functions of mathematical physics. We list a few such cases below:

1. If

$$e = \frac{Ax + B}{m} \tag{31}$$

then

(a) $E_y(x) = a_1 f_1(\zeta) + a_2 f_2(\zeta)$ (a_1, a_2 arbitrary constants)

where

(b) $$\zeta = \left(\frac{k}{A}\right)^{2/3}(Ax + B - s^2) \tag{32}$$

and $f_1(\zeta)$ and $f_2(\zeta)$ are linearly independent solutions of[4]

(c) $$\eta''(\zeta) + \zeta\eta(\zeta) = 0.$$

2. If

$$e(x) = \frac{Ax^2 + Bx + C}{m} \tag{33}$$

then

(a) $$E_y(x) = x^{-1/2}G\left[\frac{k}{4i\sqrt{A}}\left(C - s^2 - \frac{B^2}{4A}\right);\ \frac{1}{4};\ ik\sqrt{A}\left(x + \frac{B}{2A}\right)\right]$$

where

(b) $G(a; b; x) = a_1 W_{a,b}(x) + a_2 W_{-a,b}(-x)$ (a_1, a_2 arbitrary constants) (34)

and $W_{a,b}(x)$ is the Whittaker function.[5]

3. If

$$e(x) = \frac{1}{m}\left[C + \frac{A}{x + B}\right] \tag{35}$$

then

$$E_y(x) = G\left[\frac{kA}{2\sqrt{s^2 - C}};\ \frac{1}{2};\ 2k\sqrt{s^2 - C}(x + B)\right]. \tag{36}$$

4. If

$$e(x) = \frac{Ae^{2x} + Be^x + C}{m} \tag{37}$$

then

$$E_y(x) = e^{-x/2}G\left[\frac{kB}{2iA};\ k\sqrt{s^2 - C};\ 2ik\sqrt{A}e^x\right]. \tag{38}$$

5. If

$$e(x) = A\cos Bx + C$$

then the solution may be written in terms of the Mathieu functions.[6]

[4] These functions (along with their derivatives) are tabulated in Tables of the Modified Hankel Functions of order one-third and their derivatives, "Ann. Comp. Lab. Harvard Univ.," vol. II, Harvard Univ. Press; 1945.

[5] For the definition and properties of Whittaker functions see E. T. Whittaker and G. N. Watson, "A Course of Modern Analysis," (American Edition), Macmillan Company, New York, N. Y., ch. XVI; 1946.

[6] For the definition and properties of Mathieu functions see Whittaker and Watson, *op. cit*, ch. XIX.

III. Equivalences

Preliminary Remarks[7]

It is well known that a pile of uniform sheets in free space at incidence θ is equivalent to the same pile in a waveguide, provided the cut-off wavelength λ_c for the mode in question satisfies $\sin\theta=\lambda/\lambda_c$. Perpendicular polarization in free space corresponds to TE waves in the guide; parallel polarization, to TM waves.

Equivalences of this sort can be carried quite far. There are equivalences relating behavior at arbitrary incidence to that at normal incidence, equivalences relating behavior with arbitrary permeability to that with permeability unity, and so on. Here we make a systematic study of equivalences as applied to the case of a continuously varying panel.

We begin by noting that interchanging μ and ϵ in Maxwell's equations is equivalent to interchanging E with H and H with $-E$, which in turn is equivalent to changing the polarization. This enables us to restrict ourselves here to perpendicular polarization, for by interchanging μ and ϵ the following results apply to parallel polarization also.

Equivalences for Variable Incidence

In practical work it is frequently desirable to investigate transmission and reflection properties at incidence other than normal. The normal incidence equations are simpler in form than those for arbitrary incidence, and hence one is led to inquire whether they can ever be used, with minor modification, for the general case. Defining variables c and s as the cosine and sine of the angle of incidence

$$c=\cos\theta \qquad s=\sin\theta \tag{40}$$

we find the following: If we construct a new dielectric medium with parameters d', ϵ', μ' by

$$d'=d \tag{41a}$$

$$\mu'(x)=c\mu(x) \tag{41b}$$

$$\epsilon'(x)=\frac{\mu(x)\epsilon(x)-s^2}{c\mu(x)}, \tag{41c}$$

then the complex coefficients of the new medium at normal incidence are the same as those of original medium with perpendicular polarization and incidence θ.

Proof

Let us consider a panel with an incident plane wave perpendicularly polarized and striking the panel at an angle θ. We recall that the two physically important properties of the panel, namely, that its reflection coefficient $\Gamma(x)$, and its transmission coefficient $T(x)$ may be defined as

$$\Gamma(x)=\frac{Z(x)-Z_\theta}{Z(x)+Z_\theta}=\frac{\dfrac{Z(x)}{Z_\theta}-1}{\dfrac{Z(x)}{Z_\theta}+1} \qquad Z_\theta=\sqrt{\frac{\mu_0}{\epsilon_0}}\sec\theta \tag{5}$$

$$T(x)=\frac{E_y(0)}{E_y(x)}\,\frac{2Z(x)/Z_\theta}{Z(x)/Z_\theta+1} \tag{7}$$

with

$$\frac{Z(x)}{Z_\theta}=\frac{E_y(x)}{H_z(x)}\sqrt{\frac{\epsilon_0}{\mu_0}}\cos\theta=-i\omega\mu\cos\theta\,\frac{E_y(x)}{\dfrac{d}{dx}E_y(x)}, \tag{3}$$

[where the last equality follows from (2)], and where $E_y(x)$ satisfies the differential equation

$$\frac{d}{dx}\left(\frac{1}{\mu(x)}\,\frac{dE_y}{dx}\right)+\omega^2\left[\epsilon(x)-\frac{\mu_0\epsilon_0\sin^2\theta}{\mu(x)}\right]E_y=0. \tag{29}$$

Now let us consider another panel, this one at normal incidence. Let $\tilde{E}_y$ be the y-component of its $\vec{E}$ vector, and let the panel occupy the space $0\leqq x'\leqq d'$. Then $\tilde{E}_y$ satisfies the differential equation

$$\frac{d}{dx'}\left(\frac{1}{\mu'(x')}\,\frac{d\tilde{E}_y(x')}{dx'}\right)+\omega^2\epsilon'(x')\tilde{E}_y(x')=0, \tag{29'}$$

where $\mu'(x')$ and $\epsilon'(x')$ are its permeability and dielectric constant respectively.

It follows from (3), (5), and (7) above that a necessary and sufficient condition for the possibility of these two panels having the same transmission and reflection coefficients is that

$$\frac{E_y(0)}{E_y(d)}=\frac{\tilde{E}_y(0)}{\tilde{E}_y(d')} \tag{42a}$$

$$\mu(x)\cos\theta\,\frac{E_y(x)}{\dfrac{d}{dx}E_y(x)}\bigg|_{x=d}=\mu'(x')\,\frac{\tilde{E}_y(x')}{\dfrac{d}{dx'}\tilde{E}_y(x')}\bigg|_{x'=d'}. \tag{42b}$$

To assure this in the present case we set

$$x'=x \tag{43a}$$

$$\tilde{E}_y(x')=AE_y(x) \tag{43b}$$

$$\mu'(x')=\cos\theta\mu(x). \tag{43c}$$

Then (42) is surely satisfied. To assure (43b) we first need the differential equations (29) and (29') to be equal. Eq. (41c) assures this. We assume both panels have the same reflection coefficient at $x=0$. This implies by (3) and (5) that

$$E_y(0)=AE_y(0)$$

$$\frac{d}{dx}E_y(0)=A\frac{d}{dx'}\tilde{E}_y(0). \tag{44}$$

Eq. (44) together with the equality of the differential equations (29) and (29') implies (43b).

[7] The results of Section III were established by an altogether different method in R. M. Redheffer, "Equivalences and Other Relations for Dielectric Media," Mass. Inst. Tech. Res. Lab. of Electronics, Rep. No. 29; 1946.

In the foregoing discussion the condition $d'=d$ was prescribed. A different initial condition would have led to different results; for example by requiring $\mu'=\mu$ and determining the other parameters accordingly, one obtains the following: Starting with parameters x, d, $\epsilon(x)$, $\mu(x)$ one can construct a new medium with parameters

$$x' = cx \tag{45a}$$

$$d' = cd \tag{45b}$$

$$\mu'(x') = \mu(x) \tag{45c}$$

$$\epsilon'(x') = \frac{\epsilon(x)\mu(x) - s^2\mu_0\epsilon_0}{c^2\mu(x)}. \tag{45d}$$

The complex coefficients of the new medium at normal incidence are the same as those of the original medium with perpendicular polarization at incidence θ.

Proof

If

$$\tilde{E}_y(x') = E_y(x), \tag{46}$$

then the change of variable (45a) and the definition (45c) assure us that (42a) and (42b) are satisfied and thus that the two panels do have the same reflection and transmission coefficients. To assure (46) one needs (29) and (29′) to be equal. The transformation (45d) assures this.

This result is of interest for two reasons. First, the permeability of most materials differs by a negligible amount from that of free space, and hence equivalences not requiring that its value be changed have especial utility. In particular, an equation or graph which assumes $\mu=1$, so that this variable does not appear explicitly, may be used. A second feature is that the new value of d, though not equal to the original value, differs from it only by a constant factor. For this reason the argument of each new function is simply related to the argument of the original functions, and no integrals are required. It can be shown that the conditions $d'/d=$constant or $\mu'/\mu=$constant are the only ones for which this desirable behavior is obtained, and that the analog for parallel polarization is more complicated (in fact, as complicated as the general case to be considered below) because of the inconvenient form of d'.

Introduction of an Arbitrary Function

The fact is that any one of the quantities ϵ', μ', d' may be specified beforehand as a function of x, and the equations then solved for the remaining quantities. It is natural to inquire whether a more general equivalence could be obtained by leaving the specification in functional form; instead of requiring that $d'=d$ or $\mu'=\mu$ as above, we may set $d(x)=f(x)$ or $\mu(x)=f(x)$, where $f(x)$ is an arbitrary function. These more general equivalences are conveniently treated by means of the following theorem: Suppose we are given a sheet of total thickness d with parameters $\epsilon(x)$, $\mu(x)$. Let $f(x)$ be any function which has at most a finite number of discontinuities and satisfies the inequalities $M>f(x)>\delta$, for some M, δ in the interval $0\leqq x\leqq d$. Define $g(x)$ as the function inverse to $\int_0^x dy/f(y)$. If we now construct a new sheet with parameters given by

$$x' = \int_0^x dy/f(y) \tag{47a}$$

$$g(x') = x \tag{47b}$$

$$\epsilon'(x') = f[g(x')]\epsilon[g(x')] \tag{47c}$$

$$\mu'(x') = f[g(x')]\mu[g(x')], \tag{47d}$$

then the complex coefficients at normal incidence are the same for the new sheet as for the original one.

Proof

If we assume

$$\tilde{E}_y(x') = E_y(x), \tag{48}$$

and use (47a), we find

$$\frac{d}{dx}E_y(x)=\frac{1}{f(x)}\frac{d}{dx'}[\tilde{E}_y(x')]=\frac{1}{f[g(x')]}\frac{d}{dx'}\tilde{E}_y(x'). \tag{49}$$

Thus (29) restricted to normal incidence becomes

$$\frac{d}{dx'}\left[\frac{1}{\mu(x)f[g(x')]}\frac{d}{dx'}\tilde{E}_y(x')\right] + \omega^2 f[g(x')]\epsilon(x)\tilde{E}_y(x') = 0, \tag{50}$$

and

$$\frac{\mu(x)E_y(x)}{\frac{d}{dx}E_y(x)} = \frac{f[g(x')]\mu(x)\tilde{E}_y(x')}{\frac{d}{dx'}\tilde{E}_y(x')}, \tag{51}$$

from which (47c) and (47d) can be verified.

As an example we take the special case $f(x)=\sqrt{a+bx/\lambda}$, $d=d$, $\mu(x)=m$, $\epsilon(x)=e$ to obtain the following result: Suppose the dielectric constant and permeability of a lossless sheet vary linearly with position, so that $\epsilon'(x')=Ax'/\lambda+B$, $\mu(x')=Cx'/\lambda+D$ where A, B, C, and D are positive constants. If any three of these constants are chosen arbitrarily and the fourth is so determined that $AD=BC$, then the power transmission coefficient of the dielectric sheet at normal incidence becomes

$$\frac{4AC}{4AC+(A-C)^2\sin^2 2\pi[4\sqrt{AC}d'/\lambda+2\sqrt{BD}d'/\lambda]}, \tag{52}$$

where d' is its total thickness.

Returning to the question of arbitrary incidence, we recall that the equivalences were expressed in terms of a new medium at normal incidence. The result (47) may be applied to this new medium, and it is instructive to investigate the relations so obtained. By actually carrying out the calculations and comparing the algebraic

forms in each case, we find the following, which completes the discussion of arbitrary incidence: Every equivalence which can be obtained by picking an arbitrary real function for μ', ϵ', or d' and by determining the other functions accordingly, may also be obtained by using either (41) or (45) as it stands and following this by (47) with an appropriate choice of $f(x)$.

IV. Limiting-Process Methods

If one approximates a panel with continuously varying $\epsilon(x)$ and $\mu(x)$ by an array of uniform panels such that the panel occupying the space $x_n \leqq x \leqq x_{n+1}$ has constant

$$\epsilon_n = \epsilon\left(\frac{x_n + x_{n+1}}{2}\right)$$

and constant

$$\mu_n = \mu\left(\frac{x_n + x_{n+1}}{2}\right),$$

it is intuitively clear that as the number of subdivisions becomes greater and greater, the reflection and transmission coefficients of the array will approach those of the panel.[8] This may also be proved mathematically if one works with the system (2). For example, Kamke,[9] shows that if one has two systems of equations of the type (2), both with continuous coefficients, whose coefficients approach each other, then the solutions also approach each other. In our case, the coefficients of the array of panels are only piecewise continuous; however, the solution for continuous E_z and H_y can be written out explicitly. The methods Kamke uses can still be applied under these circumstances and thus one establishes the result.

As an example, we mention that by substituting

$$\frac{Z(x)}{Z_\theta} = \frac{1 + \Gamma(x)}{1 - \Gamma(x)} \tag{5}$$

in (11), one obtains the following equation for $\Gamma(x)$:

$$2\Gamma'(x) = -\frac{i\omega\mu[1 - \Gamma(x)]^2}{Z_\theta} + i\omega\left[\epsilon(x) - \mu_0\epsilon_0\frac{\sin^2\theta}{\mu(x)}\right][1 + \Gamma(x)]^2 Z_\theta. \tag{53}$$

Using the limiting process above, Redheffer[10] derived (53) and also its analog for parallel polarization, both from first principles.

[8] A proof was given in Redheffer, *loc. cit.*

[9] Kamke, *op. cit.*, sec. A, 8.4.

[10] R. M. Redheffer, "Reflection and transmission equivalences of dielectric media," Proc. IRE, vol. 39, p. 503; May, 1951.

Matrices and Product Integration

The reflection of an array of uniform sheets can be expressed as a matrix product,[11] as is well known. According to our above remarks on the limiting process, the limit of an appropriate matrix product must represent the solution of the differential equation (53).

For a second-order matrix A with complex elements a, b, c, and d, we define

$$\|A\| = |a|^2 + |b|^2 + |c|^2 + |d|^2. \tag{54}$$

By use of the "norm" (54) one can show that higher-order terms have no influence on the limit of certain matrix products. For example,

$$\lim_{n\to\infty} \prod_{m=1}^{n} (A_m^{(n)} + B_m^{(n)}) = \lim_{n\to\infty} \prod_{m=1}^{n} A_m^{(n)}, \tag{55}$$

if $\|B_m^{(n)}\| = O(1/n^2)$, and if the right-hand product exists. For a uniform dielectric sheet of (small) thickness d and complex dielectric constant ϵ, $\mu = 1$, the complex transmission t, reflection γ, and "discriminant" $d = t^2 - \gamma^2$ satisfy

$$\begin{aligned} t &= 1 + (\pi i d\epsilon^{1/2}/\lambda)(\epsilon^{1/2} + \epsilon^{-1/2}) + 0(d^2) \\ \gamma &= (\pi i d\epsilon^{1/2}/\lambda)(\epsilon^{1/2} - \epsilon^{-1/2}) + 0(d^2) \\ d &= 1 + (2\pi i d\epsilon^{1/2}/\lambda)(\epsilon^{1/2} + \epsilon^{-1/2}) + 0(d^2). \end{aligned} \tag{56}$$

Moreover, the scattering matrix of an array of such sheets is given by the matrix product

$$\begin{pmatrix} D/T & \Gamma/T \\ -P/T & 1/T \end{pmatrix} = \prod \begin{pmatrix} d/t & \gamma/t \\ -\gamma/t & 1/t \end{pmatrix}. \tag{57}$$

In view of (55) we can drop error terms in (56) to obtain, for differentiable $\epsilon(x)$, $(\mu = 1)$.

$$\begin{pmatrix} D/T & \Gamma/T \\ -P/T & 1/T \end{pmatrix} = \lim_{n\to\infty} \prod_{m=1}^{n} \left[\begin{pmatrix} 1 & 0 \\ 0 & 1 \end{pmatrix} + \frac{\pi i x}{n\lambda} \cdot \begin{pmatrix} \epsilon(mx/n) + 1 & \epsilon(mx/n) - 1 \\ \epsilon(mx/n) + 1 & \epsilon(mx/n) - 1 \end{pmatrix}\right]. \tag{58}$$

Here T is the complex transmission, Γ the complex reflection from the left, P from the right, and $D = T^2 - \Gamma P$ the discriminant, for a sheet of thickness x and dielectric constant $\epsilon = \epsilon(x)$. The result $\Gamma = \Gamma(x)$ as given by (58) is the solution of (53) for which $\Gamma(0) = 0$.

Eq. (58) as applied to (53) is related to the method of product integration.[12] It is interesting that (58) arises naturally, in the present context, from physical considerations. Much of the theory of distributed-parameter networks will undoubtedly fit in a similar framework.

[11] R. M. Redheffer, "Remarks on the basis of network theory," *M.I.T. Jour. Math. Phys.*, vol. 28, pp. 237–258; January, 1950.

[12] G. Birkhoff, "On product integration," *M.I.T. Jour. Math. Phys.*, vol. 16, pp. 109–132; January, 1937.

A Dual-Standard for Radar Echo Measurements*

M. H. COHEN† AND R. C. FISHER‡

Summary—A description is given of a corner-sphere, an aluminum sphere with an excised octant, which serves as a dual-standard echoing body. Its measured and calculated echo patterns are shown. An optical derivation is given for the echo area of the circular corner.

RADAR ECHO measurements are almost always relative, in that the echo from the body under test is compared with the echo from a standard body. A conducting sphere is commonly used for the standard. It has the two most desirable properties: (1) its echo area is accurately known, and (2) its echo pattern is not a critical function of aspect.[1]

For some applications it is difficult to work with a sphere which is large enough to be a suitable standard, and some body with a more directive echo is used. A corner reflector has been found to be satisfactory; a good approximation to its main-lobe echo area can be obtained when the dimensions are larger than several wavelengths, and its pattern is reasonably smooth so that difficult alignment procedures are not necessary.[2,3]

The Ohio State University K-Band echo-measuring equipment[4] has a dynamic range of 50 db. It is desirable to have more than one calibration point in such a range, primarily to serve as a check on the equipment. For this purpose a corner-sphere has been constructed which has the advantages of both the sphere and the corner reflector. It consists of a ten-inch aluminum sphere with an excised octant. A photograph of it is shown in Fig. 1.

This body is large enough in terms of wavelengths so that optical calculations give a very good approximation to the echo area. When only the spherical surface is visible from the radar the echo area is πa^2, or 0.051 square meters (a is the radius of the sphere.) The excised octant forms a circular corner reflector.[3] An optical derivation of the echo area of this reflector is contained in the Appendix. It is shown there that on the symmetry axis the echo area is given by

$$\sigma = 15.59(a^4/\lambda^2).$$

For the octant of the ten-inch sphere, this value is 26.0 square meters, at the operating wavelength $\lambda = 1.25$ cm.

The sphere level and the trihedral corner maximum form the two reference levels; they are 27.1 db apart. Thus a check of about half the range of the equipment can be rapidly made by taking a pattern of the corner-sphere. The complete range can be checked by taking patterns with overlapping gain settings.

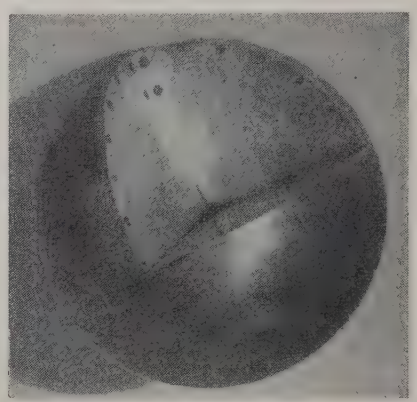

Fig. 1—Photograph of corner-sphere.

A measured echo pattern of the corner-sphere is shown in Fig. 2 (opposite page). It was suspended on nylon strings and rotated about an axis perpendicular to the line of sight, as shown in Fig. 3 (opposite page). As the body rotates the echo from the plane face is seen first. The trihedral corner, the dihedral corner, and the sphere are then seen, in that order. Those portions of the pattern which can be calculated are given in Fig. 2 by the dashed line and also by the two circled points, which represent the echoes from the flat face and the dihedral corner. Except for the flat face echo ($\theta = 0$ degree) the agreement between measured and calculated values is excellent. Apparently the body was slightly misaligned, only enough to affect the echo from the flat face, but not enough to affect that from the corner regions. This demonstrates that critical alignment is not necessary to obtain good standard values.

In the triply-reflecting region the measured curve averages $\frac{1}{2}$ to 1 db higher than the calculated one. This is within the ordinary experimental accuracy. In the region where only the sphere is visible the variations are on the order of 1 db. This approximates the smallest fluctuation ever obtained on a sphere pattern with this equipment, and represents excellent performance for the equipment, the sphere, and the sphere support.

* Original manuscript received by the PGAP, August 30, 1954. This work was reported in M. Cohen and R. Fisher, "A Dual-Standard Echoing Body," Rep. 475-11, Antenna Lab., The Ohio State Univ. Res. Foun., Columbus, Ohio; June, 1954.

† School of Elec. Engrg., Cornell Univ., Ithaca, N. Y.; formerly, Antenna Lab., Ohio State Univ., Columbus, Ohio.

‡ Dept. of Math., Ohio State Univ., Columbus, Ohio.

[1] D. E. Kerr, "Propagation of Short Radio Waves," M.I.T. Radiation Laboratory Series, vol. 13, McGraw-Hill Book Co., Inc., New York, p. 445; 1951.

[2] R. C. Spencer, "Optical Theory of the Corner Reflector," M.I.T. Rad. Lab. Rep. No. 433; March, 1944.

[3] S. D. Robertson, "Targets for microwave radar navigation," *Bell Sys. Tech. Jour.*, vol. 26, p. 852; October, 1947.

[4] D. R. Rhodes, "An Investigation of Pulsed Radar Systems for Model Measurements," Report No. 475-6, Antenna Lab., The Ohio State Univ. Res. Found., Columbus, Ohio; December, 1953.

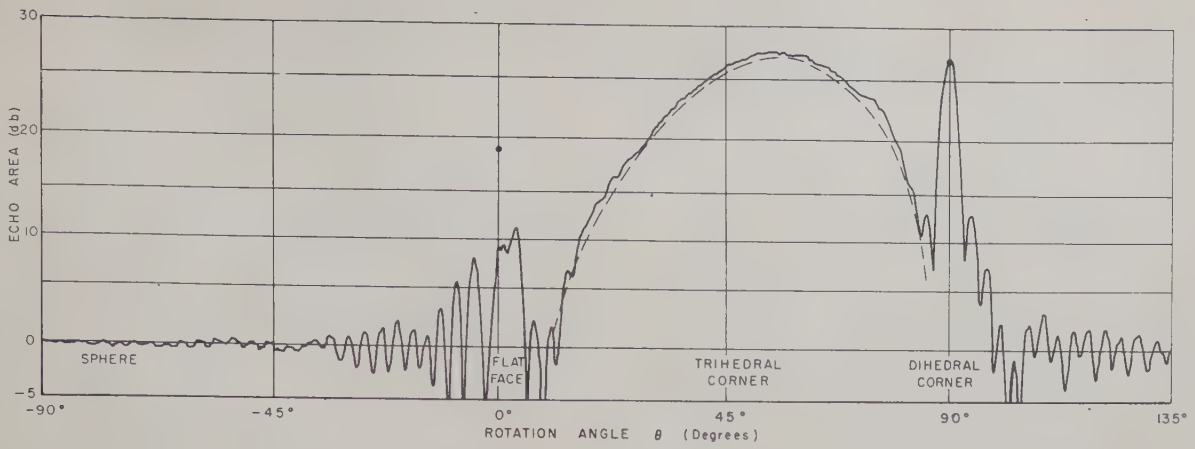

Fig. 2—Echo area pattern of 10-inch corner sphere at *K*-band. Dashed line and circled points are calculated values.

Appendix

The calculation of the echo from a circular corner reflector by an optical approximation consists of finding the equivalent flat-plate area of the target. As is well known, this amounts to calculating the area of the triply reflected region projected on a plane normal to the incident beam.[2,3] This calculation will be shown here explicitly for the plane of measurement reported above. The general procedure is, of course, valid for any aspect.

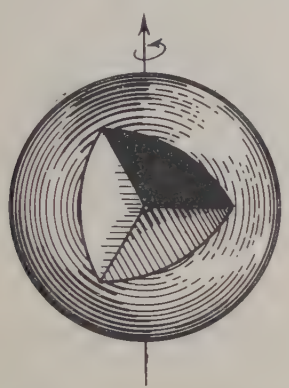

Fig. 3—Corner-sphere rotating around a vertical axis.

Let the circular corner of radius a be situated in the first octant of the $\bar{x}$ co-ordinate system. Let the x co-ordinate system be obtained by first rotating by $-\pi/4$ about the $\bar{z}$ axis and then by an angle θ about the rotated $\bar{x}$ axis. (See Fig. 4.) The co-ordinate transformation is given by $r = M\bar{r}$, where

$$M = \frac{1}{2}\begin{pmatrix} 1 & -1 & 0 \\ \cos\theta & \cos\theta & -\sin\theta \\ \sin\theta & \sin\theta & \cos\theta \end{pmatrix}.$$

The incident beam is now assumed to be parallel to the z axis. Note that the z axis coincides with the axis of symmetry of the corner when $\theta = \theta_0$, where

$$\cos\theta_0 = 1/\sqrt{3}.$$

The equivalent flat plate area $A(\theta)$ is limited by the conditions that the incident ray must pass through the surface S_E in the first octant of the $\bar{x}$ system of the sphere $\bar{x}^2+\bar{y}^2+\bar{z}^2=a^2$; and the reflected ray must appear to have passed through S_R, where S_R is the reflection of S_E about the origin. The entrance pupil is the projection of S_E on a plane normal to the incident beam; e.g. the x, y plane; and the exit pupil is the projection of S_R on the x, y plane. $A(\theta)$ is then the area of the region common to the entrance and exit pupils.

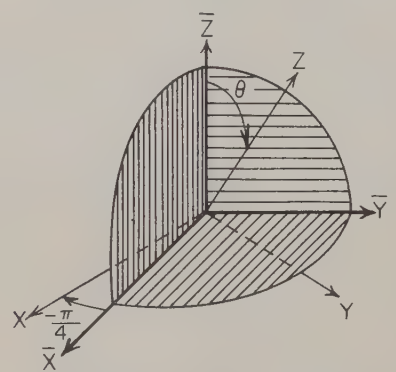

Fig. 4—Co-ordinate systems.

The boundaries of S_E and S_R are the curves of intersection of $x^2+y^2+z^2=a^2$ with the planes:

(a) $\bar{x} = 0$
(b) $\bar{y} = 0$ $\quad (\bar{x}, \bar{y}, \bar{z} \geqq 0$ for $S_E)$
(c) $\bar{z} = 0$ $\quad (\bar{x}, \bar{y}, \bar{z} \leqq 0$ for $S_R)$.

Since $\bar{r} = M^{-1}r = \tilde{M}r$ the boundaries of S_E and S_R in the x-system are portions of the curves of intersection of $x^2+y^2+z^2=a^2$ with the surfaces:

(a) $x + y\cos\theta + z\sin\theta = 0$
(b) $x - y\cos\theta - z\sin\theta = 0$
(c) $y\sin\theta - z\cos\theta = 0.$

Solving each of the equations (a), (b), (c) for z and substituting into $x^2+y^2+z^2=a^2$ yields the projections of the boundaries onto the x, y plane. Thus the entrance and exit pupils are given as portions of the curves:

1. $(1+\sin^2\theta)x^2+2xy\cos\theta+y^2=a^2\sin^2\theta$
2. $(1+\sin^2\theta)x^2-2xy\cos\theta+y^2=a^2\sin^2\theta$
3. $x^2\cos^2\theta+y^2=a^2\cos^2\theta.$

The curves 1, 2, 3 are shown in Fig. 5 for $\theta=\theta_0$. The entrance pupil is the region bounded by the arcs joining $IJKI$. The exit pupil is $LMNL$ while the equivalent flat plate area is the area of the region $ABCDEFA$. For comparison purposes the equivalent flat plate area for a triangular corner reflector with edge a is shown in Fig. 5 as the inner hexagon.

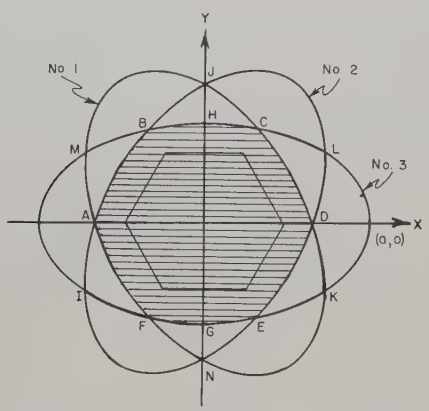

Fig. 5—Equivalent flat plate area in x, y plane for $\theta=\theta_0$.

In the general case, let y_J and y_H be the y-co-ordinates of the points H and J (see Fig. 5):

$$y_J = a\sin\theta$$

$$y_H = a\cos\theta.$$

Thus:

$$y_J < y_H \text{ for } 0 \leqq \theta < \pi/4.$$

and

$$y_H > y_J \text{ for } \pi/4 < \theta \leqq \pi/2.$$

The result is that for $\pi/4<\theta\leqq\pi/2$ the shape of the equivalent area is similar to that in Fig. 5, while for $0\leqq\theta<\pi/4$ it is similar to that in Fig. 6. The equivalent flat plate area $A(\theta)$ is thus found by integrating the appropriate regions of Figs. 5 and 6. The result is:

$$0 \leqq \theta < \pi/4,\ A(\theta) = \sqrt{2}a^2\sin\theta\sin^{-1}\left(\frac{\sqrt{2}\sin\theta}{\sqrt{1+\sin^2\theta}}\right)$$

$$\pi/4 < \theta \leqq \pi/2,\ A(\theta)$$

$$= \sqrt{2}a^2\sin\theta\left[\sin^{-1}\left(\frac{\sqrt{2}\sin\theta}{\sqrt{1+\sin^2\theta}}\right) - \sin^{-1}\left(\frac{\sqrt{2}\cos 2\theta}{\sqrt{\cos^2 2\theta+1}}\right)\right] - 2a^2\cos\theta\sin^{-1}\left(\frac{\cos 2\theta}{\sqrt{\cos^2 2\theta+1}}\right).$$

In particular, for $\theta=\theta_0=\cos^{-1}1/\sqrt{3}=54$ degrees 44 minutes, $A(\theta)$ assumes its maximum value $A(\theta_0)=1.114a^2$.

The echo area is given by

$$\sigma(\theta) = (4\pi/\lambda^2)A^2(\theta),$$

and the maximum echo area is

$$\sigma(\theta_0) = 15.59a^4/\lambda^2.$$

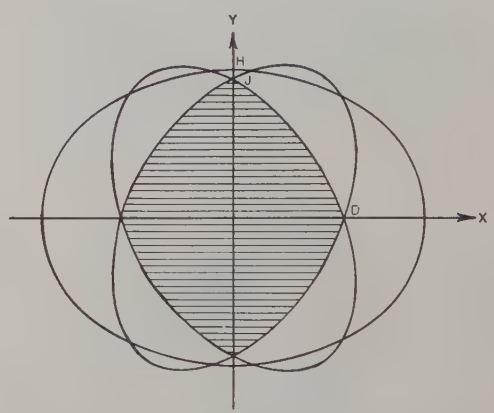

Fig. 6—Equivalent flat plate area in x, y plane for $0\leqq\theta<\pi/4$.

By a graphical method, Brown[5] determined that the maximum echo area is $15.7a^4/\lambda^2$, which is in remarkable agreement with the analytical value.

ACKNOWLEDGMENT

The corner sphere was measured by O. Click and D. R. Rhodes. This work was done under a contract between the Wright Air Development Center and The Ohio State University Research Foundation.

[5] S. K. Brown, Jr., "Effective Area of a Circular Radar Corner Reflector," NRL Progress Letter, ATI 44816; April, 1948.

Folded Unipole Antennas*

J. LEONHARD†, R. D. MATTUCK†, AND A. J. POTÉ

Summary—**Folded unipole antennas less than a quarter wavelength long are used to transform the input resistance of short vertical antennas to a more acceptable value by effecting a transformation within the antenna itself. An equivalent circuit of the folded unipole is derived. The transformation of input impedance is shown to be due to two factors: (1) the division of radiation mode currents between the driven and undriven portions of the antenna, and (2) the flow of currents in a nonradiating transmission-line mode. The effect on the input impedance of reactive elements inserted between the unfed portion and ground is investigated. The theory is verified with an experimental antenna whose input impedance is measured as a function of tuning reactance. The experimental curve is found to be in good agreement with the theory. Two methods of operating the folded unipole are proposed. In the first, only the division of radiation mode currents is utilized to effect the input impedance transformation. This method is applicable to antennas close to a quarter wave. The second method transforms the input impedance by utilizing the transmission-line mode only. It is applicable to short antennas.**

Introduction

EXTREME conditions of low input resistance are often encountered in antennas and may be due to short electrical length, or to mutual effects of other nearby radiators, or both. In consequence, coupling networks must be designed to transform the antenna resistance up to the level where it provides the desired load impedance for the driving source. This must be accomplished within certain limits of system bandwidth or phase characteristic. The general class of "folded antennas" (including folded dipoles and unipoles) represents the attempt to secure part of a desired impedance transformation within the antenna itself, thus simplifying the coupling problem.

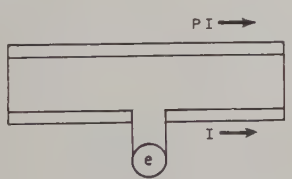

Fig. 1—Half-wave folded dipole.

The half-wave folded dipole is used extensively in high-frequency work, and the principle of its operation is well known. It consists of a half-wave dipole with another half-wave dipole close to it and joined to the first at the ends, as shown in Fig. 1. The voltage at the end of each dipole is maintained the same by the end connections; consequently, the currents in each dipole will be in phase, and maximum at the middle. Let the maximum current in the driven section be I, and that in the folded section be pI (p is determined by the relative diameters of the two sections). Let W be the power input to the dipole, and let R equal its input resistance. Then, $W=I^2R$. Assuming that all this power is radiated, we have $W=(I+pI)^2R_a$, where R_a is the radiation resistance of an ordinary dipole. Equating these two expressions for W, we obtain: $R=(1+p)^2R_a$, showing that by using the fold, the input resistance of the dipole has been increased by the factor $(1+p)^2$.

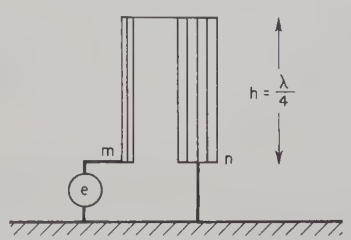

Fig. 2—Quarter-wave folded unipole.

The folded unipole is used in medium- and low-frequency broadcast work. It is essentially a folded dipole operated against ground (which, in this discussion, will be assumed perfect), and is represented schematically in Fig. 2. The fed and grounded sections of the unipole usually consist of a number of conductors (one of which is the tower itself), each carrying part of the current.

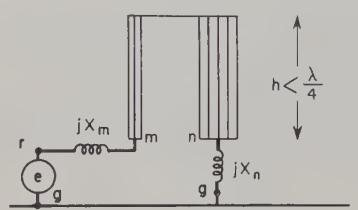

Fig. 3—Folded unipole less than a quarter wave.

In the case of the quarter-wave unipole, the impedance transformation is the same as for the half-wave dipole, provided we divide the actual resistances involved by a factor of 2. However, at very low frequencies, antennas are usually considerably less than one quarter-wavelength high, and special considerations are required. It is sometimes assumed[1] that the resistance transformation that takes place in the short radiator is the same as in the quarter-wave radiator, while the reactance may be tuned out by simply connecting to the bottom of each conductor an inductance equal to the antenna reactance. These inductors are then lumped together into X_m and X_n, as shown in Fig. 3. It will be

* Original manuscript received by the PGAP, August 30, 1954. The research in this document was first supported by the Department of State and then jointly by the Army, Navy, and Air Force under contract with the Massachusetts Institute of Technology.

† Staff Member, Lincoln Laboratory, Mass. Inst. Tech., Lexington, Mass.

[1] E. A. Laport, "Radio Antenna Engineering," McGraw-Hill Book Co., Inc., New York, N. Y., pp. 42–45; 1952.

shown that this approach is incorrect in that it neglects the existence of transmission-line currents on the antenna in addition to the ordinary antenna currents. The transmission-line mode causes the tuning inductor X_n to enter the equivalent circuit of the unipole in a complicated manner, and causes radical alteration of the input impedance. This will be shown in the derivation given in the following section.

Derivation of Equivalent Circuit of the Folded Unipole

We wish to determine the input impedance (Z_{mg}) of the unipole between point m and ground g, as a function of X_n. We will retain the inductor X_m in the derivation (its value will turn out to be proportional to that of X_n), find Z_{rg}, then subtract X_m from Z_{rg} to obtain Z_{mg}. The general procedure used will be an extension of the method employed by Roberts[2] to analyze the quarter-wave case.

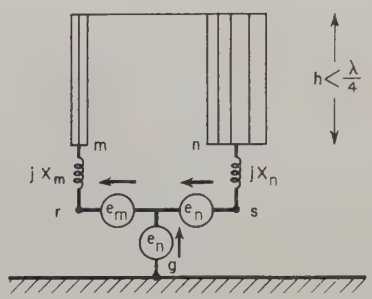

Fig. 4—Folded unipole with generator e replaced by equivalent generator network.

We start by replacing the generator e with the network shown in Fig. 4. To maintain point r at potential e, we choose e_m and e_n such that $e_m+e_n=e$; point s is maintained at ground potential by choosing the generator polarities as indicated. This new generator network is then the exact equivalent of the network in Fig. 3.

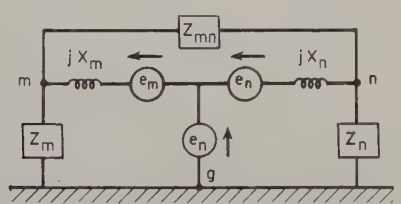

Fig. 5—Branches of unipole replaced by impedances.

We next replace the two sections of the unipole, as seen from points m and n, by impedance Z_m and Z_n to ground, and mutual impedance Z_{mn}. This is illustrated in Fig. 5. Let us now choose the ratios e_m/e_n and X_m/X_n in such manner that when the upper two generators are shorted, in-phase currents I_m and I_n flow through Z_m and Z_n (antenna mode), and when the lower generator is shorted, equal and opposite currents flow through Z_m and Z_n (transmission-line mode).

First, examine the antenna mode by shorting out the upper generators. In the limiting case, with X_m and X_n both zero, we have a simple antenna driven by voltage e_n, with in-phase currents I_{m0} and I_{n0}, flowing in the left- and right-hand sections, respectively. We let $I_{n0}/I_{m0}=p$, a ratio that depends only on the geometrical arrangement of the unipole conductors, and whose value may be calculated by using a method derived from a generalization of the procedure followed by Guertler.[3] Evidently then, $Z_m/Z_n=p$. If we now add reactance X_n to branch n, we must add reactance $X_m=pX_n$ to branch m in order to maintain the currents in phase and of ratio p. (Note that zero current flows in Z_{mn}, since the potential at point m is equal to that at point n.)

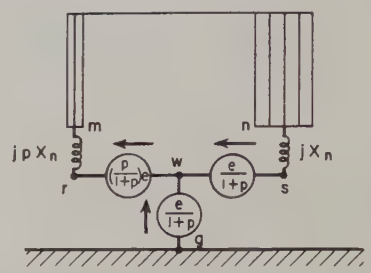

Fig. 6—Unipole with equivalent generators in terms of e and p.

Next, examine the transmission-line mode, shorting out the bottom generator. In order to maintain equal and opposite currents in Z_m and Z_n, it is easily shown that e_m must be so chosen that $e_m=pe_n$. Since $e=e_m+e_n=e_n(1+p)$ we have: $e_n=e/(1+p)$, and $e_m=[p/(1+p)]e$. We may re-draw our unipole diagram as in Fig. 6.

We are now in a position to determine the input impedance of the unipole. The current flowing at r is the sum of the transmission-line current I_T and the antenna current I_A. To obtain the transmission-line current, we short out the lower generator, and have the sum of two generator voltages driving the series combination of two inductors plus the shorted section transmission line formed by the right- and left-hand branches of the unipole. (The transmission-line inductance is designated X_L.) We thus have

$$I_T = \left[e\left(\frac{p}{1+p}\right)+\frac{e}{1+p}\right]\Big/ j(X_n+pX_n+X_L)$$
$$= e/j[X_n(1+p)+X_L]. \quad (1)$$

To find the antenna current, we first short out the two upper generators. We then note that since points m and n are at the same potential, we may connect them, thus combining the right and left portions of the unipole into a single radiator. We will designate the input impedance of this antenna by R_a-jX_a. (The values of R_a and X_a depend on the height-to-diameter ratio of

[2] W. van B. Roberts, "Input impedance of a folded dipole," *RCA Rev.*, vol. 8, pp. 289–300; June, 1947.

[3] R. Guertler, "Impedance transformation in folded dipoles," Proc. IRE, vol. 38, pp. 1042–1047; September, 1950.

the antenna and on its electrical length; formulas are available in Schelkunoff.[4]) In series with $R_a - jX_a$, we have the parallel combination of X_n and pX_n which equals $[p/(1+p)]X_n$. The driving voltage in the antenna mode is $e/(1+p)$. We thus have for the *total* antenna current

$$I_{A(\text{total})} = \left(\frac{e}{1+p}\right) \Big/ \left[R_a - jX_a + j\left(\frac{p}{1+p}\right)X_n\right]. \quad (2)$$

However, I_A is only that fraction of $I_{A(\text{total})}$ which flows in section m of the radiator. We have, then,

$$I_A = \left(\frac{1}{1+p}\right) I_{A(\text{total})}$$

or

$$I_A = e/[R_a(1+p)^2 - jX_a(1+p)^2 + jp(1+p)X_n]. \quad (3)$$

Now, the input impedance of the unipole from point r to ground is given by $Z_{rg} = e/(I_A + I_T)$. From this we must subtract $jX_m = jpX_n$, in order to obtain the true input impedance Z_{mg}, $Z_{mg} = e/(I_A + I_T) - jpX_n$. Substituting the values of I_A and I_T, we find that Z_{mg} as a function of X_n is given by

$$Z_{mg} = \frac{1}{\dfrac{1}{[R_a(1+p)^2 - jX_a(1+p)^2 + jp(1+p)X_n]} + \dfrac{1}{j[X_n(1+p) + X_L]}} - jpX_n. \quad (4)$$

From the form of this function, we see that the equivalent circuit of the unipole may be represented as is shown in Fig. 7.

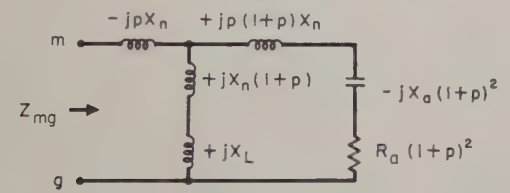

Fig. 7—Complete equivalent circuit of the folded unipole.

We may apply this circuit to the case of the quarter-wave folded unipole. Here we have $X_a = 0$ (since in the antenna mode the radiator is self-resonant), $X_n = 0$, and $X_L = \infty$ (since we have a shorted quarter-wave transmission line). Thus we obtain the result $Z_{mg} = R_a(1+p)^2$, as expected.

In the general case, we see that the effect of the unipole is, first, to multiply the input resistance and reactance of the antenna by the factor $(1+p)^2$, and second, to transform these new impedances through a T-network consisting of the transmission-line impedance and various products of X_n. The behavior of this network will be brought out more clearly in the following section in which is described the theoretical and experimental determination of Z_{mg} as a function of X_n.

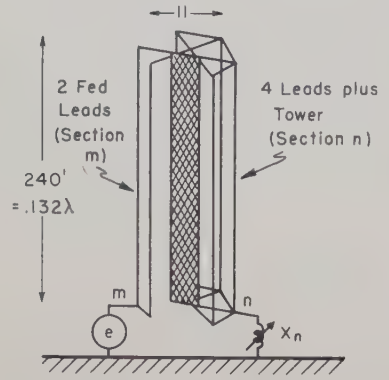

Fig. 8—The experimental folded unipole.

Experimental Verification

The antenna used for the experiment is sketched in Fig. 8. It consisted of a triangular tower 240 feet high and 1.5 feet on a side, located over a 48×48-foot ground screen to which were attached 60 radials, each 200 feet long. Six outriggers were joined to the tower, and connected to each was a downlead of No. 6 wire. These leads were 5.5 feet from the center of the tower. At the bottom, four of the leads were connected to the tower and grounded through the tuning reactor X_n, while the other two were fed by a signal generator.

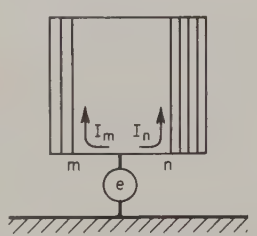

Fig. 9—The unipole operated as an ordinary base-driven antenna.

Referring to Fig. 7, we see that there are four parameters on which Z_{mg} depends (assuming X_n to be the variable), i.e., R_a, X_a, p, and X_L. These parameters were first calculated theoretically. R_a and X_a are the input resistance and reactance of the antenna formed when the right and left sections of the unipole are tied together at the base, as in Fig. 9. This antenna is, to a good approximation, a vertical cylinder 0.132 wavelength high, with a height-to-diameter ratio of 240/11 = 21.8. Using graphs based on Schelkunoff's formulas[4]

[4] S. A. Schelkunoff, "Theory of antennas of arbitrary size and shape," Proc. IRE, vol. 29, pp. 493–521; September, 1941.

for input resistance and reactance of antennas of arbitrary size and shape, values of $R_a = 7.7$ ohms and of $X_a = 170$ ohms were obtained. Using Guertler's method, the value of p was calculated to be 3.0. X_L was calculated to be 305 ohms, using a method based on the electrostatic charge ratio of infinitely long conductors having the same cross section.

$$R_{mg} = \frac{R_a K (X_n \sqrt{K} + X_L)^2}{R_a K)^2 + (X_n K - X_a K + X_L)^2}, \tag{5}$$

$$X_{mg} = -pX_n + \frac{(X_n \sqrt{K} + X_L) \cdot [(R_a K)^2 - (X_a K - X_n p \sqrt{K})(X_n K - X_a K + X_L)]}{(R_a K)^2 + (X_n K - X_a K + X_L)^2}. \tag{6}$$

The four parameters were then measured experimentally. R_a and X_a were determined by a simple bridge measurement which yielded the values $R_a = 8.5$ ohms, $X_a = 119$ ohms. R_a (measured) is larger than R_a (theoretical) due to ground losses, while the large discrepancy between X_a (measured) and X_a (theoretical) may be due to the effects of the inductance of the measuring leads, the coupling between the tower and the supporting guy wires, and the imperfect ground plane. The value of p was obtained by measuring the ratio of I_n to I_m (Fig. 9). This was done by inserting first at point n, then at point m, a ferrite-core sampling transformer whose secondary voltage varied linearly with primary current; p was then equal to the ratio of the output voltages, and was determined to be 3.0, in complete agreement with theory. Measurement at several frequencies indicated that, as predicted theoretically, p is independent of frequency to within 2 per cent.

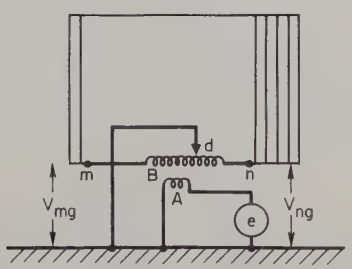

Fig. 10—Experimental measurement of X_L.

X_L was measured using the arrangement indicated schematically in Fig. 10. A signal generator e was used to drive the coil A, which was coupled to coil B. The position of the ground tap d was varied until a sampling transformer gave the same reading when inserted at m and at n, indicating that only the transmission-line mode was being excited. The sampling transformer was then calibrated absolutely to find the value of transmission-line current I_T. V_{mg} and V_{ng} were measured with a vacuum-tube voltmeter. (The ratio V_{mg} to V_{ng} turned out to equal 3.15. Comparison of this value with the theoretical value of p provides another check on the theory.) X_L was then determined from the expression $X_L = (V_{mg} + V_{ng})/I_T$ to be equal to 313 ohms, agreeing with theory to within 5 per cent.

Using the experimentally obtained values of the four parameters, the input resistance R_{mg} and reactance X_{mg} of the unipole were computed as functions of X_n from the formulas [derived from (4) with $K = (1+p)^2$ for convenience].

The curves of R_{mg} and X_{mg} are plotted versus X_n in Fig. 11. The resonance occurs at the point where $X_n K - X_a K + X_L = 0$, or $X_n = X_a - X_L/(1+p)^2 = 106.5$ ohms. Another point of interest is where R_{mg} goes to zero. This takes place when $X_n \sqrt{K} + X_L = 0$, or $X_n = -X_L/(1+p) = -78$ ohms. By taking the limits in (5) and (6), it may be shown that when X_n approaches plus or minus infinity, R_{mg} approaches R_a, and X_{mg} approaches zero.

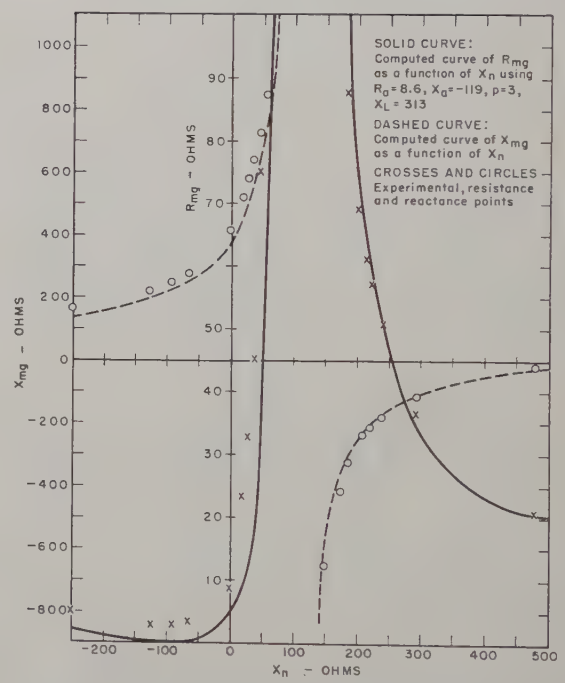

Fig. 11—Input impedance of a folded unipole with $p = 3$ as a function of inserted reactance X_n.

To check this curve experimentally, R_{mg} and X_{mg} were measured with a bridge for a wide range of values of X_n. The experimental points are plotted in Fig. 11, and it is seen that there is good agreement with the theoretical curve. It will be noticed that the experimental points do not go to zero in the negative reactance region as predicted by theory. It can be shown that this effect is due to a small loss resistance associated with the transmission-line mode.

It proved unnecessary to make corrections for the effect of base capacitance in the measurement of the

four unipole parameters and the input impedance, since experiments on a replica of the antenna base revealed the base reactance to be $-1{,}500$ ohms. However, for large value of tuning inductance it was observed that X_{mg} crossed the abscissa. This was evidently the point where the tuning inductor was in parallel resonance with the base capacitance, thus making X_n effectively infinite. It was also noted that for large X_n, R_{mg} was slightly higher than the predicted value ($R_a = 8.6$ ohms). It was demonstrated theoretically that this could be accounted for by small losses in the transmission-line mode.

Operation of the Unipole

We shall not give an exhaustive treatment of optimum methods of operating the unipole, since such optimal arrangements will depend on antenna height, desired resistance transformation, bandwidth and phase requirements, etc., making a general analysis quite unwieldy. Instead, we shall confine ourselves to the discussion of two of the many possible cases, in the hope that the results will be of some heuristic value.

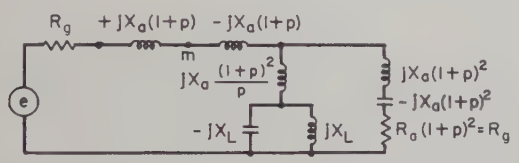

Fig. 12—Unipole operated with transmission line tuned.

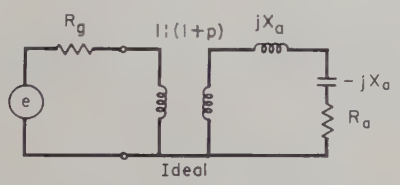

Fig. 13—Equivalent circuit using ideal transformer.

The first method derives from analogy with the quarter-wave unipole. In the quarter-wave case, the transmission-line mode provides little shunting effect because it is near the resonant point. To duplicate this situation, we connect a capacitive reactance equal to $-jX_L$ between points m and n (see Fig. 3). This tunes out the transmission line. Then, assuming that we wish to match to a generator of purely resistive internal impedance R_g, we select a value of p such that $R_g = (1+p)^2 R_a$. To tune out the reactance $X_a(1+p)^2$, we choose X_n such that $X_n = [(1+p)/p]X_a$. This leaves the series reactance $-pX_n$, which is tuned out by an inductor equal in value to $+pX_n$. This circuit is illustrated in Fig. 12. If the losses in the transmission line are small (high transmission-line Q), it can be seen that the input impedance will behave like that of the circuit of Fig. 13, where the antenna reactance is tuned out and the resistance is transformed through an ideal transformer with a turns ratio of $1:(1+p)$.

The above method effectively removes the transmission line and utilizes only the transformation properties due to the current division [i.e., the $(1+p)^2$ factor]. An alternative method sets $p=0$, and uses instead the transformation resulting from the transmission-line inductance, as shown in Fig. 14. In order to make $p=0$, we drop an additional wire from the top of the antenna down inside the tower. At the base it is connected to ground through X_n. The generator is connected to the tower and cage base as indicated through inductor X_e.

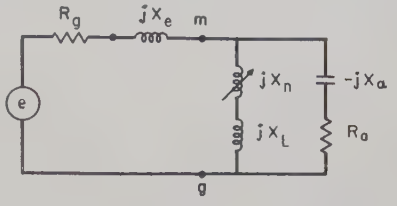

Fig. 14—Equivalent circuit utilizing the transmission line reactance ($p=0$).

We first adjust X_L to transform R_a up to R_g. The method of adjusting X_L becomes evident when we note that the center wire and tower form a section of coaxial transmission line. Thus, by adjusting wire diameter, and by placing shorting wires inside the tower at the proper point, it is possible to achieve a wide range of values of X_L. X_n is then a small inductor which may be used for fine adjustment. X_e is used to tune out whatever capacitive reactance the unipole presents.

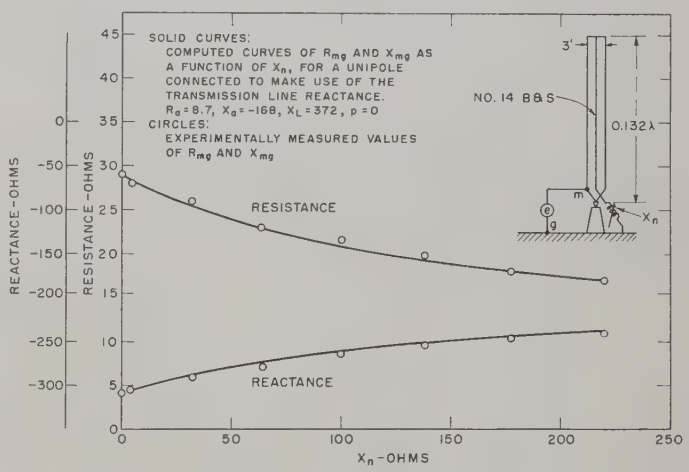

Fig. 15—Input impedance of a folded unipole with $p=0$ as a function of inserted reactance X_n.

Fig. 15 shows the computed and measured values of R_{mg} and X_{mg} plotted as a function of X_n for a folded unipole operated so that $p=0$. The antenna was a triangular tower (0.132 wavelength high and 3 feet on a side), with a single No. 14 B&S gauge copper wire connected at the top and extended vertically to the base, where a variable inductor X_n was inserted in series to ground. The curves were computed from the measured values of R_a, X_a and X_L and were checked experimen-

tally by direct measurement of R_{mg} and X_{mg}. The measured values are plotted in Fig. 15, and it is seen that there is good agreement with the computed curves.

It should be noted that if the antenna is too close to a quarter-wave long, and R_g is not too close to R_a, this method will not work, since X_e becomes imaginary when $X_a < \sqrt{R_a(R_g - R_a)}$, as is the case near a quarter wave. In this event, the first method may be employed. If the antenna is reasonably short, then X_L may be represented by an almost pure inductance, and we may show that the bandwidth and phase characteristic (aside from a slight phase shift) are approximately the same as in the circuit of Fig. 12.

Application of the Folded Unipole

The folded unipole antenna offers distinct advantages when short vertical radiators (having the undesirable feature of low radiation resistance and large reactance) must be used because of physical limitations on the height of antenna towers.

In such a case it is often desirable, because of considerations of bandwidth or phase stability, to reduce the reactance by increasing the diameter/length ratio of the antenna. This is most easily done by suspending wires from outrigger arms attached to the top of the tower. Such a structure can be modified to operate as a folded unipole antenna by exciting only a portion of the drop wires while the remaining wires are grounded through a reactance.

A T or π coupling network is generally used in conjunction with vertical antennas in order to give a nonreactive impedance of the correct magnitude to terminate a nonresonant transmission line. The coupling network may also be used to secure the proper phase relations between the radiators in a phased array. It has been shown that the input impedance of a folded unipole is influenced by the division of currents in the fed and unfed portions of the antenna and by the presence of the currents in the transmission line formed by the fed and unfed conductors, as well as by the presence of an impedance connected between the unfed section and ground. It can be seen from Fig. 7 that this results in the presence of a T-reactive network inherently associated with the transformed antenna impedance. One of the elements in this network is the reactance of the transmission line formed by the driven and the tuned sections of the antenna. Thus we are able to replace one of the lumped elements of the coupling network with a distributed parameter associated with the antenna. With careful antenna design, it should be possible to obtain a reactance which has very low losses and whose value is insensitive to temperature, vibration, etc., which will result in a more efficient and stable network.

An additional advantage accruing from the use of the unipole is that no additional elements are necessary to prevent the accumulation of a static charge on the antenna, since the antenna structure is at static ground potential.

When used in a directive array, the folded unipole has the disadvantage that it is difficult to measure directly the magnitude and phase of the radiation current in each radiator, due to the presence of the transmission-line currents. However, since the radiation-mode currents in the two sections of the antenna are in phase, while the transmission-line mode currents are equal in amplitude and in phase opposition, it is possible to obtain an indication that is proportional to the total radiation current and independent of the transmission-line currents. This is done by the use of a differential current sampling transformer with two identical input windings and a single output winding. The winding directions must be such that two in-phase input currents add in the output, while out-of-phase input currents give no output. An additional requirement is that there be negligible coupling between the two input windings. Such a transformer, consisting of a ferrite core with single-turn input windings and an electrostatically shielded, 10-turn output winding, has been used with good results.

Characteristics of Tropospheric Scattered Fields*

L. G. TROLESE†

Summary—**Experimental results obtained with transmissions at wavelengths of 3.2, 9.3, and 24 cms over a 46.3-mile path are presented. With low terminal heights the scattered field was dominant on this path. Tests with a narrow beam antenna indicate that the scattered field arrives at the receiver spread over an appreciable angle. This angle is some five to seven times as large as the Booker-Gordon theory predicts on the assumption that the scale of turbulence is large compared to the wavelength. Loss in ability to receive power in proportion to antenna gain was encountered for antennas with aperture diameters greater than about 20 wavelengths. This loss occurs for aperture sizes considerably smaller than the Booker-Gordon theory predicts.**

The speed of fading of the scattered field signal increases almost linearly with frequency. This agrees fairly well with the concept (due to Ratcliffe[1] and applied to tropospheric scattering by Booker and Gordon[2]) that fading is due to beating between various scattered field components whose frequencies differ by a fractional Doppler shift due to motion of the scatterers. The speed of fading always increases, during the day, with time of day and does not correlate with mean upper wind speed. This increase with time of day is probably connected with the repetitive diurnal meteorological cycle prevalent in Arizona.

Introduction

In 1950 Booker and Gordon[2] published their theory of tropospheric scattering which sought to explain the occurrence, in the absence of super-refraction, of fluctuating fields at a distance far beyond the horizon which are much stronger than standard diffraction theory predicts. In later papers, Gordon,[3] and Booker and deBettencourt[4] derived various approximate formulas based on this theory which can be applied to specific cases. The object of this paper is to compare the experimental results obtained on a 46.3 mile path in the Arizona desert with the predictions of the Booker-Gordon theory.[5]

Experimental Setup

A profile of the path used is shown in Fig. 1. The terrain deviates from a spherical surface by no more than 80 feet and deviations of this magnitude are not near the two terminals. Towers equipped with elevators at each terminal permitted antenna heights to be varied from 4 to 195 feet above the surface. Transmissions at wavelengths of 3.2, 9.3 and 24 cms were used in the tests with peak pulse transmitter powers of 25, 30 and 50 kw respectively.

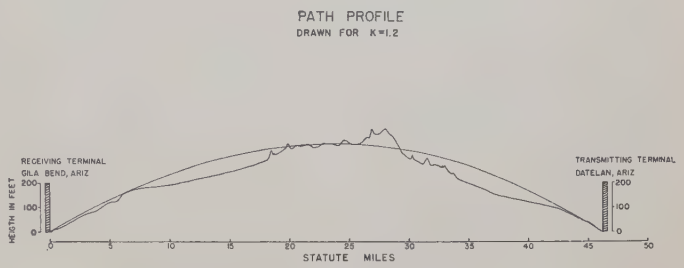

Fig. 1—Profile of path drawn for $k=1.2$.

The tests were made during the winter season when a definite repetitive diurnal meteorological cycle is prevalent. For a very large portion of the time, the daytime atmosphere is well mixed and nearly standard. After sundown, a ground-based radiation inversion quickly sets in and increases in height and intensity during the night. Shortly after sunrise, heating of the ground causes mixing in the lower atmosphere which rapidly dissipates the nocturnal inversion. Consequently, radio transmissions show no evidence of super-refractive effects during the daytime, but microwave transmissions to distances beyond the horizon are enhanced during the nighttime.

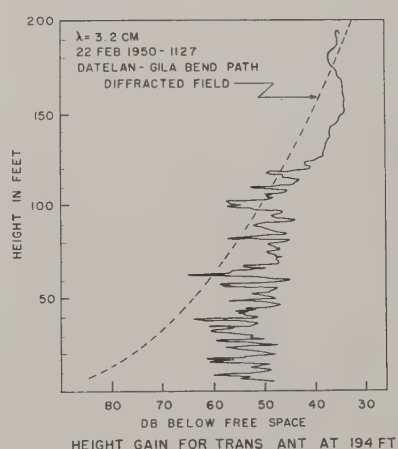

Fig. 2—Measured receiver height gain curve with transmitting antenna at 194 feet.

Height Gain Measurements

Fig. 2 shows a typical height-gain curve made during the daytime with transmission at a wavelength of 3.2 cm and a transmitting antenna height of 194 feet. When the receiving terminal is above 130 feet the received sig-

* Original manuscript received by the PGAP, December 2, 1954; revised manuscript received, March 7, 1955.

† U. S. Navy Electronics Lab., San Diego, Calif.

[1] J. A. Ratcliffe, "Diffraction from the ionosphere and the fadings of radio waves," *Nature*, vol. 163, pp. 9–11; July, 1948.

[2] H. G. Booker and W. E. Gordon, "A theory of radio scattering," Proc. IRE, vol. 38, pp. 401–412; April, 1950.

[3] W. E. Gordon, "Radio scattering in the troposphere," Proc. IRE, vol. 43, pp. 23–28; January, 1955.

[4] H. G. Booker and J. T. deBettencourt, "Theory of radio transmission by tropospheric scattering using very narrow beams," Proc. IRE, vol. 43, pp. 281–290; March, 1955.

[5] These experimental results were presented in part at the meetings of the International Scientific Radio Union at Zurich, Switzerland, by J. B. Smyth, in August, 1950. Also, presented at the Dedication Meetings, National Bureau of Standards, Boulder, Colo., September, 1954.

nal is steady and is near the value calculated for diffracted field (dashed line). As the receiving antenna is lowered below 130 feet the signal begins to fluctuate rapidly with time and shows little variation of average received field with height. Fig. 3 shows a height gain curve measured with the transmitting antenna at a height of 4 feet; in this case the average received field is independent of height of the receiving antenna and very much stronger than the calculated diffracted field. Thus, with terminals low, the received field fluctuates rapidly with time, exhibits little or no height-gain, and is very much stronger than the diffracted field value. These three characteristics of the signal lead to the conclusion that scattered field is dominant in this situation.

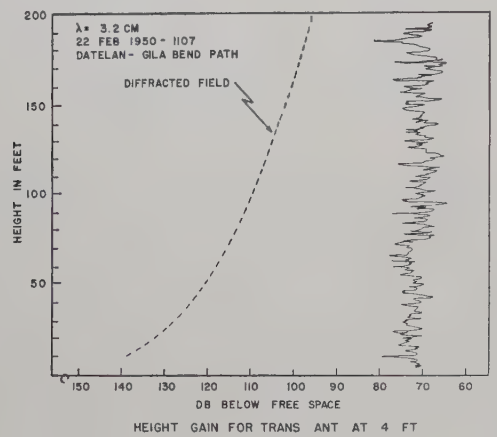

Fig. 3—Measured receiver height gain curve with transmitting antenna at 4 feet.

The Effect of Variation of Antenna Beamwidth

A series of tests were made during the daytime in which the power received with different size antenna apertures was compared using transmissions at 3.2 cm wavelength. Arrangements were made to use either a 1-foot or a 4-foot diameter paraboloid antenna at each terminal. At a wavelength of 3.2 cms the 1-foot antenna has a diameter of 9 wavelengths with a beamwidth of 7 degrees and the 4-foot antenna a diameter of 38 wavelengths with a beamwidth of 1.75 degrees. The tests were made by recording the received power for a period of 1 minute with each antenna and comparing the average of the 1-minute records. The results shown in Table I are the average of the power ratios obtained in some 10 to 15 such comparisons over a period of 10 days. The first line of the table shows the result of comparing a large and small receiving antenna aperture while using a broad-beam transmitting antenna. The ratio of received power amounted to 6 db in contrast to 12 db which would be expected under free space conditions. When both terminals were elevated from 4 feet to 194 feet, into the diffracted field domain, the same comparison yielded values close to 12 db. The second line of the table shows the result of a similar comparison except that the measurement was made with a large aperture transmitting antenna, and consequently the transmitted power was confined so as to illuminate a smaller volume. In this case, the comparison of the two receiving apertures resulted in a power ratio of 7.9 db, a value somewhat closer to the ratio of the plane wave gains of the two antennas. If the ratio of received power as measured as the transmitting aperture, rather than the receiving aperture, is changed from 9 to 38 wavelengths, comparable results are obtained as shown in lines 3 and 4 of the table. A comparison made by simultaneously changing antenna aperture size at both transmitting and receiving terminals gave a measured received power ratio of 14.8 db in contrast to a value of 24 db which would be expected under free space conditions. This is shown in the last line of the table.

TABLE I

Variation of Received Power with Antenna Aperture Size

Transmitting Antenna Diameter	Receiving Antenna Diameter	Measured Ratio of Received Power	Ratio of Plane Wave Gains
9λ	38λ / 9λ	6.0 db	12 db
38λ	38λ / 9λ	7.9 db	12 db
38λ / 9λ	9λ	5.0 db	12 db
38λ / 9λ	38λ	7.1 db	12 db
38λ / 9λ	38λ / 9λ	14.8 db	24 db

λ=3.2 cm; Antenna Height 4 Feet; 46.3 Mile Path.

Since the measurements indicate that an antenna with a 1.75 degree beam fails to absorb power proportional to its gain when receiving scattered fields, one would expect that as the antenna is rotated, the received power would not fall off in accordance with the polar diagram of the antenna. The results of rotating the 4-foot receiving antenna with a 1.75-degree beam in the horizontal plane are shown by Fig. 4 (opposite page) and in the vertical plane by Fig. 5 (opposite page). These measurements were made using a 1-foot transmitting antenna with a 7-degree beam. The left-hand diagrams show the points obtained when the measurements were made with the diffracted field dominant, and the right-hand diagrams are for measurements in the scattered field. In both cases the scattered field points tend to be spread in angle outside the beam of the antenna.

Gordon and Booker and deBettencourt have concluded that presently available measurements of atmospheric turbulence indicate the scale of turbulence, l, is very large compared to microwave wavelengths. With the additional assumption that the angle between the

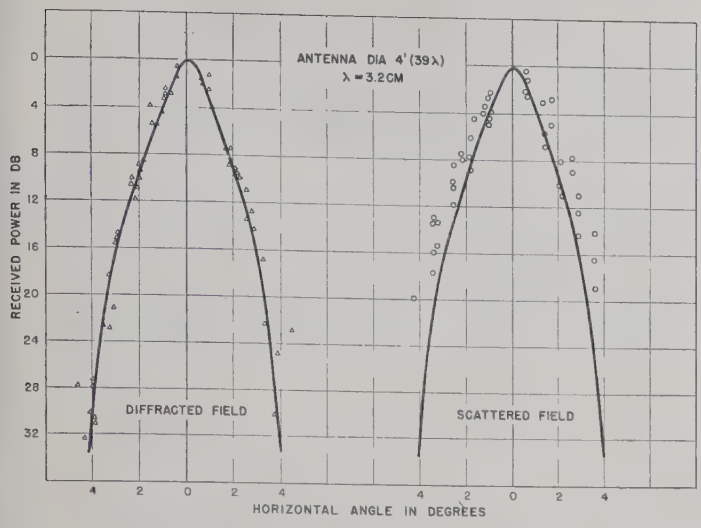

Fig. 4—Effect of rotating receiving antenna in horizontal plane.

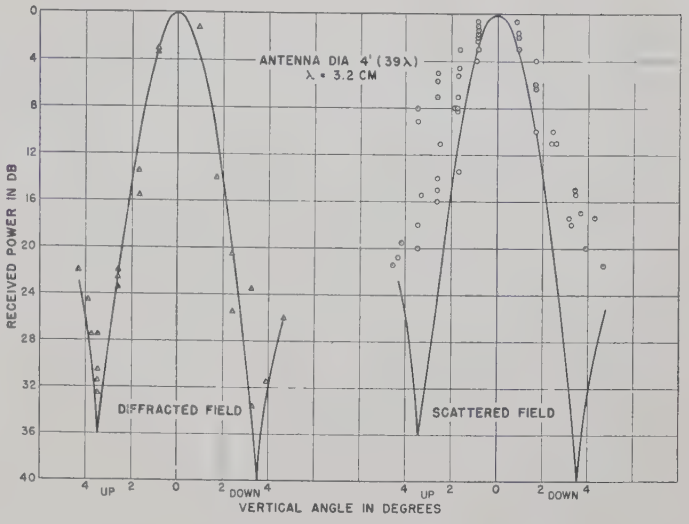

Fig. 5—Effect of rotating receiving antenna in vertical plane.

direction of incidence and the direction of scattering, θ, is small compared to one radian, Gordon derived, from the basic Booker-Gordon scattering formula, the following expressions for the horizontal angle α_c and the vertical angle θ_1, over which scattered radiation is spread at the receiver:

$$\alpha_c = 2/3\theta_0 = 2/3\frac{d}{R}, \tag{1}$$

$$\theta_1 = 1.19\theta_0 = 1.19\frac{d}{R}, \tag{2}$$

where θ_0 is the minimum value of θ imposed by the earth's curvature, d is the distance between transmitting and receiving antennas and R is the radius of the earth modified to account for refraction by a standard atmosphere. These formulas are valid provided,

$$\frac{\lambda}{2\pi l} \ll \theta \ll 1. \tag{3}$$

The horizontal angle α_c is the limiting angle and for the 46.3-mile path over which the tests were made the calaulated value of α_c is 0.35 degrees.

Booker and deBettencourt concluded that the antenna beamwidth must be appreciably smaller than α_c for the spread to be clearly visible in the direction of scattered wave, but a beamwidth five times the computed value of α_c is narrow enough in this case to show the effect.

A comparison between experiment and the theory can also be made by fitting data obtained with several antenna apertures on a chart such as that of Fig. 6, which was used by Booker and deBettencourt to illustrate the effect of antenna beamwidth on received power. This graph is based on their two equations

$$\frac{P_R}{P_F} = 0.86\frac{R^2}{d}S_p \quad \text{for} \quad \alpha \gg \alpha_c \tag{4}$$

$$\frac{P_R}{P_F} = \frac{2d\alpha^3}{(\theta_0 + \alpha/2)^5}S_p \quad \text{for} \quad \alpha \ll \alpha_c, \tag{5}$$

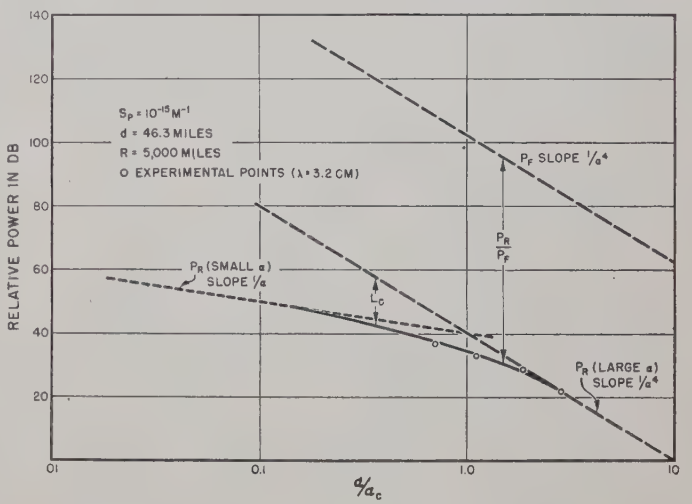

Fig. 6—Received power as a function of α/α_c.

where P_R is received power, P_F is received power in free space, α is antenna beamwidth (assuming identical transmitting and receiving antennas), and S_p is the scattering parameter of the atmosphere given by

$$S_p = \frac{1}{2\pi l}\left(\frac{\overline{\Delta\epsilon}}{\epsilon}\right)^2,$$

where $\overline{(\Delta\epsilon/\epsilon)^2}$ is the mean-square deviation of the dielectric constant from the mean. These two equations are valid provided the conditions of (3) are met. For α large compared to α_c, the antennas function as if in free space and P_R and P_F both vary as $1/\alpha^4$, P_R/P_F is independent of beamwidth and (4) applies. When α is small compared to α_c, P_R/P_F varies as α^3 according to (5) and consequently P_R is proportional to $1/\alpha$. The chart of Fig. 6 has been drawn for the 46.3-mile path, assuming a value of S_p equal to 10^{-15} meter^{-1}. The quantity labeled Lc on the graph which increases as the ratio α/α_c decreases, has been termed the "aperture-

medium coupling loss" by Booker and deBettencourt.[6] Experimentally determined values of Lc are available from measurements made in Arizona. Using 3.2-cm transmissions, measurements were made of received power as the transmitter and receiver were simultaneously shifted from 4-foot to 1-foot, $2\frac{1}{2}$-foot to 1-foot, and $1\frac{1}{2}$- to 1-foot diameter antennas. Or in terms of beamwidth received power was measured as α was changed successively from $1\frac{3}{4}$ to 7, 2.8 to 7, and 4.6 to 7 degrees. Changing antenna diameter from 1 to $1\frac{1}{2}$ feet or α from 7 to 4.6 degrees resulted in a power change of 6.9 db as compared to 7.0 db which would be expected under free space conditions. Thus, it is apparent that Lc must be zero for $\alpha=7$ degrees and the value of received power measured with this beamwidth should lie on the dashed line with slope $1/\alpha^4$ valid for large α. Consequently, the measured values of P_R should be placed on the graph so as to form a smooth transition between the dashed lines having slopes $1/\alpha$ and $1/\alpha^4$, with the value for $\alpha=7$ degrees on the latter line. The experimental values placed in this fashion are shown as circles on the graph, and this fixes α_c as equal to 2.5 degrees. This value is 7 times larger than the value of 0.35 degrees computed from Gordon's formula (1).

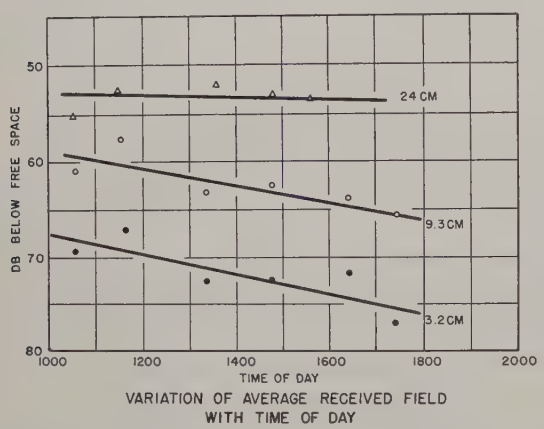

Fig. 7—Variation of received field with time of day.

Variation of Received Field with Wavelength

The measured variation of average received field strength with time of day is shown in Fig. 7 for wavelengths of 3.2, 9.3 and 24 cms. These measurements were made with transmitting and receiving antennas 4 feet in diameter located 4 feet above the ground. The received power decreases somewhat with time of day, with the decrease greatest for the shortest wavelength. However, this variation with time of day is not large. The variation of the ratio P_R/P_F with wavelength is more pronounced, as shown in Fig. 8. The variation with wavelength is slightly less in the morning than in the afternoon. The 4-foot diameter antennas used at a wavelength of 24 cms have a beamwidth of 14 degrees so that formula (4) valid for large α should apply. Assuming $S_p=10^{-15}$ meter^{-1} the computed value using this formula is shown as point (1) on Fig. 8, which is about 8 db below the measured values. If S_p were assumed equal to 10^{-14} meter^{-1} the computed value of P_R/P_F for 24 cm would be shifted by 10 db and the agreement would be better. For 4-foot antennas at 3.2 cms the beamwidth is 1.75 degrees, some five times the computed value for α_c of 0.35 degree, and one would expect on the basis of the theory that the formula for large α would be applicable. However, this would predict no dependence of P_R/P_F on wavelength. If α_c is assumed to be 2.5 degrees and $S_p=10^{-15}$ M^{-1} and a value of P_R/P_F for 3.2 cms is determined from Fig. 6, point (2) on Fig. 8 is obtained which is in agreement with the data for this wavelength. But then the value for 24 cms is 8 db off and it would appear that this experimental data shows more wavelength dependence than allowed for by the Booker-Gordon theory.

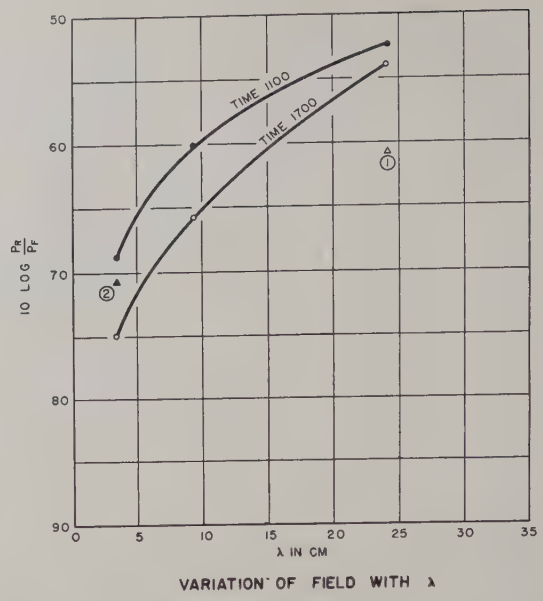

Fig. 8—Variation of received field with wavelength.

Fluctuating Characteristics

The scattered fields fluctuate rapidly with time as shown in the sample records of Fig. 9 (opposite page), which were made with Brush recorders at 3.2, 9.3, and 24 cm transmissions and quite obviously the character of the fluctuations are a function of wavelength. Booker and Gordon utilized a concept by Ratcliffe[1] to explain the fluctuations. Ratcliffe defined a quantity, S, the speed of fading by

$$S=\frac{\overline{|U_\tau|}}{\tau\overline{E}}, \tag{6}$$

where E is the signal amplitude, U_τ is the difference between successive values of E taken at intervals τ

[6] This loss sometimes has been referred to incorrectly as a "loss of antenna gain." Gain, as defined usually, is a constant for a given antenna (e.g. S. Silver, "Microwave Antenna Theory and Design," M.I.T. Radiation Lab. Ser., McGraw-Hill Book Co., Inc., New York, N. Y., vol. 12, p. 3: 1949).

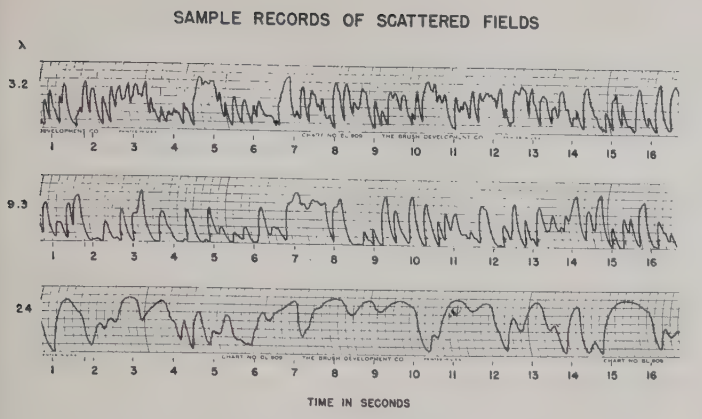

Fig. 9—Typical records of scattered field signals for three wavelengths.

seconds apart, with τ sufficiently small so that E does not vary greatly in one interval. He has shown that the speed of fading can be related to a fractional Doppler shift in frequency due to effective speed of the scatterers, V, by the following relation

$$S = \frac{2Vf \sin \theta/2}{C}, \qquad (7)$$

where f is the radio frequency, C the velocity of light and θ is the angle between the direction of incidence and the direction of scattering. Thus the speed of fading should vary directly as the radio frequency. Using (6), the speed of fading was calculated for a number of cases at three frequencies (or wavelengths of 3.2, 9.3 and 24 cms). Fig. 10 is a typical sample of the results which

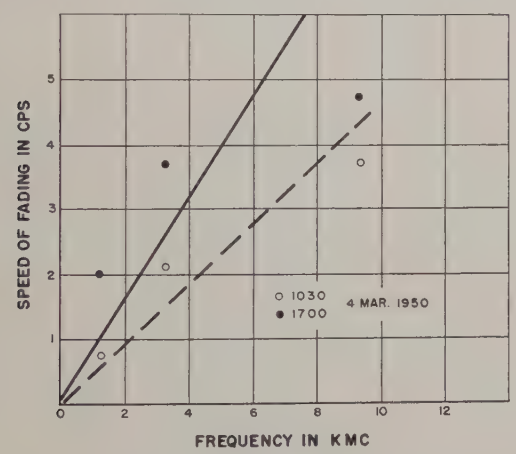

Fig. 10—Variation of speed of fading with frequency.

were obtained. The points obtained from data taken at 10:30 in the morning fit fairly well on a straight line but the afternoon points are a poorer fit to (7). Data taken simultaneously at more than three frequencies would be desirable to determine if the speed of fading follows formula (7) or some other relationship.

Fig. 11 shows a plot of the variation of speed of fading with time of day. For all three wavelengths the speed of fading increases slowly with time of day. Earlier than 10:00 in the morning or later than 6:00 in the

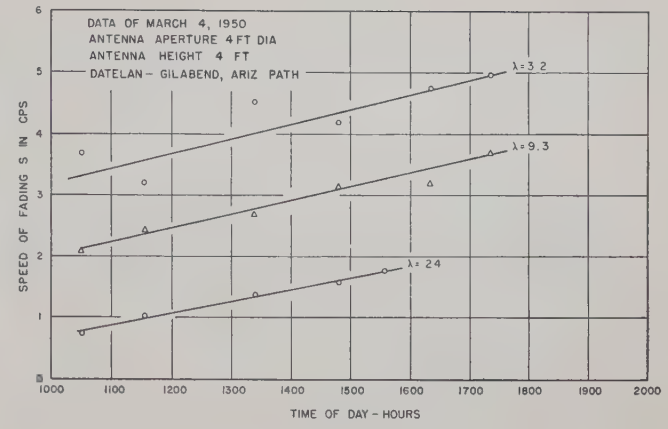

Fig. 11—Variation of speed of fading with time of day.

evening the presence of the radiation inversion causes the refracted field component to swamp out the scattered field. This gradual increase of speed of fading was consistently observed every time scattered field recordings were made. This would seem to indicate that fading is not due to the fact that scatterers drift with

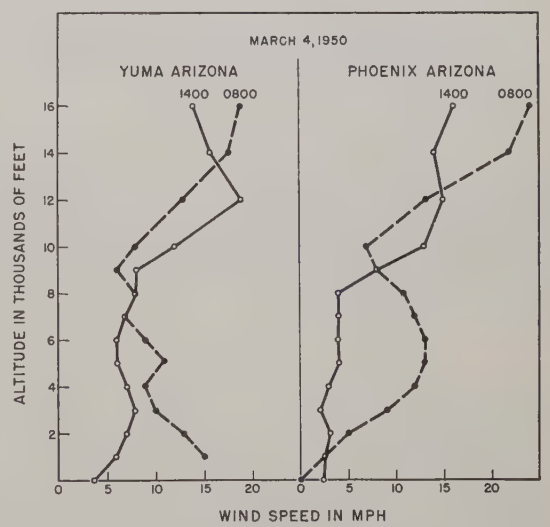

Fig. 12—Wind speed as a function of altitude.

the mean wind. Fig. 12 shows profiles of wind speed aloft for the same day that the data of Fig. 11 was taken. Two sets of wind data are shown, one taken at Yuma, Arizona, 100 miles west of the propagation path, and the second taken at Phoenix, Arizona, 100 miles northeast of the path. Below 7,000 feet the wind speed is greater at 0800 than at 1400. With antenna beamwidth of $1\frac{3}{4}$ degrees and a pathlength of 46.3 miles, the important scattering volume should lie below 4,000 or 5,000 feet altitude, so it is apparent that the trend in upper wind is opposite to the trend in speed of fading. It appears more likely that the increase of speed of fading during the day is connected with the diurnal meteorological cycle. The nocturnal radiation inversion is dissipated in the morning by heating of the ground and a turbulent layer is propagated upward as the day

progresses and ground heating is intensified. Consequently the velocity V in formula (7) is probably an effective velocity due to the upward motion of the turbulence during the day.

Conclusions

Scattered fields measured on a 46.3-mile path in Arizona with low terminal heights arrive at the receiving antenna spread over an appreciable angle. This angle is some 5 to 7 times as large as the angle computed using an approximate formula derived by Gordon based on the assumption that the scale of turbulence is large compared to the wavelength. Appreciable aperture to medium coupling loss occurs for antennas with beamwidth considerably larger than this computed angle.

The ratio of received power to power received in free space measured at wavelengths of 3.2, 9.3 and 24 cms shows a greater wavelength dependence than predicted by the Booker-Gordon theory.

The speed of fading measured at wavelengths of 3.2, 9.3 and 24 cms increases with increasing frequency or decreasing wavelength. The increase of speed of fading with frequency follows fairly well the linear relationship inherent in Booker and Gordon's equation based on Ratcliffe's concept. The speed of fading on this path always increases during the day and does not correlate with mean upper wind speed. This increase with time of day is probably connected with the diurnal meteorological cycle.

Acknowledgment

The author is indebted to W. C. Hoffman, C. A. Potter, and J. B. Smyth for many helpful discussions; and to E. L. Culler and M. D. Rocco who assisted with the computations.

Use of Folded Monopoles in Antenna Arrays*

J. B. LEWIS†

Summary—**The use of folded elements in antenna arrays is reviewed and then discussed with regard to an array of vertical monopoles to which an improved impedance match of the feed system is required. A method of calculating the driving point impedances from the self and mutual impedances of related unfolded elements is given.**

Introduction

IN THE DESIGN of antenna arrays of vertical monopoles, the driving point impedances of the elements may be too low to be matched conveniently and efficiently to the phasing network, and the possibility of using some folded elements in the array offers a method of increasing these impedances. The extensive use of a folded element in Yagi antennas is a similar application of this technique. The self impedance of a resonant length, folded dipole has been investigated previously,[1,2] and expressions for the self impedance transformation ratios using wires of unequal diameter[3] and for the self impedance of nonresonant length, folded dipoles have been published.[4] The use of folded monopoles as array elements where mutual impedances must be considered, and the effect on these impedances and on the driving point impedances of using nonresonant lengths are considered here.

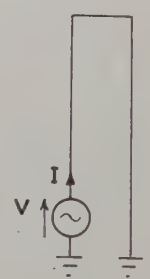

Fig. 1—Folded monopole.

Theoretical Development

Self Impedance of a Folded Monopole

Consider first a resonant length, folded monopole (approximately a quarter wavelength) shown in Fig. 1. This element may be represented as the superposition of parallel monopoles and shorted transmission line in Fig. 2 (opposite page).[5] If it is assumed that terminal current of the transmission line is very small, and radiated power from this line is negligible, a single frequency equivalent unfolded monopole may be used to represent the elements of Fig. 2, insofar as radiated power is con-

* Original manuscript received by the PGAP, December 15, 1954; revised manuscript received March 21, 1955. This work was supported by the Bureau of Ships, Navy Department.

† Elec. Engrg. Dept., Univ. of Tennessee, Knoxville, Tenn.

[1] R. W. P. King, H. R. Mimno, and A. H. Wing, "Transmission Lines, Antennas, and Wave Guides," McGraw-Hill Book Co., Inc., New York, N. Y., p. 224; 1945.

[2] W. van B. Roberts, "Input impedance of a folded dipole," *RCA Review*, vol. 8, p. 129; June, 1947.

[3] R. Guertler, "Impedance transformation in folded dipoles," Proc. IRE, vol. 38, p. 1042; September, 1950.

[4] R. E. Beam and P. Andris, "Input impedance of folded dipole antennas," *Proc. NEC*, vol. 8, pp. 678–691; 1952.

[5] King, Mimno, and Wing, *loc. cit.*

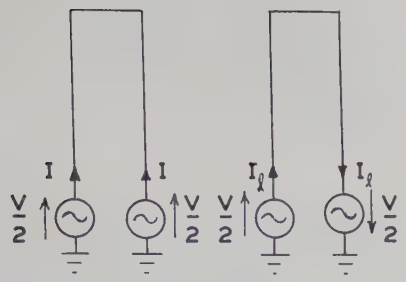

Fig. 2—Parallel monopoles (a) and shorted transmission line (b).

cerned. This equivalent unfolded monopole is a monopole with a total current distribution equal to the sum of the currents in Fig. 2(a), and is shown in Fig. 3. The power input in both Figs. 1 and 3 is VI; however, the input impedance in Fig. 1 is $Z_{11}' = V/I$, whereas the input impedance in Fig. 3 is $Z_{11} = V/4I$, so that

$$Z_{11}' = 4Z_{11}. \tag{1}$$

This result assumes that two wires of equal diameter are used in the folded monopole. In all impedance expressions, primes are used when the corresponding element is folded.

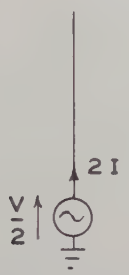

Fig. 3—Equivalent unfolded monopole.

In the more general case where the element is of nonresonant length, the terminal current in Fig. 1 is taken as $I' + I_l$. Here I' is the terminal current of each of the elements in Fig. 2(a), $I_l = V/Z_l$ is the terminal current of Fig. 2(b), and Z_l is the input impedance of the transmission line, for the given length, frequency, wire size, and spacing. The equivalent unfolded monopole of Fig. 3 has a terminal current of $2I'$, and the transmission line is assumed to have negligible loss and radiation. The input impedance in Fig. 1 is then

$$Z_{11}' = \frac{V}{I' + I_l} = \frac{V}{I'}\left[\frac{1}{1 + \dfrac{2Z_d}{Z_l}}\right],$$

where $Z_d = V/2I'$, the driving point impedance of either element in Fig. 2(a). The input impedance in Fig. 3 is now $Z_{11} = V/4I'$, and therefore,

$$a^2 = \frac{Z_{11}'}{Z_{11}} = \frac{4}{1 + \dfrac{2Z_d}{Z_l}} = \frac{4Z_l}{Z_l + 2Z_d}. \tag{2}$$

This impedance transformation ratio, a^2, is for the case of two similar wires of nonresonant length. Other more general cases of more than two conductors and of conductors of unequal size have been calculated in the literature but are not considered here. For close conductor spacing, Z_d approaches $2Z_{11}$ where Z_{11} is the self impedance of a single isolated monopole of the given dimensions, so that $Z_{11}' = a^2 Z_{11}$ appears as the parallel combination of $4Z_{11}$ and Z_l. For a resonant length, Z_l approaches an infinite value and a^2 approaches 4.

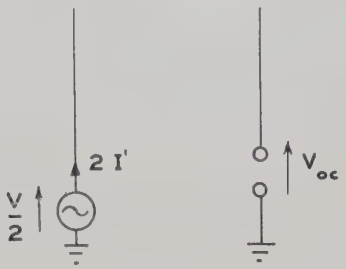

Fig. 4—Coupled monopoles.

Mutual Impedance between Folded Monopoles

The mutual impedance between unfolded and folded array elements of the type discussed above must also be found. In Fig. 4 are shown two unfolded vertical monopoles of any length. Element 1 is the equivalent of a folded monopole of two like wires, and the mutual impedance Z_{21} is defined as $V_{0c}/2I'$. For element 1 folded, the terminal current is $I' + I_l$, and therefore

$$Z_{21}' = \frac{V_{0c}}{I' + I_l} = \frac{V_{0c}}{I'}\left[\frac{1}{1 + \dfrac{2Z_d}{Z_l}}\right].$$

The ratio Z_{21}'/Z_{21} is then

$$\frac{Z_{21}'}{Z_{21}} = \frac{2}{1 + \dfrac{2Z_d}{Z_l}}. \tag{3}$$

It can also be shown that $Z_{12}' = Z_{21}'$. Z_{21} can be calculated from the length and spacing of the elements. If element 2 is also folded, it can be shown that the open circuit voltage is doubled in this case of two like wires and the ratio of mutual impedance between two folded elements becomes

$$\frac{Z_{21}''}{Z_{21}} = \frac{4}{1 + \dfrac{2Z_d}{Z_l}}, \tag{4}$$

which is the same as (2). The elements are assumed to be spaced far enough apart to neglect coupling effects in the transmission lines.

Driving Point Impedances

It is more convenient to regard the impedance transformation ratio as $a^2\rho$ (a in this case being 2), where a is a voltage and current transformation ratio and ρ is a

complex modifying factor to account for the shunting effect of Z_l. A close analogy to the well-known "referred" coupled circuit theory is then possible. If one considers first an array of n unfolded monopoles, the voltage equations are:

$$\begin{aligned} V_1 &= I_1Z_{11} + I_2Z_{12} + \cdots + I_kZ_{1k} + \cdots + I_nZ_{1n} \\ &\cdots\cdots\cdots\cdots\cdots\cdots \\ V_k &= I_1Z_{k1} + I_2Z_{k2} + \cdots + I_kZ_{kk} + \cdots + I_nZ_{kn} \\ &\cdots\cdots\cdots\cdots\cdots\cdots \\ V_n &= I_1Z_{n1} + I_2Z_{n2} + \cdots + I_kZ_{nk} + \cdots + I_nZ_{nn}. \end{aligned} \tag{5}$$

If the kth element is then folded, a similar set of equations is:

$$\begin{aligned} V_1 &= I_1 \ Z_{11} + I_2 \ Z_{12} + \cdots + \frac{I_k}{2} 2\rho Z_{1k} + \cdots + I_n \ Z_{1n} \\ &\cdots\cdots\cdots\cdots\cdots\cdots\cdots\cdots\cdots\cdots \\ 2V_k &= I_1 2\rho Z_{k1} + I_2 2\rho Z_{k2} + \cdots + \frac{I_k}{2} 4\rho Z_{kk} + \cdots + I_n 2\rho Z_{kn} \\ &\cdots\cdots\cdots\cdots\cdots\cdots\cdots\cdots\cdots\cdots \\ V_n &= I_1 \ Z_{n1} + I_2 \ Z_{n2} + \cdots + \frac{I_k}{2} 2\rho Z_{nk} + \cdots + I_n \ Z_{nn}. \end{aligned} \tag{6}$$

Eq. (6) may be solved for the driving point impedances where in general $Z_{dj} = V_j/I_j$ and $Z_{dj}' = 2V_j/I_j/2$. Folding the kth element changes the driving point impedances of all the elements. However, for resonant length elements where $\rho = 1$, only the kth element impedance is increased by 4; the other elements are unaffected.

Experimental Results[6]

An experimental investigation was made to check some of the results of the preceding section. The measurements were made with a commercial vhf bridge on a model operated at 450 mc, and the model elements were resonant length brass rods 3/32 inch in diameter mounted on an elevated horizontal ground plane sixteen feet square. Three sets of measurements were made to check the mutual impedances using two elements spaced 0.4λ apart. In each case, a driving point impedance was measured at each element with the other shorted, and this measured value was compared with a value calculated using the theoretical values[7] of $Z_{11} = 35 \ \angle 0$ degree and $Z_{12} = Z_{21} = 16.9 \ \angle -81.0$ degree. The results are shown in Table I below.

Conclusion

The theoretical expressions of the second section, which are based on certain approximations discussed in the references, have been checked in part. The use of folded elements in an antenna array appears to be a satisfactory method of increasing driving point impedances, and these impedances can be calculated, as shown, with reasonable accuracy.

TABLE I

Impedance	Theoretical Value	Measured Value
Z_{11}	35/0 degree	35/0 degree
Z_{11}'	140/0 degree	141/0 degree
Z_{d1} (unfolded-unfolded)	42.8/3.4 degrees	43/5.5 degrees
Z_{d2} (unfolded-unfolded)	42.8/3.4 degrees	45/6.5 degrees
Z_{d1}' (unfolded-folded)	42.8/3.4 degrees	41.5/2.0 degrees
Z_{d2}' (unfolded-folded)	171.2/3.4 degrees	163/5 degrees
Z_{d1}'' (folded-folded)	171.2/3.4 degrees	162/−4 degrees
Z_{d2}'' (folded-folded)	171.2/3.4 degrees	178/3 degrees

Acknowledgment

The author wishes to acknowledge the assistance of C. E. Blakely with the experimental work.

[6] J. B. Lewis and C. E. Blakely, "Use of Folded Monopoles in Antenna Arrays," Engineering Experiment Station Report, University of Tennessee; September 1, 1954.

[7] R. King, "Self and Mutual Impedances of Parallel Identical Antennas," Cruft Lab. Tech. Rep. No. 118; November 1950.

A New Interpretation of the Integral Equation Formulation of Cylindrical Antennas*

C. T. TAI†

Summary—**The validity of the conventional integral equation formulation of cylindrical antennas is often criticized because of an approximation of the kernel of the integral equation. If the antenna is of the form of a cylindrical tube there is an exact integral equation formulation. By means of the variational technique the integral equation for the cylindrical tube can be solved approximately. When the length of the tube is large compared to its diameter, the input impedance of the structure is found to be the same as if one had used the approximate integral equation at the very beginning of the analysis. This new procedure therefore clarifies one main ambiguity involved in the early works of the theory of cylindrical antennas based upon the approximate integral equation. It also enables us to treat the problem of relatively thick cylindrical antennas.**

Introduction

MANY ARTICLES have been written on the subject of cylindrical antennas using the integral equation technique.[1–4] Most of them are based upon Hallén's original integral equation for a thin antenna and his iteration method of solving it. Because of an approximation to the kernel of the integral equation, the result obtained has often been criticized. In the case of a transmitting antenna it is known, however, that the numerical results for the input impedance of the antenna, based upon various iteration procedures, are acceptable provided that the proper order of solution is used. The evidence is partly supported by Schelkunoff's theory of cylindrical antennas,[5] which is based upon an entirely different method, yet his result can also be obtained by a so-called $\mu\Omega$ expansion as shown by Hallén.[6]

The purpose of this paper is to examine the problem again, starting with the exact integral equation for a cylindrical shell. By means of a variational method, the integral equation can be solved approximately. No attempt is made to simplify the exact kernel of the integral equation. The exact kernel is retained in the entire analysis. Approximations are introduced only in evaluating certain definite integrals. These approximations are valid when the length of the antenna is large compared to its radius. Under this condition it is found that the expression for the input impedance of the antenna is the same as if one had used the approximate integration equation at the very beginning of the analysis. The finding demonstrates the fact that as far as the final result is concerned the use of the approximate integral equation is justified even though the equation itself may not have the unique meaning of a properly behaved integral equation. The new procedure also indicates the feasibility of treating problems involving relatively thick antennas. There seems, however, no simple way of handling some definite integrals except by numerical integration.

The Exact Integral Equation for a Cylindrical Shell and Its Approximate Form

It is known from the literature[7,8] that the boundary value problem of a perfectly conducting cylindrical shell as a center-driven antenna can be formulated exactly in terms of an integral equation containing the current distribution function $I(z)$ as the unknown function.

$$E^i(z) = \frac{j\omega\mu}{4\pi}\int_{-l}^{l} I(z')\left[1 + \frac{1}{k^2}\frac{\partial^2}{\partial z^2}\right]G(z - z', a)dz', \quad (1)$$

where $E^i(z)$ denotes the impressed field applied at the center of the antenna and distributed uniformly around the cylindrical shell, and

$$G(z - z', a) = \frac{1}{2\pi}\int_0^{2\pi}\frac{e^{-jkr}}{r}d\phi, \quad (2)$$

where

$$r = \sqrt{(z - z')^2 + \left(2a\sin\frac{\phi}{2}\right)^2}$$

l = half-length of the antenna
a = radius of the antenna
$k = 2\pi/\lambda$.

Hallén's integral equation is obtained by replacing the exact expression for $G(z-z', a)$ by an approximate expression

$$G_h(z - z', a) = \frac{e^{-jkr_a}}{r_a}, \quad (3)$$

where

$$r_a = \sqrt{(z - z')^2 + a^2}.$$

* Original manuscript received by PGAP, November 5, 1954. The work herein has been supported by Air Force Contract AF 19(604)-266. This paper was presented at the 1954 IRE West Coast Convention.

† Dept. Elec. Engrg., Ohio State Univ., Columbus, Ohio; formerly with Stanford Res. Inst., Stanford, Calif.

[1] E. Hallén, "Theoretical investigations into the transmitting and receiving qualities of antennae," *Nova Acta Upsal.*, no. 4, p. 11; 1938.

[2] M. C. Gray, "A modification of Hallén's solution of the antenna problem," *Jour. Appl. Phys.*, vol. 15, p. 61; 1944.

[3] R. King and D. Middleton, "The cylindrical antenna; current and impedance," *Quar. Appl. Math.*, vol. 3, p. 302; 1946.

[4] S. A. Schelkunoff, "Advanced Antenna Theory," John Wiley & Sons, Inc., New York, N. Y., ch. 5; 1952.

[5] Schelkunoff, *ibid.*, ch. 1.

[6] E. Hallén, "Admittance Diagrams for Antennas and the Relation between Antenna Theories," Cruft Lab., Harvard Univ., Cambridge, Mass., Tech. Rep. No. 46; 1948.

[7] E. Hallén, "Properties of long antennas," *Jour. Appl. Phys.*, vol. 19, p. 1141; 1948.

[8] Schelkunoff, *op. cit.*, ch. 4.

Eq. (1) is then reduced to

$$E^i(z) = \frac{j\omega\mu}{4\pi}\int_{-l}^{l} I(z')\left(1+\frac{1}{k^2}\frac{\partial^2}{\partial z^2}\right)G_h(z-z', a)dz'. \quad (4)$$

This approximation creates certain questions regarding the true significance of this mathematical step and its consequence. These questions have been raised and discussed by both Schelkunoff[9] and Whinnery.[10] In this investigation, we avoid this ambiguous step by considering (1) as the basic equation.

Variational Solution and the Evaluation of Integrals

To analyze (1) let us first define a normalized function $f(z)$ such that

$$\text{and} \qquad \left.\begin{aligned} E^i(z) &= Vf(z) \\ \int_{-l}^{l} f(z)dz &= 1 \end{aligned}\right\}, \quad (5)$$

where V, by definition, denotes the applied voltage to the antenna. A parametric equation can then be obtained by multiplying (1) by $I(z)$ and integrating with respect to z from $-l$ to l. Dividing the resultant equation by $[\int_{-l}^{l} f(z)I(z)dz]^2$ one obtains

$$\frac{V}{\int_{-l}^{l} f(z)I(z)dz} = \frac{j\eta}{4\pi}\cdot\frac{\int_{-l}^{l}\int_{-l}^{l} I(z)I(z')K(z-z')dzdz'}{\left[\int_{-l}^{l} f(z)I(z)dz\right]^2} \quad (6)$$

where

$$K(z-z') = k\left(1+\frac{1}{k^2}\frac{\partial^2}{\partial z^2}\right)G(z-z', a)$$

$$\eta = (\mu/\epsilon)^{1/2} = 120\pi \text{ ohms.}$$

Denoting the quantity at the left side of (6) by Z_i, which corresponds to the input impedance of the antenna, it can be shown that the value of Z_i evaluated using the right member of (6) is stationary with respect to a small variation of $I(z)$ when the latter satisfies (1). This variational method of determining the impedance of a cylindrical antenna was first applied by Storer[11] to (4). The method is quite distinct from both Hallén's and Schelkunoff's methods yet it is simple and attractive. In calculating Z_i, using the variational formula, one major problem is the proper choice of trial function for $I(z)$. The functions which have been found adequate to use are so far limited to

$$I(z) = \sin k(l-|z|) + A_s[1-\cos k(l-|z|)] \quad (7)$$

and

$$I(z) = \sin k(l-|z|) + A_t k(l-|z|)\cos k(l-|z|). \quad (8)$$

The constant A_s or A_t is determined according to the extreme property of Z_i such that

$$\frac{\partial Z_i}{\partial A_s} = 0 \quad \text{or} \quad \frac{\partial Z_i}{\partial A_t} = 0.$$

The first trial function was due to Storer, and the latter was suggested by this writer.[12]

The advantage of using (8) is that the impedance function will be finite for all values of l while Storer's function is only good for $l<\lambda$. In the present work, we can use the same functions as the trial functions. To perform the integration, it is convenient to change a variable and write

$$G(z-z', a) = \frac{2}{\pi}\int_0^{2a} \frac{e^{-jk\sqrt{(z-z')^2+\xi^2}}}{\sqrt{(z-z')^2+\xi^2}} \cdot \frac{d\xi}{\sqrt{(2a)^2-\xi^2}}. \quad (9)$$

In the case of a δ-gap, (6) reduces to

$$Z_i = \frac{j\eta}{4\pi I^2(0)}\int_0^{2a}\frac{2d\xi}{\pi\sqrt{(2a)^2-\xi^2}} \cdot \int_{-l}^{l}\int_{-l}^{l} I(z)I(z')K_h(z-z')dzdz', \quad (10)$$

where

$$K_h(z-z') = k\left(1+\frac{1}{k^2}\frac{\partial^2}{\partial z^2}\right)G_h(z-z', \xi)$$

and

$$G_h(z-z', \xi) = \frac{e^{-jk\sqrt{(z-z')^2+\xi^2}}}{\sqrt{(z-z')^2+\xi^2}}.$$

It has been shown[11,12] that when $l \gg \xi (\xi \leqq 2a)$ the double integral with respect to z and z' using the functions described by (7) or (8) can readily be evaluated. Thus, if (8) is used as the trial function, one finds that

$$j\int_{-l}^{l}\int_{-l}^{l} I(z)I(z')K_h(z-z')dzdz' = \gamma_{11}(\xi) + 2\gamma_{12}(\xi)A_t + \gamma_{22}(\xi)A_t^2. \quad (11)$$

The coefficients $\gamma_{11}(\xi)$, $\gamma_{12}(\xi)$, and $\gamma_{22}(\xi)$ consist of a *linear* function of Ω_ξ and some terms independent of ξ, for example,

[9] S. A. Schelkunoff, "Concerning Hallén's integral equation for cylindrical antennas," Proc. IRE, vol. 33, pp. 872–878; December, 1945.

[10] J. R. Whinnery, "The Integral Equation Solution of the Antenna Problem," U. S. Navy Elec. Res., Univ. of California, Berkeley, Calif., Rep. No. 128; 1947.

[11] J. Storer, "Variational Solution to the Problem of the Symmetrical Cylindrical Antenna," Cruft Lab., Harvard Univ., Tech. Rep. No. 101; 1950.

[12] C. T. Tai, "A Variational Solution to the Problem of Cylindrical Antennas," Aircraft Radiation Systems Lab., Stanford Res. Inst., Stanford, Calif., Tech. Rep. No. 12; 1950.

$$\gamma_{11}(\xi) = 2L2x + e^{2jx}(\ln 2 - \tfrac{1}{2}\Omega_\xi - L4x + 2L2x) + e^{-2jx}(-\ln 2 + \tfrac{1}{2}\Omega_\xi), \tag{12}$$

where

$$Lx = \int_0^x \frac{1 - e^{-ju}}{u}\,du = \overline{C}ix + Six$$

$$x = kl, \qquad \Omega_\xi = 2 \ln \frac{2l}{\xi}.$$

Substituting (11) into (10) and performing the integration with respect to ξ, one notices that

$$\frac{2}{\pi}\int_0^{2a} \frac{d\xi}{\sqrt{(2a)^2 - \xi^2}} = 1$$

and

$$\frac{2}{\pi}\int_0^{2a} \frac{\Omega_\xi d\xi}{\sqrt{(2a)^2 - \xi^2}} = \Omega = 2 \ln \frac{2l}{a},$$

hence,

$$Z_i = \frac{\eta}{4\pi} \frac{[\gamma_{11} + 2\gamma_{12}A_i + \gamma_{22}A_i^2]}{[\sin x + A_i x \cos x]^2}, \tag{13}$$

where γ_{11}, γ_{12}, and γ_{22} are obtained by substituting Ω for Ω_ξ in $\gamma_{11}(\xi)$, $\gamma_{12}(\xi)$, and $\gamma_{22}(\xi)$. The interesting result of the present analysis is that (13) is the same as the expression previously derived using (4) as the basic equation. The fact that (13) can be derived using this alternative but more logical approach should remove the ambiguity that has often been attached to the approximation in deriving (4). As far as the final result for the input impedance is concerned the variational solution based upon (4) is therefore a good approximate solution of the exact integral equation defined by (1).

One further advantage of the present manipulation lies in the problem of thick antennas. If the condition specifying the characteristics of a thin antenna $l \gg a$ is not satisfied, (4) can not be used. On the other hand, (10) is still valid. The double integration with respect to z and z' can be expressed in terms of generalized sine and cosine integrals. The remaining integration with respect to ξ, however, can not be evaluated in a closed form although it seems feasible to do it numerically. Until some numerical values are compiled, we will not give any detailed discussion.

The Radiation Field Produced by a Slot in a Large Circular Cylinder*

L. L. BAILIN†

Summary—General results obtained previously by Silver and Saunders for slots of arbitrary shape are applied to the cases of narrow-width half-wavelength slots oriented transverse and parallel to the axis of infinite cylinders with fairly large radii. Sufficient theoretical data are given to describe accurately the major portion of the three-dimensional pattern of both the principal and cross-polarized components of the radiation fields of these slots. Perfectly conducting cylinders of circumferences of 8 and 12 wavelengths are considered.

Introduction

THE BASIC problem of communicating to and from high-speed aircraft has stimulated research work into the theory and application of slotted-cylinder antennas,[1] both in this country and abroad. It will be the purpose of this paper to aid this work by accurately describing the element factor of a slot which can be used in the design of such practical antennas.

In a recent paper,[2] Silver and Saunders have developed general expressions for the external field produced by a slot of arbitrary shape in the wall of an infinite circular cylinder, on the assumption that the tangential electric field in the slot is a prescribed function. The present paper deals with the application of these results to the cases of the slots oriented transverse and parallel to the axis of cylinders with fairly large radii. In each case, we will assume that the width of the slot is very much smaller than its length and that the excitation has a simple cosine distribution along its length and is uniform over its width. Such slots are easy to construct and excite; consequently, they are useful in application to microwave antenna design or as antenna pattern-range calibrating devices. Thus, we shall present the numerical data necessary to accurately describe the portion of the three-dimensional pattern which is of major interest of both the principal and cross-polarized components of the radiation fields of these slots.

The results given in this paper are restricted to the far-zone field of various slots which are a half-wavelength long. The far-zone field expressions are given in terms of an infinite series of terms involving the reciprocal of integral order Hankel functions or their derivations where the arguments are functions of ka; where $k=2\pi/\lambda$ and a is the radius of the cylinder. This series converges rapidly for small values of ka. However, as the cylinder becomes larger, the series representation for the far field converges more slowly and a greater number of terms are required to approximate the sum of the infinite series to a given accuracy. It can be shown that it takes about two ka terms to obtain three-significant-figure accuracy in the field components where ka is the circumference of the cylinder in wavelength. Since tabulated values for Hankel functions of large argument and order are unavailable and difficult to compute, the calculations presented here were restricted to cylinders with circumferences of 8 and 12 wavelengths. Thus only slight extensions of presently available tables of the Hankel functions[3] for these arguments were necessary. Computations were made for azimuthal angle, ϕ, for 0 (5 degrees) 160 degrees (2 degrees, 3 degrees) 180 degrees and for the polar angle, θ, in the range from 30 degrees to 90 degrees. In θ, rational values of sin θ which are approximately 5 degrees apart were chosen for convenience.

Relevant Formulas

The slot configuration and the various co-ordinates to be used are shown in Fig. 1 (opposite page). The slot is bounded axially by the planes $z=\pm l/2$ and in azimuth by planes $\phi=\pm\phi_0$ or in the notation used in reference 2, we have for the boundaries of the slot,

$$z_1=-l/2,\quad z_2=+l/2;\quad \phi_1(z)=-\phi_0,\quad \phi_2(z)=+\phi_0.$$

We shall assume that a narrow half-wavelength circumferential slot is defined by $\phi_0=\pi/2ka$ and $l\to 0$, and that the corresponding axial slot is given by $l=\pi/k$ and $\phi_0\to 0$. For the field distribution in the slot, we shall proceed as did Silver and Saunders[4] in a supplementary paper and assume that the field components in the slot are separable functions of ϕ and z. Thus

* Original manuscript received by the PGAP, April 22, 1954; revised manuscript received February 18, 1955. Work reported here was performed at Hughes Aircraft Co., sponsored by Air Force Cambridge Res. Lab., Cambridge, Mass., under Contract AF 19(604)-262, and was described in Hughes Aircraft Co. Tech. Mem. No. 309.

† Microwave Lab., Res. and Dev. Labs., Hughes Aircraft Co., Culver City, Calif.

[1] G. Sinclair, E. C. Jordan, and E. W. Vaughan, "Measurement of aircraft-antenna patterns using models," PROC. IRE, vol. 35, pp. 1451–52; December, 1947.
G. Sinclair, "The patterns of slotted-cylinder antennas," PROC. IRE, vol. 36, pp. 1487–92; December, 1946.
J. A. Stratton, "Electromagnetic Theory," McGraw-Hill Book Co., Inc., New York, N. Y. Chap. VI; 1941.
G. Sinclair, "The patterns of antennas located near cylinders of elliptical cross section," PROC. IRE, vol. 39, p. 660; June, 1951.
A. Alford, "Long slot antennas," *Proc. Nat. Elect. Conf.*, vol. 2, p. 143; 1946.
A. S. Pistolkors, "Radiation from transverse slit on the surface of a circular cylinder," *Jour. Tech. Phys. of USSR*, vol. 17, p. 377; 1947. (In Russian.)
C. H. Papas, "Radiation from transverse slot in an infinite cylinder," *Jour. Math. Phys.*, vol. 28, p. 227; January, 1950.
R. M. Sprague and A. Alford, "A four slot cylindrical antenna for VOR service," *IRE Convention Record*, Part I, pp. 12–24; 1954.

[2] S. Silver and W. K. Saunders, "External field produced by a slot in an infinite circular cylinder," *Jour. Appl. Phys.*, vol. 21, pp. 153–158; February, 1950.

[3] U. S. National Bureau of Standards Computation Laboratory Tables of $Y_n(x)$ and Harvard University Laboratory Tables of $Jn(x)$.

[4] S. Silver and W. K. Saunders, "The radiation from a transverse rectangular slot in a circular cylinder," *Jour. Appl. Phys.*, vol. 21, pp. 745–749; August, 1950.

$$E_\phi(a, \phi, z) = f_1(\phi, z) = F_1(\phi)G_1(z)$$
$$E_z(a, \phi, z) = f_2(\phi, z) = F_2(\phi)G_2(z). \quad (1)$$

For the half-wavelength circumferential slot, we shall take the excitation element to be a single mode of E_z. Thus

$$F_1 = G_1 = 0,$$

and

$$F_2(\phi) = \cos\frac{\pi\phi}{2\phi_0} \quad \text{and} \quad G_2(z) = \frac{V_0}{l}, \quad (2)$$

where V_0 is the voltage across the center of the slot and where l is considered small. Similarly, for the half-wavelength axial slot, the excitation element is a single mode of E_ϕ where

$$F_2 = G_2 = 0$$

and

$$F_1(\phi) = \frac{V_0}{2a\phi_0} \quad \text{and} \quad G_1(z) = \cos\frac{\pi z}{l} \quad (3)$$

and ϕ_0 is considered small.

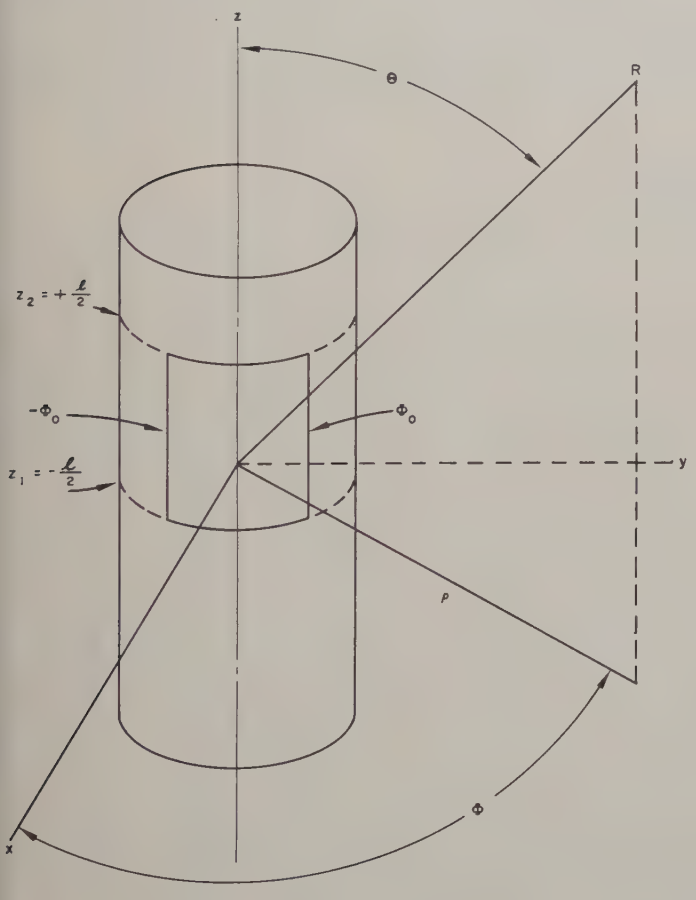

Fig. 1

The general expressions for the far-zone field with the harmonic time dependence exp $[j\omega t]$ suppressed are given in (23) of reference 2 as

$$E_\theta = -jA\sum_{n=-\infty}^{\infty}\left[\frac{C_n}{\sin\theta}\int_{-l/2}^{l/2} G_2(\xi)e^{jk\xi\cos\theta}d\xi \cdot \int_{-\phi_0}^{\phi_0} F_2(\beta)e^{jn\beta}d\beta\right], \quad (4)$$

and

$$E_\phi = A\sum_{n=-\infty}^{\infty}\left[D_n\left(\int_{-l/2}^{l/2} G_1(\xi)e^{jk\xi\cos\theta}d\xi \int_{-\phi_0}^{\phi_0} F_1(\beta)e^{jn\beta}d\beta + \frac{n\cot\theta}{ka\sin\theta}\int_{-l/2}^{l/2} G_2(\xi)e^{jk\xi\cos\theta}d\xi \cdot \int_{-\phi_0}^{\phi_0} F_2(\beta)e^{jn\beta}d\beta\right)\right] \quad (5)$$

where

$$C_n = \frac{j^n e^{-jn\phi}}{H_n^{(2)}(ka\sin\theta)}; \qquad D_n = \frac{j^n e^{-jn\phi}}{H_n^{(2)\prime}(ka\sin\theta)},$$

and

$$A = \frac{1}{2\pi^2}\frac{e^{-jkR}}{R}.$$

For the special cases considered in this paper, (4) and (5) can be simplified considerably as shown in the next section.

Description of Computations

Case I—Narrow Circumferential Slot

$\phi_0 = \pi/2ka$, $l \to 0$. If we insert (2) into (4) and (5) and combine terms of positive and negative n, we have

$$E_\theta = -jAV_0 2ka\left(\frac{1}{\sin\theta}\right)\sum_{n=\infty}^{\infty}\frac{\epsilon_n j^n\cos(n\phi)}{H_n^{(2)}(ka\sin\theta)} \cdot \left[\frac{\cos\left(\frac{n\pi}{2ka}\right)}{(ka)^2 - n^2}\right] \text{ and} \quad (6)$$

$$E_\phi = -jAV_0 2ka\left(\frac{\cot\theta}{ka\sin\theta}\right)\sum_{n=1}^{\infty}\frac{2nj^n\sin(n\phi)}{H_n^{(2)\prime}(ka\sin\theta)} \cdot \left[\frac{\cos\left(\frac{n\pi}{2ka}\right)}{(ka)^2 - n^2}\right], \quad (7)$$

where

$$\epsilon_n = 1 \quad n = 0$$
$$= 2 \quad n > 0.$$

Tables I(a), (b) (page 130) and II(a), (b) (page 131) give, respectively, the magnitude and phase of the principal component of the electric field computed from (6) and normalized to unity at $\phi = 0$ degree, $\theta = 90$ degrees for $ka = 8$ and 12. These tables list the normalized principal component in the form:

TABLE I(a)

CIRCUMFERENTIAL HALF-WAVELENGTH SLOT—Magnitude of E_θ; $ka=8$

$\phi°$ \ $\theta°$	30|0	35|1	39|6	45|4	49|7	55|6	59|6	64|2	69|6	74|3	80|9	90|0
0	1|019	1|014	1|010	1|007	1|005	1|004	1|003	1|002	1|001	1|001	1|000	1|000
5	1|015	1|010	1|006	1|003	1|001	999	998	997	996	995	995	995
10	1|004	998	994	990	987	985	983	982	981	980	979	979
15	985	978	973	968	965	962	960	958	956	955	954	953
20	960	952	946	939	935	931	928	925	922	921	919	918
25	928	918	911	903	898	892	888	885	881	879	876	875
30	891	879	871	861	854	847	842	838	833	830	827	826
35	849	835	825	813	806	796	791	785	780	776	773	771
40	802	787	775	762	753	742	736	729	723	719	714	712
45	752	735	722	707	697	685	678	671	664	659	654	651
50	700	681	667	651	640	627	619	611	603	598	592	590
55	647	626	611	593	582	568	559	551	543	537	531	529
60	592	571	555	536	524	509	501	492	483	478	472	469
65	538	516	499	480	468	453	444	435	426	421	415	412
70	485	463	446	426	414	399	390	381	372	367	361	358
75	434	411	394	375	362	348	339	330	322	316	311	308
80	385	363	345	326	314	300	292	284	276	270	265	263
85	339	317	300	282	270	257	249	241	234	229	224	222
90	296	275	259	241	230	217	210	203	196	192	187	185
95	257	236	221	204	194	183	176	169	163	159	155	153
100	221	201	187	172	163	152	146	140	134	130	127	125
105	188	170	157	143	135	125	120	114	109	106	103	102
110	160	143	131	119	111	102	097	093	088	086	083	082
115	135	119	108	097	090	083	079	075	071	068	066	065
120	113	099	089	079	073	067	063	060	056	054	052	051
125	093	082	073	064	059	053	050	047	044	043	041	040
130	076	066	059	052	047	042	039	037	035	033	032	031
135	063	053	047	041	038	033	031	029	027	026	025	024
140	052	043	037	032	029	026	025	023	021	020	019	019
145	044	036	030	025	023	020	019	017	016	016	015	015
150	036	030	025	020	018	015	014	013	012	011	011	011
155	028	024	021	017	015	013	011	010	009	009	008	008
160	020	017	015	013	012	010	010	009	008	008	007	007
162	017	014	013	012	011	009	008	008	007	007	006	006
165	014	011	009	008	008	007	007	006	006	006	005	005
168	013	009	007	006	005	005	004	004	004	004	004	004
170	014	010	007	005	005	004	003	003	003	003	003	003
172	015	011	008	006	005	004	003	003	003	002	002	002
175	017	013	010	008	006	005	005	004	004	003	003	003
178	018	014	011	009	008	006	006	005	005	004	004	004
180	019	014	012	009	008	007	006	005	005	005	004	004

TABLE I(b)

CIRCUMFERENTIAL HALF-WAVELENGTH SLOT—Phase of E_θ; $ka=8$

$\phi°$ \ $\theta°$	30|0	35|1	39|6	45|4	49|7	55|6	59|6	64|2	69|6	74|3	80|9	90|0
0	231|2–	196|3–	167|2–	132|5–	109|4–	80|6–	63|3–	46|0–	28|7–	17|2–	5|7–	0|0
5	232|2–	197|3–	168|4–	133|8–	110|8–	82|0–	64|8–	47|6–	30|4–	18|9–	7|4–	1|7–
10	234|9–	200|4–	171|8–	137|6–	114|8–	86|3–	69|3–	52|3–	35|2–	23|9–	12|6–	6|9–
15	239|3–	205|5–	177|4–	143|8–	121|5–	93|5–	76|8–	60|1–	43|4–	32|3–	21|1–	15|6–
20	245|6–	212|6–	185|2–	152|5–	130|7–	103|5–	87|3–	71|0–	54|7–	43|9–	33|0–	27|6–
25	253|5–	221|7–	195|3–	163|6–	142|6–	116|3-	100|6–	84|9–	69|1–	58|7–	48|2–	42|9–
30	263|2–	232|7–	207|3–	177|0–	156|9–	131|7–	116|7–	101|6–	86|5–	76|5–	66|5–	61|5–
35	274|4–	245|5–	221|4–	192|7–	173|5–	149|7–	135|4–	121|1–	106|9–	97|3–	87|8–	83|1–
40	287|3–	260|1–	237|5–	210|5–	192|6–	170|2–	156|8–	143|4–	129|9–	121|0–	112|1–	107|7–
45	301|6–	276|3–	255|4–	230|4–	213|7–	193|0–	180|5–	168|1–	155|7–	147|4–	139|1–	135|0–
50	317|4–	294|3–	275|1–	252|2–	237|0–	218|0–	206|6–	195|3–	183|9–	176|3–	168|7–	165|0–
55	334|4–	313|6–	296|4–	275|8–	262|1–	245|1–	234|9–	224|7–	214|4–	207|6–	200|8–	197|4–
60	352|8–	334|5–	319|3–	301|1–	289|1–	274|1–	265|1–	256|1–	247|1–	241|1–	235|1–	232|2–
65	372|4–	356|6–	343|6–	328|1–	317|8–	304|9–	297|2–	289|5–	281|8–	276|6–	271|5–	268|9–
70	392|9–	380|0–	369|3–	356|4–	348|0–	337|3–	330|9–	324|6–	318|3–	314|0–	309|8–	307|7–
75	414|6–	404|5–	396|1–	386|1–	379|5–	371|2–	366|3–	361|3–	356|4–	353|1–	349|8–	348|1–
80	437|1–	429|9–	424|0–	417|0–	412|3–	406|5–	403|0–	399|5–	396|0–	393|6–	391|3–	390|1–
85	460|4–	456|4–	452|9–	448|9–	446|2–	442|9–	440|9–	438|9–	436|9–	435|5–	434|2–	433|5–
90	484|5–	483|5–	482|8–	481|8–	481|2–	480|4–	479|9–	479|4–	478|9–	478|6–	478|2–	478|1–
95	509|2–	511|4–	513|3–	515|5–	517|0–	518|8–	519|8–	520|9–	522|0–	522|7–	523|3–	523|7–
100	534|6–	540|0–	544|5–	550|0–	553|5–	557|9–	560|6–	563|2–	565|9–	567|6–	569|4–	570|2–
105	560|5–	569|1–	576|3–	585|0–	590|7–	597|8–	602|0–	605|2–	610|4–	613|2–	616|0–	617|4–
110	586|7–	598|7–	608|6–	620|5–	628|4–	638|3–	644|1–	649|9–	655|6–	659|5–	663|4–	665|3–
115	613|2–	628|7–	641|4–	656|4–	666|5–	679|1–	686|6–	694|0–	701|4–	706|3–	711|2–	713|7–
120	639|8–	658|9–	674|5–	692|9–	705|0–	720|2–	729|3–	738|5–	747|5–	753|6–	759|6–	762|6–
125	666|8–	689|1–	707|7–	729|7–	744|0–	761|8–	772|4–	783|1–	793|8–	800|9–	808|0–	811|5–
130	694|4–	719|5–	740|8–	766|3–	783|2–	803|9-	816|1–	828|2–	840|4–	848|4–	856|6–	860|6–
135	722|7–	750|6–	774|1–	802|7–	821|9–	845|7–	859|8–	873|8–	887|6–	896|7–	905|8–	910|4–
140	751|2–	782|8–	808|5–	839|4–	860|3–	886|8–	902|7–	918|6–	934|4–	944|9–	955|3–	960|5–
145	778|3–	814|9–	844|1–	878|0–	900|3–	928|4–	945|4–	962|6–	979|9–	991|6–	1003|1–	1009|0–
150	803|0–	844|5–	878|2–	917|3–	942|4–	973|1–	991|2–	1009|2–	1027|2–	1039|3-	1051|4–	1057|6–
155	826|5–	870|9–	908|1–	952|3–	981|4-	1016|9	1037|7-	1058|3–	1078|4-	1091|7–	1104|8–	1111|3–
160	853|1–	897|4–	935|6–	982|3–	1013|7–	1053|0–	1076|5–	1099|9–	1123|1–	1138|5–	1153|9–	1161|5–
162	866|0–	910|7–	949|4–	995|0–	1024|9–	1063|0–	1087|2–	1112|6–	1138|8–	1156|2–	1173|3–	1164|9–
165	893|0–	935|2–	971|2–	1015|9–	1046|7–	1086|0–	1109|9–	1134|1–	1158|5–	1174|7–	1191|1–	1199|3–
168	922|6–	968|8–	1005|7–	1049|2–	1078|2–	1115|0–	1137|7–	1160|6–	1184|0–	1192|0-	1215|6–	1223|6–
170	939|5–	990|5–	1031|4–	1078|5–	1108|9–	1146|1–	1168|1–	1190|0–	1212|2–	1227|0–	1241|9–	1249|5–
172	952|3–	1007|0–	1052|5–	1104|1–	1138|2–	1179|9–	1204|4–	1228|5–	1252|1–	1267|7–	1283|1–	1290|8–
175	964|1–	1022|0–	1069|7–	1126|3–	1163|7–	1210|2–	1237|9–	1265|4–	1292|9–	1311|1–	1329|3–	1338|4–
178	969|7–	1028|7–	1077|3–	1135|3–	1173|7–	1221|6–	1250|0 ·	1278|4–	1306|8–	1325|7–	1344|6–	1354|0–
180	970|7–	1029|8–	1078|7–	1136|9–	1175|4–	1223|3–	1252|0–	1280|5–	1309|0–	1327|9–	1346|9–	1356|3–

TABLE II(a)

CIRCUMFERENTIAL HALF-WAVELENGTH SLOT—Magnitude of E_θ; $ka=12$

$\phi°$ \ $\theta°$	30|0	35|1	39|9	45|1	50|1	54|8	60|1	65|3	70|3	75|2	79|5	90|0
0	1|010	1|007	1|005	1|004	1|003	1|002	1|001	1|001	1|000	1|000	1|000	1|000
5	1|006	1|003	1|001	999	998	997	996	996	995	995	995	995
10	994	991	988	986	984	983	981	980	980	979	979	978
15	975	970	967	964	961	959	957	956	954	953	953	952
20	948	943	938	934	930	927	924	922	920	918	917	916
25	915	908	902	897	892	888	884	880	877	875	874	872
30	876	867	860	853	847	841	836	832	828	825	824	822
35	832	821	812	804	796	790	783	778	773	770	768	765
40	783	771	760	750	741	734	726	720	715	711	708	705
45	731	717	705	693	684	675	666	659	653	649	646	643
50	676	660	647	635	624	614	605	597	591	586	582	579
55	619	603	589	575	563	553	543	535	528	523	519	516
60	563	545	530	515	503	493	482	474	467	461	458	454
65	506	487	472	457	444	434	423	414	407	402	399	395
70	451	432	416	401	388	378	367	358	352	346	343	340
75	398	378	363	348	335	325	315	306	300	295	291	288
80	348	328	313	298	286	276	266	258	252	247	244	241
85	301	282	267	253	241	232	223	215	209	205	202	200
90	258	239	225	212	201	192	184	177	172	168	165	163
95	218	201	188	175	165	157	150	144	139	136	133	131
100	183	167	155	144	135	127	121	115	111	108	106	104
105	153	138	126	116	108	102	096	091	088	085	083	082
110	126	112	102	093	086	081	075	071	068	066	065	063
115	103	091	082	074	068	063	059	055	053	051	050	049
120	083	073	065	058	053	049	045	042	040	039	038	037
125	067	058	051	045	041	038	035	032	031	029	028	028
130	054	046	040	035	032	029	026	024	023	022	021	021
135	043	036	031	027	024	022	020	018	017	016	016	015
140	034	028	024	021	018	016	015	014	013	012	012	011
145	026	022	019	016	014	012	011	010	009	009	009	008
150	021	016	014	012	010	009	008	007	007	006	006	006
155	017	013	010	008	007	007	006	006	005	005	005	005
160	014	011	009	007	006	005	004	004	003	003	003	003
162	012	010	008	007	006	005	004	003	003	003	003	003
165	009	008	007	006	005	004	004	003	003	003	003	002
168	006	005	004	004	004	003	003	003	003	002	002	002
170	005	004	003	003	003	002	002	002	002	002	002	002
172	006	004	003	002	002	002	001	001	001	001	001	001
175	007	005	004	003	002	002	001	001	001	001	001	001
178	009	007	005	004	003	003	002	002	002	002	002	002
180	009	007	005	004	004	003	003	002	002	002	002	002

TABLE II(b)

CIRCUMFERENTIAL HALF-WAVELENGTH SLOT—Phase of E_θ; $ka=12$

$\phi°$ \ $\theta°$	30|0	35|1	39|9	45|1	50|1	54|8	60|1	65|3	70|3	75|2	79|5	90|0
0	345|3–	293|3–	247|2–	201|1–	160|8–	126|3–	91|8–	63|1–	40|2–	22|9–	11|5–	0|0
5	346|6–	294|8–	248|8–	202|9–	162|8–	128|5–	94|1–	65|5–	42|6–	25|4–	14|0–	2|6–
10	350|7–	299|4–	253|9–	208|6–	168|9–	134|9–	100|9–	72|7–	50|0–	33|1–	21|7–	10|4–
15	357|3–	307|0–	262|4–	217|8–	178|9–	145|5–	112|2–	84|5–	62|2–	45|6–	34|5–	23|4–
20	366|5–	317|5–	274|1–	230|7–	192|8–	160|4–	127|9–	100|9–	79|3–	63|1–	52|3–	41|5–
25	378|3–	331|0–	289|1–	247|2–	210|6–	179|2–	147|9–	121|8–	101|0–	85|3–	74|9–	64|5–
30	392|5–	347|3–	307|1–	267|1–	232|0–	202|0–	172|1–	147|1–	127|2–	112|2–	102|2–	92|2–
35	409|2–	366|2–	323|2–	290|2–	257|0–	228|7–	200|2–	176|6–	157|7–	143|5–	134|1–	124|6–
40	428|0–	387|8–	352|1–	316|6–	285|4–	258|9–	232|2–	210|1–	192|4–	179|1–	170|2–	161|4–
45	449|1–	411|8–	378|8–	345|9–	317|1–	292|4–	267|9–	247|3–	231|0–	218|7–	210|5–	202|3–
50	472|2–	438|2–	408|1–	378|0–	351|7–	329|3–	306|8–	288|1–	273|2–	262|0–	254|5–	247|1–
55	497|3–	466|7–	439|7–	412|8–	389|3–	369|1–	349|0–	332|3–	318|9–	308|8–	302|1–	295|4–
60	524|1–	497|3–	473|6–	450|0–	429|4–	411|7–	394|1–	379|4–	367|6–	358|8–	352|9–	347|1–
65	552|6–	529|8–	509|6–	489|4–	471|8–	456|8–	441|8–	429|3–	419|3–	411|8–	406|8–	401|8–
70	582|6–	563|9–	547|4–	530|9–	516|5–	504|2–	491|9–	481|7–	473|5–	467|4–	463|3–	459|2–
75	614|0–	599|6–	586|9–	574|2–	563|1–	553|7–	544|2–	536|3–	530|0–	525|3–	522|1–	519|0–
80	646|6–	636|7–	627|9–	619|1–	611|5–	604|9–	598|4–	593|0–	588|6–	585|3–	583|2–	581|0–
85	680|4–	675|0–	670|2–	665|5–	661|4–	657|8–	654|3–	651|3–	649|0–	647|2–	646|0–	644|8–
90	715|2–	714|4–	713|7–	713|1–	712|6–	712|1–	711|6–	711|2–	710|9–	710|6–	710|4–	710|2–
95	750|7–	754|8–	758|3–	761|8–	764|9–	767|5–	770|2–	772|4–	774|1–	775|3–	776|2–	777|0–
100	787|1–	795|8–	803|7–	811|4–	818|2–	824|0–	829|8–	834|5–	838|3–	841|2–	843|1–	844|9–
105	824|0–	837|7–	849|8–	861|8–	872|3–	881|2–	890|2–	897|6–	903|5–	907|9–	910|9–	913|8–
110	861|4–	880|0–	896|4–	912|8–	927|0–	939|1–	951|2–	961|3–	969|4–	975|3–	979|4–	983|4–
115	899|3–	922|9–	943|6–	964|2–	982|2–	997|6–	1012|9–	1025|6–	1035|7–	1043|4–	1048|5–	1053|6–
120	937|5–	965|9–	991|1–	1016|0–	1037|7–	1056|4–	1074|9–	1090|3–	1102|6–	1111|8–	1117|8–	1124|0–
125	976|2–	1009|2–	1038|7–	1068|2–	1093|7–	1115|4–	1137|1–	1155|3–	1169|7–	1180|5–	1187|7–	1194|9–
130	1014|9–	1053|0–	1086|6–	1120|3–	1149|8–	1174|9–	1199|7–	1220|3–	1236|8–	1249|2–	1257|5–	1265|7–
135	1053|1–	1097|0–	1135|0–	1172|6–	1205|6–	1234|0–	1262|4–	1285|8–	1304|5–	1318|3–	1327|6–	1336|8–
140	1091|3–	1140|0–	1183|4–	1225|7–	1262|1–	1293|2–	1324|5–	1350|6–	1371|6–	1387|3–	1397|8–	1408|1–
145	1131|0–	1182|9–	1230|1–	1277|8–	1319|1–	1353|7–	1387|9–	1416|1–	1438|7–	1455|8–	1467|1–	1478|5–
150	1172|5–	1228|7–	1278|0–	1328|3–	1373|2–	1412|0–	1450|7–	1482|6–	1507|7–	1526|4–	1538|7–	1551|0–
155	1210|5–	1275|4–	1330|4–	1383|6–	1429|6–	1469|5–	1510|0–	1544|3–	1572|1–	1593|0–	1607|0–	1621|0–
160	1242|3–	1314|1–	1377|4–	1439|3–	1491|9–	1535|7–	1578|6–	1613|5–	1641|4–	1662|3–	1676|1–	1690|2–
162	1254|5–	1326|7–	1392|6–	1457|4–	1513|2–	1560|1–	1606|1–	1643|5–	1673|0–	1694|9–	1709|4–	1723|9–
165	1275|5–	1347|7–	1413|7–	1480|5–	1539|1–	1589|3–	1639|2–	1680|4–	1713|3–	1737|8–	1754|2–	1770|3–
168	1307|4–	1375|5–	1438|6–	1504|4–	1562|6–	1613|6–	1664|7–	1707|5–	1741|8–	1767|5–	1784|7–	1801|8–
170	1337|8–	1405|8–	1465|9–	1527|7–	1583|7–	1632|9–	1682|9–	1725|4–	1759|3–	1781|9–	1802|3–	1819|5–
172	1366|1–	1442|6–	1506|6–	1568|5–	1621|8–	1667|7–	1714|2–	1753|5–	1785|6–	1809|9–	1826|3–	1843|0–
175	1390|9–	1475|7–	1550|0–	1623|6–	1687|1–	1741|2–	1794|5–	1838|6–	1873|3–	1899|4–	1916|7–	1934|0–
178	1400|7–	1487|7–	1562|1–	1641|1–	1707|5–	1764|3–	1821|0–	1868|1–	1905|5–	1933|4–	1951|8–	1970|4–
180	1402|3–	1489|7–	1566|9–	1643|6–	1710|3–	1767|4–	1824|4–	1871|6–	1909|1–	1937|2–	1955|6–	1974|1–

TABLE III(a)—Circumferential Half-Wavelength Slot, Magnitude of E_a; $ka=8$

$\phi°$ \ $\theta°$	30|0	35|1	39|6	45|4	49|7	55|6	59|6	64|2	69|6	74|3	80|9	90|0
0	000	000	000	000	000	000	000	000	000	000	000	000
5	068	069	062	059	053	048	043	036	029	023	013	000
10	136	137	124	118	106	094	085	072	057	045	026	000
15	204	201	184	173	157	138	125	107	085	067	039	000
20	269	262	243	225	207	180	162	140	111	087	050	000
25	333	318	300	273	253	219	197	170	136	105	061	000
30	392	369	352	317	295	256	228	197	158	122	071	000
35	446	415	397	357	330	289	256	220	176	137	079	000
40	493	458	436	394	361	317	281	240	192	149	087	000
45	531	497	466	426	387	339	303	258	204	159	092	000
50	560	531	491	452	410	355	318	272	214	166	096	000
55	580	559	512	469	429	366	327	282	223	172	099	000
60	595	577	530	477	441	376	332	285	227	176	101	000
65	607	582	544	479	443	382	336	285	226	176	102	000
70	618	578	549	480	438	382	337	284	223	173	100	000
75	627	568	543	481	431	373	333	282	220	169	097	000
80	628	559	524	477	425	359	321	275	216	166	094	000
85	617	554	502	461	418	347	305	261	207	160	092	000
90	590	547	484	434	401	338	292	245	193	150	087	000
95	552	531	473	404	373	323	282	235	181	139	080	000
100	511	499	460	384	342	298	266	224	173	131	074	000
105	480	453	434	372	321	268	239	206	163	125	071	000
110	465	407	391	355	311	248	214	182	145	113	065	000
115	458	377	343	321	293	239	202	165	127	098	056	000
120	447	368	310	275	258	224	195	159	119	089	050	000
125	417	364	301	240	216	192	174	148	115	087	048	000
130	364	346	301	232	193	158	141	123	099	078	045	000
135	296	301	284	235	195	146	121	099	078	061	036	000
140	237	238	239	220	194	153	126	099	071	053	029	000
145	216	181	177	175	167	145	126	103	077	057	031	000
150	240	172	137	120	116	109	101	088	070	054	031	000
155	272	205	155	108	086	069	062	055	046	037	022	000
160	282	233	191	142	112	079	062	047	033	024	013	000
162	276	235	199	155	126	093	074	056	039	028	037	000
164	265	231	201	162	136	104	085	067	082	035	046	000
165	257	227	199	163	139	108	090	071	052	038	021	000
166	248	221	196	163	140	111	152	074	094	041	055	000
168	224	204	184	157	234	111	155	078	101	044	024	000
170	196	181	165	144	128	106	091	076	058	044	025	000
172	163	152	141	124	112	094	082	069	053	041	023	000
174	126	118	110	099	089	076	067	056	044	034	019	000
175	106	100	094	084	076	065	058	049	038	029	017	000
176	086	081	076	068	062	053	047	040	031	024	014	000
178	043	041	039	035	032	028	024	021	016	013	007	000
180	000	000	000	000	000	000	000	000	000	000	000	000

TABLE III(b)—Circumferential Half-Wavelength Slot, Phase of E_ϕ; $ka=8$

$\phi°$ \ $\theta°$	30|0	35|1	39|6	45|4	49|7	55|6	59|6	64|2	69|6	74|3	80|9	90|0
0	44|1–	8|7–	18|5	53|1	74|7	104|7	120|1	137|1	155|4	166|6	177|0	182|3
5	45|0–	9|6–	17|4	51|9	73|3	103|3	118|7	135|5	153|7	164|9	175|4	180|7
10	47|6–	12|5–	14|0	48|4	69|5	99|0	114|5	131|0	148|7	159|9	170|5	175|7
15	51|9–	17|2–	8|6	42|5	63|2	91|8	107|5	123|5	140|4	151|5	162|3	167|5
20	57|8–	23|9–	1|1	34|1	54|5	81|8	97|6	113|2	129|1	139|9	150|6	155|9
25	65|1–	32|5–	8|2–	23|4	43|4	69|0	84|7	99|9	115|1	125|2	135|7	140|9
30	73|9–	43|2–	19|4–	10|3	30|0	53|9	68|9	83|9	98|2	107|8	117|6	122|7
35	84|1–	55|7–	32|4–	5|1–	14|1	36|6	50|5	64|9	78|7	87|7	96|8	101|5
40	95|6–	70|0–	47|4–	22|3–	4|2–	17|1	29|9	43|1	56|4	65|0	73|5	77|8
45	108|5–	85|7–	64|3–	41|3–	24|8–	4|4–	7|2	19|1	31|3	39|5	47|6	51|5
50	123|0–	102|6–	83|2–	61|6–	47|3–	28|4–	17|4–	6|9–	3|9	11|4	19|0	22|7
55	139|0–	120|4–	103|8–	83|5–	71|2–	54|5–	44|3–	34|7–	25|3–	18|9–	12|1–	8|7–
60	156|5–	139|2–	125|7–	107|3–	96|2–	82|4–	73|4–	64|5–	56|2–	50|7–	45|1–	42|3–
65	175|3–	159|3–	148|3–	132|9–	122|8–	111|6–	104|3–	96|5–	88|9–	84|1–	79|5–	77|2–
70	194|9–	180|8–	171|5–	160|1–	151|1–	141|5–	136|1–	130|2–	123|8–	119|5–	115|5–	113|6–
75	214|7–	203|9–	195|7–	188|0–	181|3–	172|9–	168|7–	164|7–	160|3–	157|0–	153|6–	151|9–
80	234|5–	228|2–	221|1–	216|1–	212|4–	206|1–	202|5–	199|7–	197|2–	195|4–	193|3–	192|1–
85	254|5–	253|0–	248|3–	244|5–	243|5–	240|8–	238|3–	236|1–	234|6–	233|8–	233|1–	232|8–
90	275|0–	277|5–	276|7–	274|2–	274|5–	275|7–	275|4–	274|5–	273|5–	273|2–	273|2–	273|3–
95	296|8–	301|3–	305|2–	305|9–	306|5–	309|8–	312|1–	313|8–	314|6–	314|8–	315|1–	315|3–
100	320|3–	325|3–	332|6–	338|8–	340|7–	344|4–	347|9–	351|9–	355|5–	357|4–	359|0–	359|6–
105	345|6–	350|5–	359|1–	370|9–	376|4–	381|4–	384|8–	389|3–	394|7–	398|4–	401|9–	403|7–
110	370|9–	378|2–	386|2–	401|0–	410|8–	420|4–	424|8–	429|2–	434|4–	438|5–	443|0–	445|3–
115	394|5–	408|0–	416|1–	430|4–	442|5–	457|7–	465|5–	472|1–	477|8–	481|7–	485|8–	488|0–
120	415|7–	436|9–	449|1–	462|3–	473|9–	491|5–	502|5–	513|0–	522|4–	528|0–	533|0–	535|4–
125	435|0–	462|4–	481|8–	499|0–	509|3–	525|3–	536|7–	549|2–	561|8–	570|1–	578|0–	581|8–
130	454|4–	484|4–	509|7–	536|1–	550|0–	565|1–	574|7–	585|9–	598|4–	607|4–	616|7–	621|5–
135	476|5–	505|4–	533|1–	566|8–	587|5–	609|7–	620|9–	631|2–	641|7–	649|1–	657|2–	661|5–
140	505|7–	529|4–	555|6–	591|6–	616|4–	646|5–	663|5–	679|2–	693|3–	701|9–	710|0–	713|9–
145	541|5–	563|3–	583|9–	616|3–	641|1–	674|0–	694|0–	714|0–	733|6–	746|3–	758|7–	764|7–
150	572|2–	605|8–	627|5–	652|1–	671|9–	701|3–	720|8–	741|2–	762|2–	776|4–	790|7–	797|8–
155	592|0–	637|1–	671|5–	707|0–	726|6–	748|7–	762|7–	778|4–	795|8–	808|3–	821|4–	828|1–
160	604|2–	654|6–	695|8–	743|9–	774|6–	811|1–	831|3–	850|2–	867|4–	877|9–	888|0–	892|8–
162	607|7–	659|3–	701|8–	752|2–	785|1–	825|3–	848|7–	871|4–	893|2–	907|1–	920|5–	926|9–
164	610|6–	663|0–	706|5–	758|3–	792|5–	834|9–	859|9–	884|7–	909|1–	925|2–	941|0–	948|8–
165	611|9–	664|6–	708|4–	760|8–	795|4–	838|5–	864|0–	889|5–	914|7–	931|3–	947|8–	956|0–
166	613|0–	666|1–	710|2–	763|0–	797|9–	841|5–	867|5–	893|4–	919|1–	936|2–	953|1–	961|6–
168	615|0–	668|6–	713|0–	766|5–	802|0–	846|3–	872|8–	899|3–	925|7–	943|3–	960|7–	969|5–
170	616|6–	670|5–	715|3–	769|2–	805|1–	849|9–	876|7–	903|4–	930|3–	948|1–	965|9–	974|8–
172	617|9–	672|1–	717|1–	771|3–	807|4–	852|4–	879|4–	906|5–	933|5–	951|5–	969|4–	978|4–
174	618|9–	673|2–	718|4–	772|8–	809|0–	854|3–	881|4–	908|6–	935|7–	953|8–	971|9–	980|9–
175	619|3–	673|6–	719|0–	773|4–	809|6–	855|0–	882|2–	909|4–	936|6–	954|7–	972|8–	981|8–
176	619|5–	674|0–	719|4–	773|9–	810|2–	855|6–	882|8–	910|0–	937|2–	955|4–	973|5–	982|6–
178	619|9–	674|5–	719|9–	774|5–	810|9–	856|3–	883|6–	910|8–	938|1–	956|3–	974|4–	983|5–
180	620|1–	674|7–	720|1–	774|7–	811|1–	856|6–	883|8–	911|1–	938|3–	956|6–	974|7–	983|8–

TABLE IV(a)—Circumferential Half-Wavelength Slot, Magnitude of E_ϕ; $ka = 12$

ϕ° \ θ°	30|0	35|1	39|9	45|1	50|1	54|8	60|1	65|3	70|3	75|2	79|5	90|0
0	000	000	000	000	000	000	000	000	000	000	000	000
5	072	070	065	059	055	049	042	036	029	022	015	000
10	144	138	129	118	108	097	084	071	057	043	031	000
15	214	205	191	175	161	144	125	104	084	064	045	000
20	282	267	249	231	210	188	163	136	110	084	059	000
25	345	325	305	283	255	230	198	166	133	101	072	000
30	403	379	358	330	298	269	230	193	155	118	083	000
35	454	429	406	371	337	301	260	217	174	132	093	000
40	499	476	447	407	371	330	285	237	190	144	102	000
45	541	516	479	440	398	355	305	255	203	154	109	000
50	579	548	506	467	419	376	320	267	214	161	114	000
55	610	568	530	485	436	389	333	276	221	167	118	000
60	629	581	548	495	449	396	341	282	224	170	120	000
65	635	592	555	500	452	401	341	284	226	170	120	000
70	631	600	550	503	447	401	339	280	224	169	119	000
75	627	597	542	497	441	390	335	274	217	165	116	000
80	624	578	535	479	433	378	322	267	211	158	111	000
85	615	552	521	459	414	366	306	253	202	152	107	000
90	589	532	491	444	387	346	293	238	188	142	100	000
95	547	516	455	420	368	318	273	225	176	131	092	000
100	506	436	432	382	347	299	247	205	164	123	086	000
105	481	439	411	350	311	279	231	185	146	110	078	000
110	466	393	372	332	279	245	211	172	133	098	068	000
115	435	372	323	302	264	219	182	152	122	091	064	000
120	380	357	295	256	237	207	166	130	102	077	055	000
125	319	319	287	229	196	178	154	124	094	068	047	000
130	291	259	256	225	180	147	124	106	085	064	045	000
135	296	223	201	196	176	145	110	085	066	050	036	000
140	290	230	174	147	141	131	110	086	064	046	031	000
145	244	230	188	139	106	092	083	073	059	045	032	000
150	169	184	179	154	121	092	066	050	039	030	021	000
155	130	113	121	124	116	101	081	062	045	032	021	000
160	172	113	079	065	065	061	053	043	033	023	000	
162	191	135	093	063	049	045	043	039	033	026	019	000
164	205	155	114	079	054	039	030	025	021	017	013	000
165	208	163	125	089	063	045	031	023	018	014	010	000
166	209	169	133	099	073	053	036	025	018	012	008	000
168	204	173	144	115	090	070	052	037	026	018	012	000
170	189	167	145	121	100	082	064	048	036	026	017	000
172	165	149	136	115	099	083	067	053	041	030	020	000
174	132	122	111	099	086	075	062	050	039	029	020	000
175	113	105	096	086	076	066	056	045	035	026	018	000
176	092	086	080	072	064	056	047	039	030	023	016	000
178	047	045	042	038	034	030	025	021	017	012	009	000
180	000	000	000	000	000	000	000	000	000	000	000	000

TABLE IV(b)—Circumferential Half-Wavelength Slot, Phase of E_ϕ; $ka = 12$

ϕ° \ θ°	30|0	35|1	39|9	45|1	50|1	54|8	60|1	65|3	70|3	75|2	79|5	90|0
0	520|1-	468|5-	421|5-	376|3-	337|8-	302|3-	269|2-	239|9-	218|1-	200|7-	188|7-	179|5-
5	521|4-	469|9-	423|2-	378|2-	339|7-	304|5-	271|4-	242|3-	220|4-	203|1-	191|4-	182|0-
10	525|1-	474|1-	428|2-	383|9-	345|3-	310|9-	278|0-	249|5-	227|5-	210|6-	199|2-	189|5-
15	531|1-	481|1-	436|7-	393|2-	354|8-	321|7-	288|9-	261|4-	239|3-	222|9-	212|0-	201|7-
20	539|6-	491|0-	448|4-	405|9-	368|2-	336|4-	304|1-	277|7-	256|1-	240|1-	229|5-	218|5-
25	550|5-	504|0-	463|2-	421|9-	385|6-	355|0-	323|8-	298|2-	277|5-	262|0-	251|7-	239|7-
30	563|9-	519|8-	480|8-	441|0-	406|7-	377|1-	347|6-	322|9-	303|4-	288|5-	278|6-	265|5-
35	579|8-	538|4-	501|1-	463|5-	431|2-	403|0-	375|3-	351|8-	333|2-	319|4-	310|0-	296|5-
40	598|1-	559|3-	523|9-	489|3-	458|8-	432|6-	406|4-	384|7-	367|1-	354|1-	345|4-	333|1-
45	618|6-	582|2-	549|6-	517|8-	489|2-	465|4-	441|0-	421|1-	405|0-	392|8-	384|6-	375|3-
50	640|7-	607|0-	577|9-	548|7-	522|8-	501|0-	479|1-	460|5-	446|1-	435|2-	427|8-	422|6-
55	664|2-	634|0-	608|5-	581|8-	559|3-	539|3-	520|0-	503|4-	490|2-	480|6-	474|1-	472|2-
60	689|0-	663|4-	640|7-	617|4-	597|7-	580|4-	563|2-	549|2-	537|6-	528|8-	523|2-	521|4-
65	715|5-	694|5-	674|4-	655|5-	638|0-	624|0-	609|0-	597|0-	587|5-	580|2-	575|2-	570|5-
70	743|9-	726|7-	710|1-	694|9-	680|6-	668|9-	657|4-	647|1-	639|3-	633|6-	629|7-	621|8-
75	773|8-	759|5-	747|9-	735|3-	725|4-	715|7-	707|0-	699|7-	693|3-	688|7-	685|7-	677|4-
80	804|6-	793|6-	786|6-	777|4-	770|8-	764|7-	758|0-	753|3-	749|5-	746|2-	744|0-	740|4-
85	835|1-	829|7-	825|5-	821|6-	817|0-	814|6-	811|3-	808|0-	806|2-	804|9-	804|0-	808|2-
90	865|8-	867|1-	865|1-	866|3-	865|3-	864|7-	865|3-	865|1-	864|4-	864|1-	864|1-	870|3-
95	897|9-	904|1-	907|0-	910|3-	914|8-	916|7-	919|1-	922|3-	924|5-	925|6-	926|2-	927|6-
100	932|2-	940|2-	950|0-	955|7-	963|2-	970|1-	975|1-	979|2-	983|6-	987|1-	989|3-	985|2-
105	967|4-	977|3-	991|2-	1003|7-	1012|1-	1021|8-	1032|1-	1039|0-	1044|0-	1048|1-	1051|1-	1046|6-
110	1000|8-	1017|5-	1031|6-	1050|5-	1064|3-	1074|3-	1086|6-	1098|1-	1106|6-	1112|2-	1115|8-	1120|4-
115	1031|9-	1058|4-	1075|0-	1094|7-	1115|2-	1130|4-	1143|2-	1155|0-	1165|8-	1174|3-	1180|0-	1195|1-
120	1063|4-	1095|6-	1121|4-	1141|4-	1162|4-	1183|3-	1202|9-	1216|7-	1227|1-	1235|3-	1241|2-	1254|1-
125	1099|3-	1130|0-	1163|7-	1193|0-	1213|6-	1233|4-	1256|7-	1276|8-	1291|9-	1302|3-	1308|7-	1311|2-
130	1139|6-	1168|0-	1201|2-	1239|4-	1269|6-	1291|0-	1311|5-	1331|2-	1348|7-	1362|4-	1371|6-	1369|1-
135	1175|4-	1214|3-	1243|0-	1279|6-	1316|5-	1347|8-	1375|6-	1395|6-	1410|7-	1422|5-	1430|9-	1430|9-
140	1203|2-	1256|9-	1295|9-	1327|7-	1360|0-	1392|9-	1428|0-	1457|0-	1479|0-	1494|5-	1504|1-	1524|9-
145	1227|8-	1287|6-	1340|3-	1387|1-	1420|4-	1446|6-	1476|4-	1504|9-	1529|5-	1548|5-	1561|3-	1585|8-
150	1259|7-	1314|4-	1370|5-	1428|0-	1476|9-	1515|6-	1549|6-	1574|4-	1593|4-	1608|1-	1618|6-	1634|5-
155	1315|0-	1356|4-	1402|4-	1458|0-	1510|3-	1556|2-	1602|1-	1639|5-	1668|7-	1689|8-	1703|5-	1705|3-
160	1360|1-	1424|9-	1472|0-	1511|8-	1551|4-	1591|6-	1635|7-	1674|4-	1706|0-	1730|0-	1746|1-	1752|2-
162	1370|0-	1442|2-	1501|1-	1551|2-	1587|8-	1619|8-	1657|1-	1692|0-	1721|7-	1744|1-	1760|4-	1766|1-
164	1377|1-	1453|5-	1519|2-	1581|3-	1630|2-	1666|7-	1698|8-	1725|9-	1749|8-	1768|3-	1782|9-	1786|6-
165	1379|9-	1457|6-	1525|3-	1590|8-	1645|1-	1687|8-	1725|6-	1753|5-	1774|9-	1791|6-	1803|2-	1808|1-
166	1382|3-	1461|0-	1530|2-	1598|0-	1655|6-	1702|8-	1747|2-	1780|9-	1805|4-	1821|8-	1833|4-	1850|0-
168	1386|2-	1466|4-	1537|3-	1607|7-	1668|7-	1720|4-	1771|4-	1813|0-	1845|6-	1869|7-	1885|2-	1913|1-
170	1389|2-	1470|3-	1542|1-	1613|8-	1676|3-	1729|7-	1782|8-	1826|9-	1862|1-	1888|2-	1905|7-	1930|1-
172	1391|4-	1473|0-	1546|4-	1617|9-	1681|1-	1735|2-	1789|2-	1834|2-	1870|1-	1897|2-	1915|0-	1937|5-
174	1393|1-	1475|0-	1547|9-	1620|6-	1684|3-	1738|8-	1793|2-	1838|5-	1874|8-	1902|1-	1920|1-	1941|6-
175	1393|7-	1475|8-	1548|7-	1621|6-	1685|4-	1740|0-	1794|6-	1840|0-	1876|3-	1903|6-	1921|8-	1943|0-
176	1394|2-	1476|4-	1549|5-	1622|5-	1686|3-	1740|9-	1795|6-	1841|1-	1877|5-	1905|0-	1923|0-	1944|0-
178	1394|9-	1477|1-	1550|3-	1623|4-	1687|4-	1742|1-	1796|9-	1842|5-	1879|0-	1906|5-	1924|6-	1945|3-
180	1395|1-	1477|4-	1550|6-	1623|8-	1687|8-	1742|5-	1797|4-	1843|0-	1879|5-	1907|0-	1925|1-	1945|8-

TABLE V(a)—Axial Half-Wavelength Slot, Magnitude of E_ϕ; $ka=8$

ϕ° \ θ°	30|0	35|1	39,6	45|4	49|7	55|6	59|6	64|2	69|6	74|3	80|9	90|0
0	411	481	548	627	687	759	810	859	908	943	981	1 000
5	410	480	548	627	687	759	809	859	908	943	980	999
10	409	480	546	626	685	759	807	857	908	943	979	997
15	407	479	544	625	682	759	805	854	907	942	977	995
20	405	477	541	623	679	758	802	850	905	941	975	993
25	401	476	537	621	675	755	800	847	900	937	973	990
30	396	473	532	618	671	749	797	843	893	930	967	986
35	391	470	527	613	667	741	790	839	887	921	958	977
40	386	464	523	605	662	732	781	832	881	913	947	966
45	381	456	518	594	654	724	768	820	873	905	938	955
50	377	445	511	582	642	715	756	804	858	893	927	944
55	372	434	501	572	625	703	745	788	837	874	910	929
60	364	422	486	562	609	684	731	773	816	849	885	904
65	353	413	468	549	594	660	708	755	797	825	856	873
70	339	403	450	529	579	635	678	727	775	803	831	845
75	322	391	434	503	558	615	649	691	740	773	804	818
80	305	374	421	475	528	593	625	657	697	729	762	779
85	290	351	406	452	493	561	599	631	661	684	711	727
90	279	326	383	435	464	519	560	599	631	650	669	680
95	270	303	352	415	443	479	511	551	591	615	636	645
100	260	287	320	384	421	453	472	498	534	560	587	600
105	244	277	296	343	386	430	448	463	482	500	522	534
110	221	265	283	307	340	393	420	440	454	463	473	479
115	194	245	273	288	302	340	371	401	426	439	449	453
120	169	214	253	280	286	299	316	341	371	391	410	418
125	154	181	219	262	279	286	289	296	310	324	341	350
130	152	157	180	225	254	279	286	288	289	290	293	295
135	155	153	155	178	206	244	264	279	289	292	293	293
140	153	160	156	153	160	186	207	230	252	265	277	282
145	140	161	167	163	157	152	156	165	181	193	208	215
150	114	144	163	175	177	172	167	161	156	154	154	154
155	079	109	133	160	174	187	191	193	193	191	188	187
160	049	065	084	112	131	154	167	179	190	197	203	205
162	046	051	064	086	104	110	141	155	169	177	185	189
165	054	048	046	053	063	080	091	104	118	127	136	141
168	071	065	059	052	048	047	049	053	060	065	071	075
170	083	081	077	071	066	059	055	052	049	048	047	048
172	093	095	095	093	091	087	085	082	078	076	073	072
175	106	113	118	122	125	128	129	130	131	132	133	133
178	113	123	131	140	145	153	157	161	166	169	172	173
180	115	125	133	143	149	158	163	168	173	176	180	181

TABLE V(b)—Axial Half-Wavelength Slot, Phase of E_ϕ; $ka=8$

ϕ° \ θ°	30|0	35|1	39|6	45|4	49|7	55|6	59|6	64|2	69|6	74|3	80|9	90|0
0	226|8–	192|6–	164|8–	130|5–	108|1–	79|6–	62|5–	45|7–	28|6–	17|1–	5|6–	0|0
5	227|6–	193|6–	165|9–	131|8–	109|4–	81|1–	64|0–	47|2–	30|2–	18|7–	7|4–	1|7–
10	230|1–	196|6–	169|0–	135|5–	113|2–	85|3–	68|5–	51|7–	35|0–	23|8–	12|5–	6|9–
15	234|2–	201|6–	174|4–	141|6–	119|6–	92|4–	75|9–	59|4–	42|9–	32|0–	21|0–	15|5–
20	239|9–	208|6–	181|7–	150|2–	128|6–	102|1–	86|2–	70|0–	53|9–	43|4–	32|8–	27|4–
25	247|3–	217|2–	191|3–	160|9–	140|1–	114|4–	99|2–	83|7–	68|0–	57|8–	47|6–	42|5–
30	256|3–	227|6–	202|9–	173|7–	154|1–	129|3–	114|8–	100|1–	85|1–	75|3–	65|5–	60|6–
35	267|0–	239|5–	216|5–	188|6–	170|3–	146|7–	132|9–	119|1–	105|1–	95|7–	86|3–	81|6–
40	279|1–	253|0–	231|9–	205|4–	188|4–	166|7–	153|4–	140|5–	127|7–	119|0–	110|1–	105|7–
45	292|7–	268|0–	248|8–	224|4–	208|5–	188|8–	176|5–	164|3–	152|5–	144|7–	136|6–	132|5–
50	307|3–	284|7–	267|1–	245|3–	230|4–	212|8–	201|8–	190|6–	179|6–	172|5–	165|3–	161|7–
55	322|9–	303|0–	286|8–	268|0–	254|3–	238|4–	229|0–	219|0–	209|0–	202|4–	196|0–	192|9–
60	339|2–	322|7–	307|8–	291|9–	280|2–	265|7–	257|5–	249|4–	240|6–	234|7–	228|9–	226|1–
65	356|4–	343|5–	330|4–	316|8–	307|6–	294|8–	287|6–	280|9–	274|0–	269|1–	264|1–	261|6–
70	374|7–	364|9–	354|6–	342|6–	335|7–	325|9–	319|5–	313|7–	308|3–	304|7–	300|9–	298|9–
75	394|0–	386|7–	379|9–	369|9–	364|5–	358|0–	353|3–	348|4–	343|8–	341|1–	338|5–	337|2–
80	414|8–	409|0–	405|7–	398|8–	394|4–	390|6–	388|0–	384|8–	381|2–	379|1–	377|1–	376|2–
85	436|7–	432|1–	431|3–	429|1–	425|9–	423|5–	422|8–	421|9–	420|3–	418|9–	417|6–	416|9–
90	459|1–	456|8–	457|1–	459|5–	459|1–	457|8–	457|9–	458|7–	459|5–	459|7–	459|6–	459|5–
95	481|1–	483|0–	483|9–	489|1–	492|3–	494|1–	494|7–	496|0–	498|1–	499|8–	501|4–	502|1–
100	502|2–	509|9–	512|6–	518|6–	524|5–	531|0–	533|5–	535|5–	538|0–	540|0–	542|4–	543|7–
105	522|7–	536|1–	543|1–	549|5–	556|2–	566|4–	572|0–	576|6–	580|4–	582|7–	585|2–	586|5–
110	543|4–	560|5–	573|2–	583|2–	589|6–	600|5–	608|2–	615|9–	622|9–	627|0–	630|7–	632|3–
115	565|8–	583|8–	600|9–	618|0–	626|3–	636|6–	644|2–	652|9–	662|3–	668|6–	674|6–	677|5–
120	591|2–	607|6–	626|4–	650|0–	663|4–	676|8–	684|0–	691|9–	701|0–	707|8–	714|9–	718|6–
125	619|4–	634|8–	652|1–	678|4–	696|4–	716|8–	727|1–	736|3–	744|8–	750|7–	757|1–	760|5–
130	646|8–	666|9–	681|9–	706|1–	725|5–	750|9–	765|6–	779|5–	791|9–	799|5–	806|5–	809|9–
135	669|7–	699|6–	718|4–	739|1–	756|0–	781|3–	797|8–	814|6–	831|4–	842|3–	852|7–	857|8–
140	687|8–	726|3–	754|4–	781|2–	796|2–	816|8–	831|2–	847|3–	864|6–	876|6–	888|7–	894|8–
145	702|8–	746|2–	781|2–	819|8–	842|4–	866|1–	878|7–	891|4–	905|0–	915|0–	925|7–	931|3–
150	717|3–	762|0–	800|2–	845|7–	875|1–	910|1–	929|6–	947|7–	964|2–	974|3–	983|8–	988|5–
155	736|4–	778|2–	816|3–	863|9–	895|9–	936|0–	959|8–	983|4–	1005|5–	1021|6–	1036|5–	1043|8–
160	775|2–	805|5–	837|7–	882|1–	913|7–	954|4–	979|2–	1004|2–	1029|2–	1045|9–	1062|7–	1071|0–
162	800|0–	826|8–	853|4–	893|1–	922|9–	954|8–	986|9–	1011|7–	1036|7–	1053|6–	1070|4–	1078|9–
165	833|2–	871|3–	896|7–	925|7–	948|4–	981|6–	1003|6–	1026|6–	1050|5–	1066|7–	1083|1–	1091|4–
168	852|4–	902|7–	941|9–	984|2–	1008|5–	1034|9–	1049|9–	1065|9–	1083|4–	1095|0–	1109|4–	1116|4–
170	860|0–	913|8–	957|5–	1008|5–	1041|1–	1079|7–	1101|2–	1121|4–	1139|9–	1151|4–	1162|2–	1167|6–
172	865|0–	920|6–	966|3–	1020|7–	1056|5–	1100|7–	1126|9–	1152|8–	1178|3–	1195|0–	1211|6–	1219|7–
175	869|6–	926|4–	973|3–	1029|4–	1066|6–	1113|1–	1140|8–	1168|6–	1196|2–	1214|6–	1233|0–	1242|2–
178	871|8–	928|9–	976|3–	1032|9–	1070|5–	1117|5–	1145|6–	1173|7–	1201|7–	1220|3–	1239|0–	1248|3–
180	872|2–	929|4–	976|8–	1033|6–	1071|2–	1118|2–	1146|3–	1174|5–	1202|5–	1221|2–	1239|9–	1249|2–

TABLE VI(a)—Axial Half-Wavelength Slot, Magnitude of E_ϕ; $ka=12$

ϕ° \ θ°	30|0	35|1	39|9	45|1	50|1	54|8	60|1	65|3	70|3	75|2	79|5	90|0
0	414	487	554	626	694	753	817	871	918	952	976	1|000
5	414	486	554	626	694	753	817	871	917	952	976	1|000
10	413	485	554	626	693	753	816	871	916	951	976	1|000
15	411	484	553	625	691	753	814	870	914	950	975	999
20	409	482	552	623	689	751	812	868	914	948	972	997
25	407	481	550	620	688	747	811	865	911	947	970	994
30	405	479	546	618	685	744	808	861	907	944	967	991
35	402	475	541	615	680	740	803	858	902	937	962	987
40	399	469	536	610	673	735	795	852	897	930	954	979
45	394	462	532	602	667	726	789	841	889	923	946	969
50	385	455	525	591	660	715	780	831	875	911	935	959
55	376	448	513	581	647	704	764	819	861	893	917	943
60	367	439	498	570	629	690	746	799	845	876	897	920
65	359	426	485	554	612	668	728	775	819	854	876	898
70	349	408	472	531	595	643	703	752	789	820	843	867
75	336	390	454	509	569	620	669	721	761	788	806	826
80	317	376	428	489	537	591	639	679	720	751	771	789
85	296	360	402	464	509	551	606	644	673	700	720	741
90	281	336	382	428	482	516	558	603	635	656	669	684
95	269	307	361	396	442	486	517	549	583	609	625	639
100	254	284	329	374	400	440	483	507	527	546	562	579
105	231	269	294	343	374	394	430	466	489	501	509	518
110	204	252	272	300	343	368	383	406	433	454	467	477
115	183	223	258	270	295	331	358	369	377	389	399	411
120	175	190	230	257	264	279	311	338	352	358	361	364
125	170	174	190	229	252	256	261	278	299	316	326	335
130	152	172	170	184	217	241	252	251	252	256	261	268
135	122	159	171	167	170	191	219	238	247	249	249	248
140	097	124	156	171	168	162	165	179	196	210	219	228
145	097	094	114	145	166	174	171	164	159	157	158	160
150	109	100	090	096	117	140	161	173	178	179	179	178
155	105	115	112	101	090	087	095	109	124	135	143	150
160	077	100	115	124	124	120	112	103	096	091	089	087
162	061	085	104	119	127	130	130	126	121	117	113	110
165	037	055	074	094	110	121	131	137	140	142	143	143
168	030	029	038	052	069	082	096	107	116	122	126	130
170	041	033	028	029	037	047	058	069	077	084	089	093
172	056	051	044	037	031	028	027	030	034	038	041	044
175	077	078	078	076	075	073	070	067	065	063	062	061
178	089	094	099	104	107	110	113	116	117	119	120	121
180	091	098	103	109	114	118	122	126	129	131	132	134

TABLE VI(b)—Axial Half-Wavelength Slot, Phase of E_ϕ, $ka=12$

ϕ° \ θ°	30|0	35|1	39|9	45|1	50|1	54|8	60|1	65|3	70|3	75|2	79|5	90|0
0	341|8–	290|6–	245|2–	199|7–	159|8–	125|5–	91|4–	62|8–	39|9–	22|9–	11|5–	0|0
5	343|0–	292|1–	246|8–	201|6–	161|7–	127|7–	93|6–	65|1–	42|4–	25|4–	14|0–	2|6–
10	346|9–	296|6–	251|8–	207|0–	167|7–	134|0–	100|3–	72|3–	49|7–	32|8–	21|6–	10|4–
15	353|2–	304|0–	260|1–	216|0–	177|6–	144|5–	111|4–	83|9–	61|9–	45|3–	34|2–	23|3–
20	362|2–	314|3–	271|5–	228|6–	191|3–	159|1–	127|0–	100|1–	78|7–	62|6–	51|9–	41|1–
25	373|5–	327|3–	285|9–	244|7–	208|7–	177|6–	146|7–	120|8–	100|0–	84|6–	74|3–	63|9–
30	387|2–	342|9–	303|4–	264|1–	229|5–	200|0–	170|0–	145|6–	125|9–	111|1–	101|2–	91|4–
35	403|0–	361|0–	323|8–	286|7–	253|9–	226|1–	197|9–	174|7–	156|0–	141|9–	132|6–	123|2–
40	420|8–	381|5–	347|1–	312|1–	281|6–	255|5–	229|3–	207|4–	190|1–	176|9–	168|2–	159|3–
45	440|5–	404|6–	372|8–	340|3–	312|4–	288|0–	264|1–	243|8–	227|7–	215|7–	207|7–	199|6–
50	462|1–	429|9–	400|6–	371|3–	345|8–	323|8–	301|9–	283|7–	268|9–	257|9–	250|7–	243|4–
55	485|8–	457|1–	430|5–	404|9–	381|8–	362|5–	342|6–	326|5–	313|5–	303|6–	296|9–	290|4–
60	511|3–	485|6–	462|8–	440|4–	420|3–	403|3–	386|3–	371|9–	360|6–	352|2–	346|5–	340|7–
65	538|1–	515|7–	497|2–	477|6–	461|1–	446|3–	432|2–	420|1–	410|2–	403|1–	398|4–	393|7–
70	565|6–	547|6–	532|8–	516|7–	503|5–	491|8–	479|8–	470|5–	462|6–	456|5–	452|6–	448|7–
75	593|9–	581|4–	569|2–	558|0–	547|1–	538|9–	529|8–	522|2–	516|6–	512|3–	509|3–	506|2–
80	623|4–	616|1–	607|2–	600|2–	592|8–	586|8–	581|5–	576|2–	571|9–	569|1–	567|3–	565|6–
85	654|8–	650|9–	647|0–	642|7–	640|2–	636|4–	633|6–	631|7–	629|6–	627|7–	626|6–	625|6–
90	687|4–	685|9–	687|8–	686|6–	687|4–	688|0–	687|2–	687|3–	687|9–	688|1–	688|1–	687|9–
95	719|8–	722|8–	727|9–	732|6–	735|1–	739|1–	742|7–	744|6–	746|3–	748|1–	749|5–	750|8–
100	751|1–	761|6–	768|1–	778|5–	785|2–	790|4–	797|5–	803|4–	807|2–	809|6–	811|4–	813|4–
105	782|4–	800|1–	810|8–	822|8–	835|7–	844|4–	852|3–	860|6–	867|7–	872|8–	875|9–	878|7–
110	815|9–	836|3–	855|1–	868|8–	883|8–	898|2–	910|4–	919|3–	927|0–	933|5–	938|1–	942|8–
115	852|4–	872|3–	896|7–	918|2–	933|5–	949|0–	966|7–	980|5–	990|1–	996|8–	1001|4–	1006|1–
120	888|4–	912|1–	935|9–	965|0–	987|3–	1003|1–	1020|4–	1037|3–	1051|3–	1061|5–	1067|9–	1074|0–
125	920|1–	955|2–	978|8–	1007|6–	1036|9–	1060|5–	1080|3–	1095|7–	1109|3–	1120|5–	1128|3–	1136|4–
130	948|5–	993|7–	1027|6–	1054|7–	1082|4–	1110|2–	1138|5–	1160|1–	1175|5–	1186|1–	1193|2–	1200|4–
135	979|6–	1025|9–	1070|3–	1109|1–	1135|4–	1160|2–	1188|5–	1214|5–	1235|8–	1251|3–	1261|4–	1271|1–
140	1020|6–	1059|3–	1104|6–	1153|5–	1193|8–	1223|4–	1249|1–	1270|7–	1289|9–	1305|6–	1316|6–	1327|9–
145	1065|1–	1106|8–	1143|1–	1189|6–	1235|2–	1275|0–	1313|1–	1342|2–	1363|2–	1377|6–	1386|9–	1396|1–
150	1096|0–	1157|7–	1202|4–	1239|6–	1276|8–	1314|5–	1355|7–	1391|3–	1419|8–	1441|0–	1454|9–	1468|7–
155	1116|0–	1187|9–	1249|7–	1306|8–	1349|8–	1381|2–	1411|6–	1440|0–	1465|3–	1485|6–	1499|6–	1513|9–
160	1133|8–	1207|3–	1274|0–	1340|9–	1398|6–	1447|0–	1493|5–	1530|2–	1557|6–	1576|9–	1589|0–	1600|6–
162	1143|4–	1215|0–	1281|7–	1349|4–	1408|8–	1459|4–	1516|7–	1550|6–	1582|7–	1606|4–	1621|8–	1636|9–
165	1170|4–	1231|7–	1294|8–	1361|5–	1421|3–	1473|0–	1524|9–	1568|2–	1602|8–	1628|7–	1645|9–	1663|1–
168	1230|9–	1278|1–	1324|0–	1383|6–	1437|2–	1487|1–	1538|3–	1581|5–	1616|4–	1642|6–	1660|1–	1677|6–
170	1261|1–	1329|3–	1379|5–	1422|2–	1464|4–	1506|9–	1553|6–	1594|5–	1628|0–	1653|6–	1670|7–	1687|9–
172	1275|6–	1355|0–	1423|1–	1487|5–	1538|4–	1576|4–	1610|2–	1638|7–	1663|6–	1683|9–	1698|1–	1712|9–
175	1285|4–	1368|9–	1442|7–	1516|2–	1580|1–	1634|6–	1688|9–	1733|8–	1769|7–	1796|5–	1814|2–	1831|9–
178	1289|2–	1373|7–	1448|4–	1522|9–	1588|0–	1643|7–	1699|2–	1745|5–	1782|5–	1810|2–	1828|7–	1847|1–
180	1289|9–	1374|4–	1449|3–	1524|0–	1589|1–	1644|9–	1700|5–	1746|9–	1784|0–	1811|8–	1830|2–	1848|7–

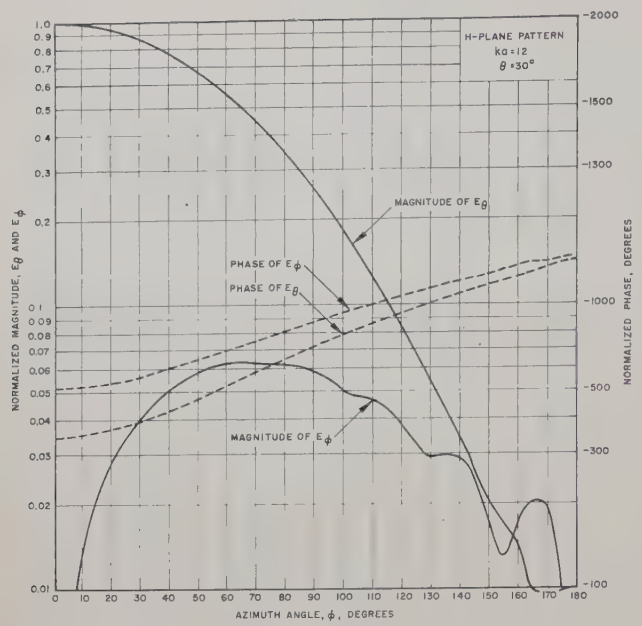

Fig. 2—Circumferential half-wavelength slot.

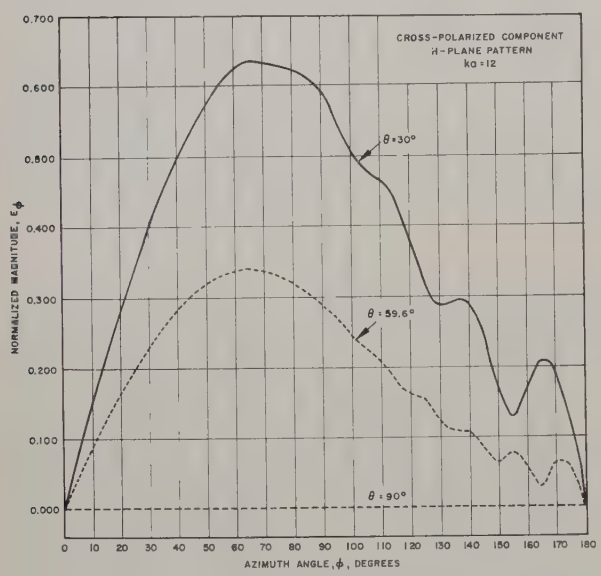

Fig. 4—Circumferential half-wavelength slot.

(magnitude of E_θ)$e^{j(\text{phase of } E_\theta \text{ in degrees})}$,

where the normalization is accomplished by dividing each result by

$$N_I = (-jaV_0 2ka) \sum_{n=0}^{\infty} \frac{\epsilon_n j^n}{H_n^2(ka)} \left[\frac{\cos\left(\frac{n\pi}{2ka}\right)}{(ka)^2 - n^2} \right]$$

$$= [-jAV_0{}^2 ka][.394]e^{j[92.220^0]} \qquad (8)$$

for $ka = 8$ and

$$N_I = (-jAV_0 2ka)[.262]e^{j[324.06^0]} \qquad (9)$$

for $ka = 12$. Although these results are given for $\phi = 0 \rightarrow 180$ degrees and $\theta = 30$ degrees$\rightarrow$90 degrees, they may be extended to the range $\phi = 180$ degrees$\rightarrow$360 degrees and $\theta = 90$ degrees$\rightarrow$150 degrees since both the phase

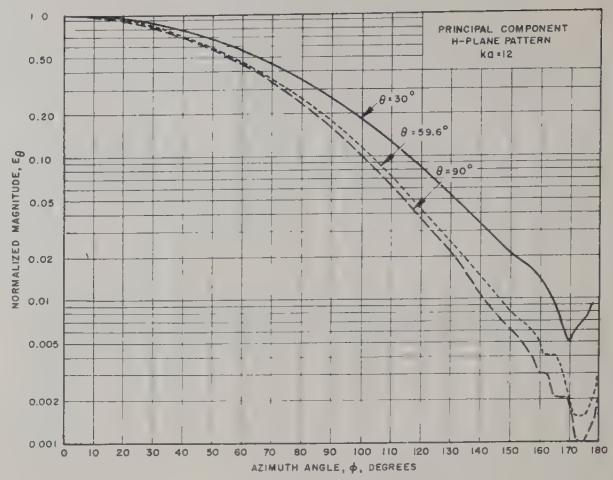

Fig. 3—Circumferential half-wavelength slot.

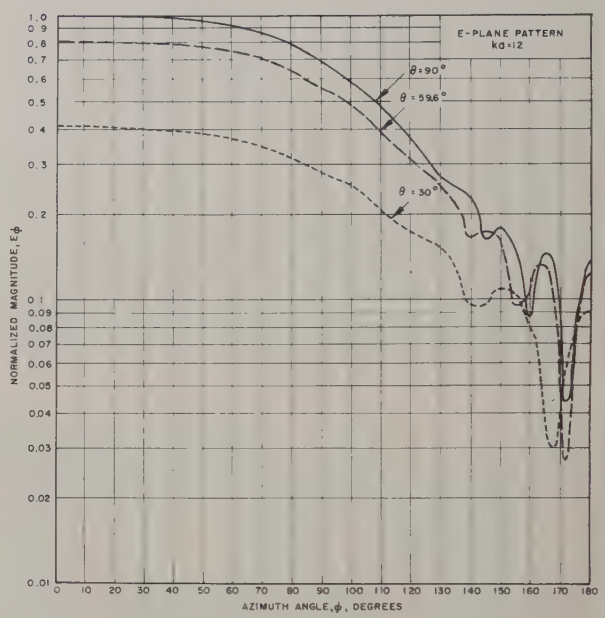

Fig. 5—Axial half-wavelength slot.

and magnitude of this component are symmetrical abou the planes $\phi = 180$ degrees and $\theta = 90$ degrees. The rang in θ is limited because the fundamental equations (4 and (5) are not valid for small values of θ. Tables III(a) (b) (page 132) and IV(a), (b) (page 133) describe similarly, the cross-polarized component of the electri field computed from (7) and suitably normalized to th corresponding principal component by dividing eac result by (8) or (9). Here, the results may be extende to the range of $\phi = 180$ degrees$\rightarrow$360 degrees an $\theta = 90$ degrees$\rightarrow$150 degrees by changing the sign of th magnitude or by changing the phase by 180 degree since this component is antisymmetrical about th planes $\phi = 180$ degrees and $\theta = 90$ degrees.

Fig. 2 compares the normalized magnitude and phas of the principal and the cross-polarized components i the H-plane cone, $\theta = 30$ degrees. The curves show tha the cross-polarized component is more strongly affecte by the diffraction phenomena in the semicircle ove

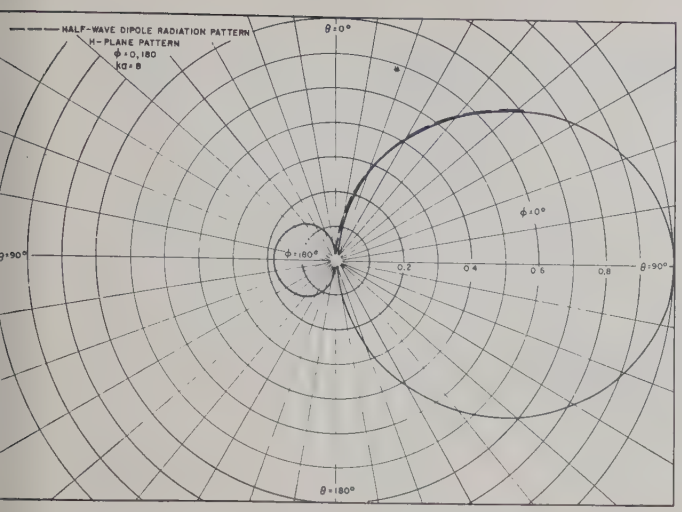

Fig. 6—Axial half-wavelength slot.

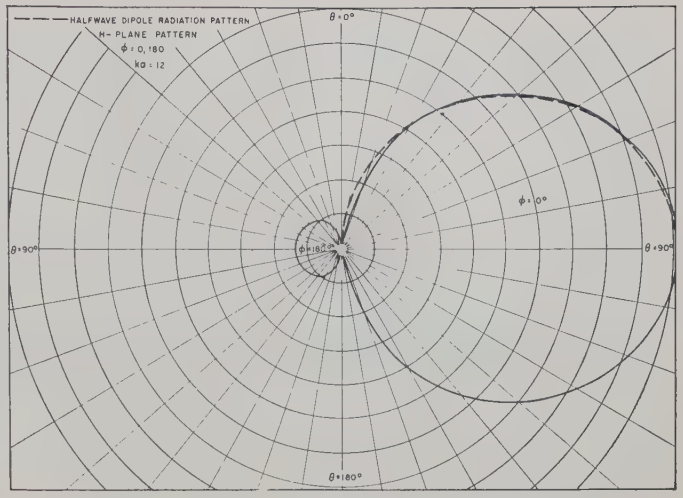

Fig. 7—Axial half-wavelength slot.

which the slot is optically invisible ($90 \leqq \phi \leqq 270$) than the principal component. This effect is to be anticipated by an elementary consideration of Sommerfeld diffraction theory. Fig. 3 describes the H-plane pattern of the principal component as a function of polar angle θ. The increase in the magnitude of E_θ as θ decreases is due to the finite curvature of the slot itself. This curvature introduces a phase difference into the radiation from the different portions of the source and, consequently, a reduction of the effective strength of the source. Since this phase difference decreases as θ departs from the principal H-plane ($\theta = 90$ degrees), the magnitude of E_θ should increase slightly for all values of ϕ. Fig. 4 shows the deterioration of the cross-polarized components as θ approaches 90 degrees.

Case II—Narrow Axial Slot

$l = \lambda/2$, $\phi_0 \to 0$. If again we insert (3) into (4) and (5) and combine terms of positive and negative n, we have

$$E_\theta = 0 \tag{10}$$

and

$$E_\phi = A \frac{V_0}{a} \frac{\lambda}{\pi} \left[\frac{\left(\cos \frac{\pi}{2} \cos \theta \right)}{\sin \theta} \right] \frac{1}{\sin \theta} \cdot \sum_{n=0}^{\infty} \frac{\epsilon_n j^n \cos (n\phi)}{H_n^{(2)\prime}(ka \sin \theta)} . \tag{11}$$

Tables V(a), (b) (page 134) and VI(a), (b) (page 135) give, respectively, the magnitude and phase of the electric field computed from (11) and normalized to unity at $\phi = 0$ degrees, $\theta = 90$ degrees for $ka = 8$ and 12. The normalization for this case was obtained by dividing each result by

$$N_{II} = \left(\frac{AV_0\lambda}{a\pi} \right) \sum_{n=0}^{\infty} \frac{\epsilon_n j^n}{H_n^{(2)\prime}(ka \sin \theta)} = \left[\frac{AV_0\lambda}{a\pi} \right] [24.888] e^{j[191.69°]}$$

for $ka = 8$ and

$$N_{II} = \left[\frac{AV_0\lambda}{a\pi} \right] [37.475] e^{j[59.874°]}$$

for $ka = 12$. These tables may also be extended to the range $\phi = 180$ degrees $\to 360$ degrees and $\theta = 90$ degrees $\to 150$ degrees, since both the phase and magnitude are symmetrical about the planes $\phi = 180$ degrees and $\theta = 90$ degrees.

Fig. 5 shows the deterioration of the E-plane pattern as a function of θ. Here the diffraction effects in the optically invisible region are quite pronounced in contrast to the fields of the circumferential slot. Figs. 6 and 7 describe the H-plane patterns in the two principal planes: $\phi = 0$, 180 degrees. For these large cylinders the pattern at $\phi = 0$ is very nearly given by the radiation field of a half-wave dipole which is indicated by the dotted line in the figures and the bracket in (11).

ACKNOWLEDGMENT

The author wishes to thank Annabelle Cordova and the numerical computation group at Hughes Aircraft Company for their computing services.

communications

Fresnel Antenna Patterns*

L. W. LECHTRECK†

THE PURPOSE of this article is to present graphs useful in the evaluation of the effects of quadratic aperture phase errors on antenna near and far fields. Two types of aperture amplitude illumination were considered: (1) uniform, and (2) cosine with zero edge intensity. Four graphs give the radiation characteristics for various phase coefficients. In Fig. 1 (opposite page), the aperture illumination is

$$\mathcal{E}(x) = 1e^{jbx^2} \quad \text{for} \quad -1 \leqq x \leqq +1.$$

The radiation pattern is

$$\sqrt{b}\,\mathcal{E}(u)\alpha C\left(\frac{u}{2\sqrt{b}}+\sqrt{b}\right)^2 \mp C\left(\frac{u}{2\sqrt{b}}-\sqrt{b}\right)^2 + iS\left(\frac{u}{2\sqrt{b}}+\sqrt{b}\right)^2 \mp iS\left(\frac{u}{2\sqrt{b}}-\sqrt{b}\right)^2.$$

In Fig. 2 (opposite page), the aperture illumination is

$$\mathcal{E}(x) = \cos\left(\frac{\pi}{2}x\right)e^{jbx^2}$$

for $-1 \leqq x \leqq +1$. The resultant radiation is

$$-\sqrt{b}\,\mathcal{E}(u)\alpha e^{-j(\pi u/2b)}\left[C(N_1)^2 \pm C(N_2)^2 + jS(N_1)^2 \pm jS(N_2)^2\right] + \left[C(M_1)^2 \pm C(M_2)^2 + jS(M_1)^2 \pm jS(M_2)^2\right];$$

where $u = \pi a/\lambda \sin\theta$, a = total aperture length, λ = wavelength, θ = radiation angle from normal, b = coefficient of phase deviation from plane front, C and S are Fresnel integrals, $\mathcal{E}(u)$ = field intensity at angle θ,

$$N_1 = -\sqrt{b}+\frac{u}{2\sqrt{b}}+\frac{\pi}{4\sqrt{b}}, \quad M_1 = -\sqrt{b}+\frac{u}{2\sqrt{b}}-\frac{\pi}{4\sqrt{b}},$$

and

$$N_2 = \sqrt{b}+\frac{u}{2\sqrt{b}}+\frac{\pi}{4\sqrt{b}}, \quad M_2 = +\sqrt{b}+\frac{u}{2\sqrt{b}}-\frac{\pi}{4\sqrt{b}}.$$

Figs. 3 and 4 (page 140) show the variation in radiation side lobes and nulls with small phase errors.

$$b = 2\pi\frac{\Delta L}{\lambda}.$$

The results are directly applicable to: both planes of radiation of large pyramidal horns, where

$$\Delta L \doteq \frac{A^2}{8L},$$

A = aperture length, and L = slant length; and to near-field measurements of a rectangular aperture where L is now the radiation distance. The curves are also useful in securing qualitative information about nonrectangular radiators such as the defocused parabolic reflector in which

$$b = 2\pi\frac{d}{\lambda}(1-\cos\phi),$$

* Original manuscript received by the PGAP, September 22, 1954; revised manuscript received, January 21, 1955.
† Emerson Electric Mfg. Co., St. Louis 21, Mo.

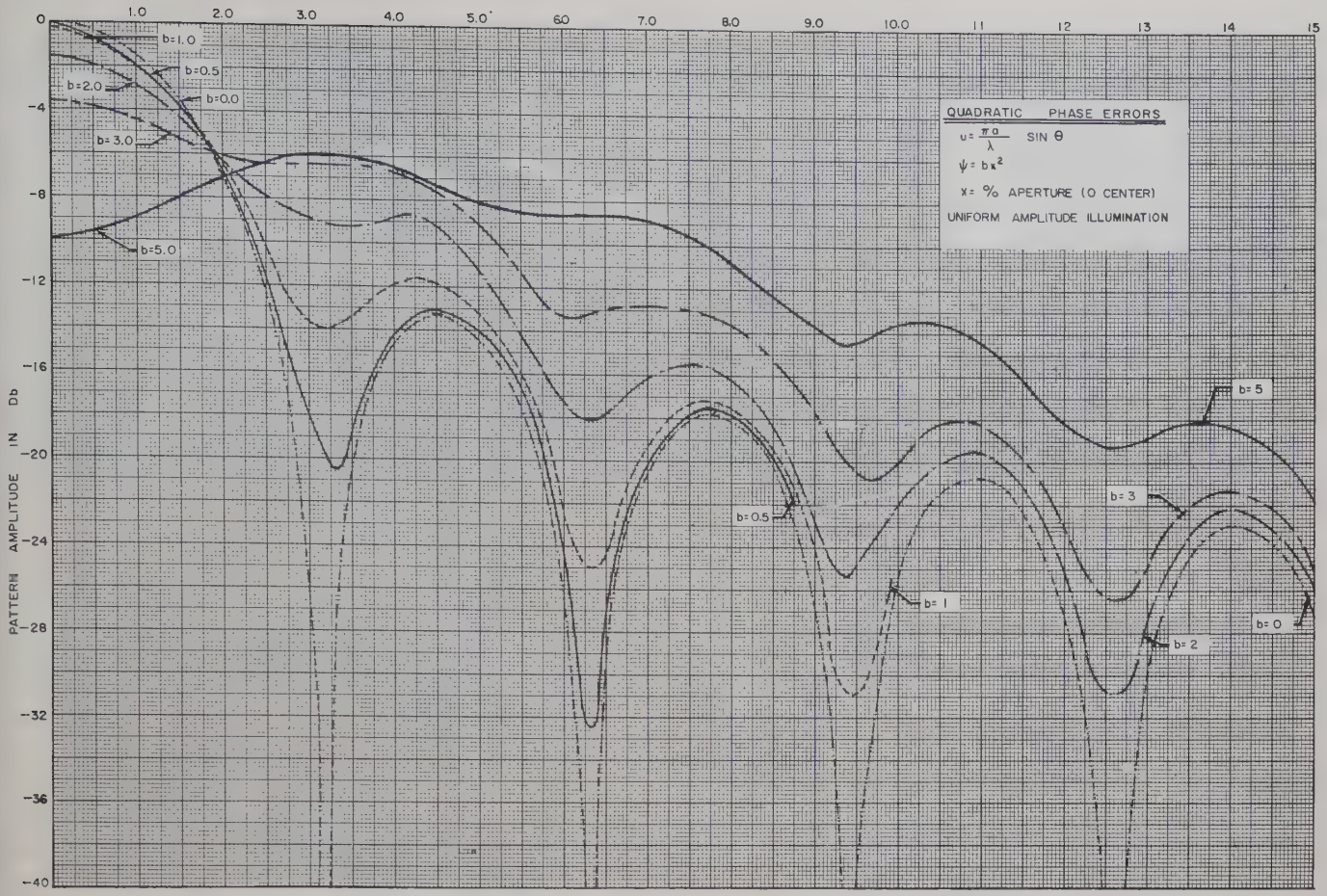
QUADRATIC PHASE ERRORS
$u = \frac{\pi a}{\lambda} \sin\theta$
$\psi = bx^2$
x = % APERTURE (0 CENTER)
UNIFORM AMPLITUDE ILLUMINATION
PATTERN AMPLITUDE IN Db
b=1.0
b=0.5
b=0.0
b=2.0
b=3.0
b=5.0
b=5
b=3
b=0.5
b=1
b=0
b=2

Fig. 1

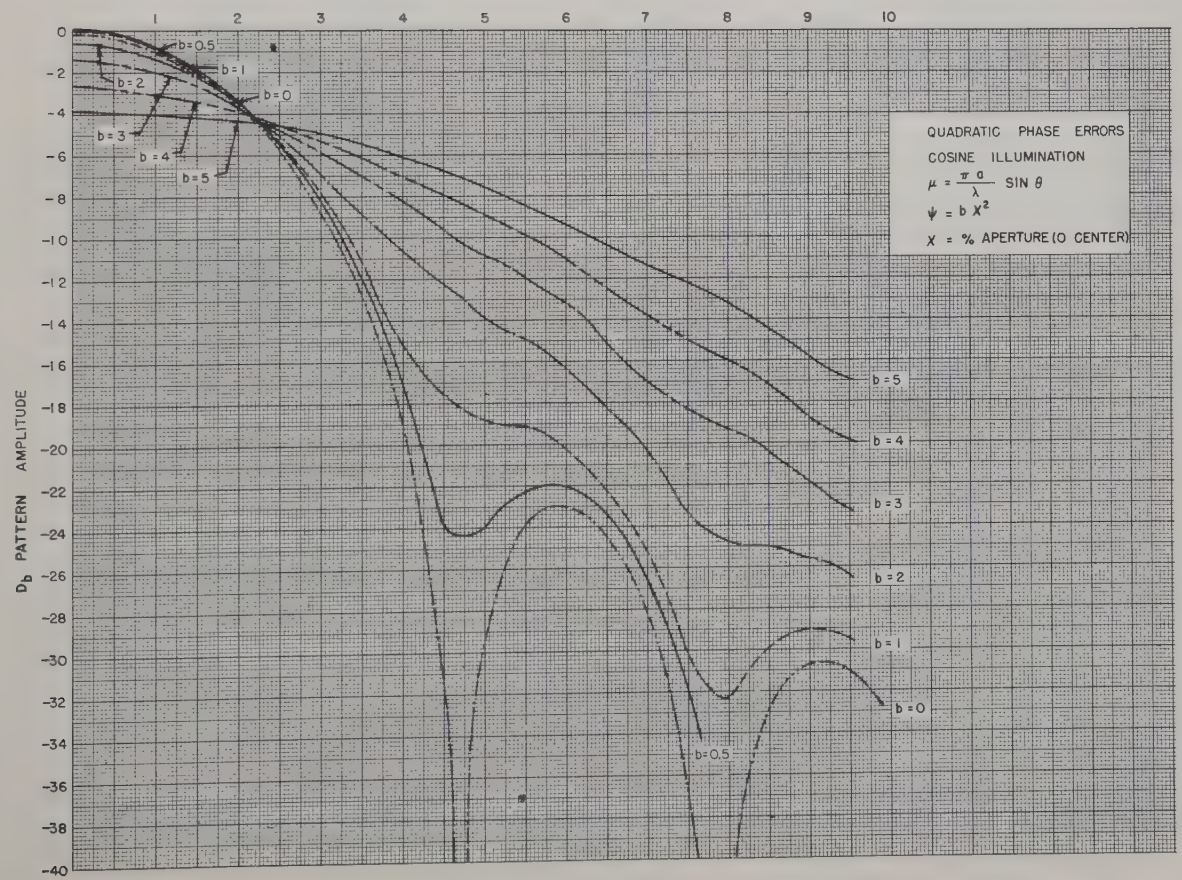
QUADRATIC PHASE ERRORS
COSINE ILLUMINATION
$\mu = \frac{\pi a}{\lambda} \sin\theta$
$\psi = b X^2$
X = % APERTURE (0 CENTER)
D_b PATTERN AMPLITUDE
b=0.5
b=1
b=2
b=0
b=3
b=4
b=5
b=5
b=4
b=3
b=2
b=1
b=0
b=0.5

Fig. 2

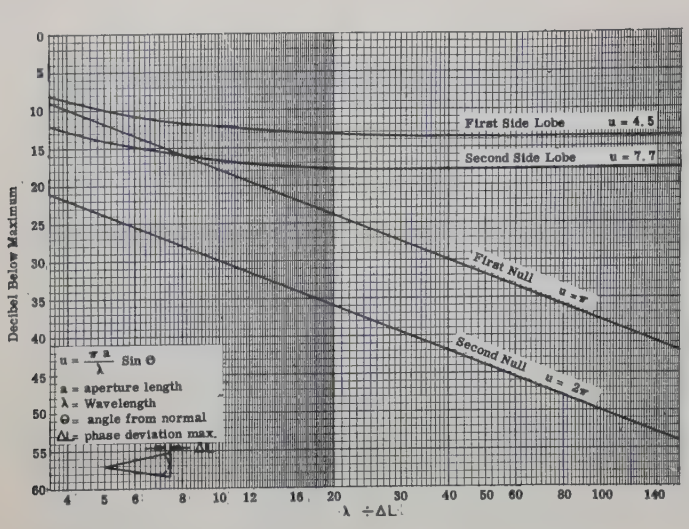

Fig. 3—Side-lobes and nulls for quadratic phase error, uniform aperture illumination.

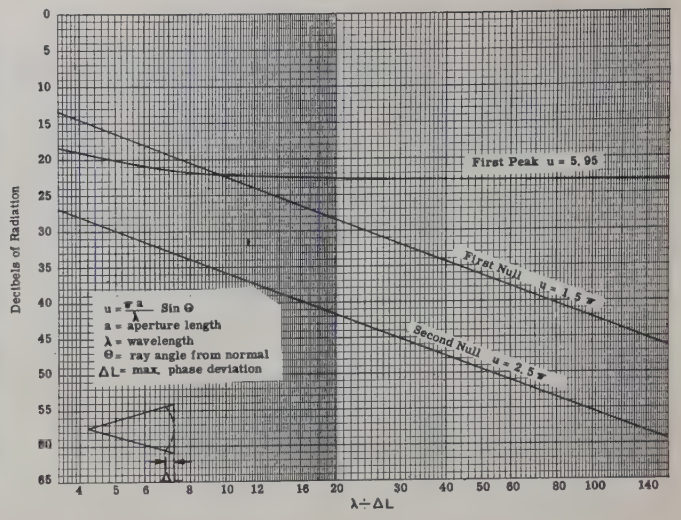

Fig. 4—Side-lobes and nulls for quadratic phase error cosine illumination.

where

d = axial feed displacement from the principal focus, λ = free space wavelength, and ϕ = half-angle subtended by dish at feed.

The curves are directly applicable to pulse analysis where the ramp frequency shift is proportional to the phase constant b, the pulse amplitude to the illumination, and the spectrum frequency to the argument u.

Parasitic Arrays Excited by Surface Waves*

R. S. ELLIOTT† AND E. N. RODDA†

TRAPPING media, such as corrugated surfaces and grounded-dielectric surfaces, have been used with success both as transmission lines[1] and as antennas.[2–4] The antennas are characterized by endfire radiation which is not desirable for some applications. An attempt has been made to use these trapping media as transmission lines feeding parasitic arrays, with the hope that controllable radiation patterns could be obtained. The versatility of beams tilted anywhere from endfire to broadside, of csc² shaping, etc., was the desired end product of the investigation.

Arrays of dipoles, loops, wickets, and plates were used as the parasites and were first placed over the *S*-band corrugated surface of Fig. 1(a) (opposite page). The surface was $7\lambda_0$ long and $3\frac{1}{2}\lambda_0$ wide and was excited by a corrugated hog horn.[5] The reference pattern for this antenna with no parasites present is shown in Fig. 2 (opposite page). The degree of trapping was found experimentally to correspond to $\lambda_0/\lambda_g = 1.07$.

The first attempts at altering the endfire radiation consisted of placing arrays of thin plates over the corrugated surface as suggested by Fig. 1(b). These plates were 14 inches long in the transverse dimension and the widths were varied from $\frac{1}{2}$ inch to two inches. The plates were rotated at various angles around an axis parallel to the corrugations and were placed at several distances above the corrugations. No interesting changes in the radiation pattern were observed.

Arrays of dipoles were next tried. In the first series of experiments, the dipoles were kept parallel to the surface

* Original manuscript received by the PGAP, September 27, 1954; revised manuscript received, March 21, 1955. The research described here was supported by the Air Force Cambridge Research Center under Contract AF 19(604)-262.

† Hughes Res. and Dev. Labs., Hughes Aircraft Co., Culver City, Calif.

[1] G. Goubau, "Surface waves and their application to transmission lines," *Jour. Appl. Phys.*, vol. 21, pp. 1119–28; November, 1950.

[2] "Ridge and Corrugated Antenna Studies," Quarterly Progress Reports 1 through 6, Stanford Res. Inst.; July, 1949–January, 1951.

[3] J. C. Simon and G. Weill, "Un nouveau type d'aerien à rayonnement longitudinal," *Ann. Radioelect.*, vol. 8, pp. 183–193; July, 1953.

[4] R. S. Elliott, "On the theory of corrugated plane surfaces," *Trans. IRE*, vol. AP-2, pp. 71–81; April, 1954.

[5] For a more complete description of the apparatus, see R. S. Elliott and E. N. Rodda, "Parasitic Arrays Excited by Surface Waves," Tech. Memo. No. 344, Hughes Res. and Dev. Labs.; March 15, 1954.

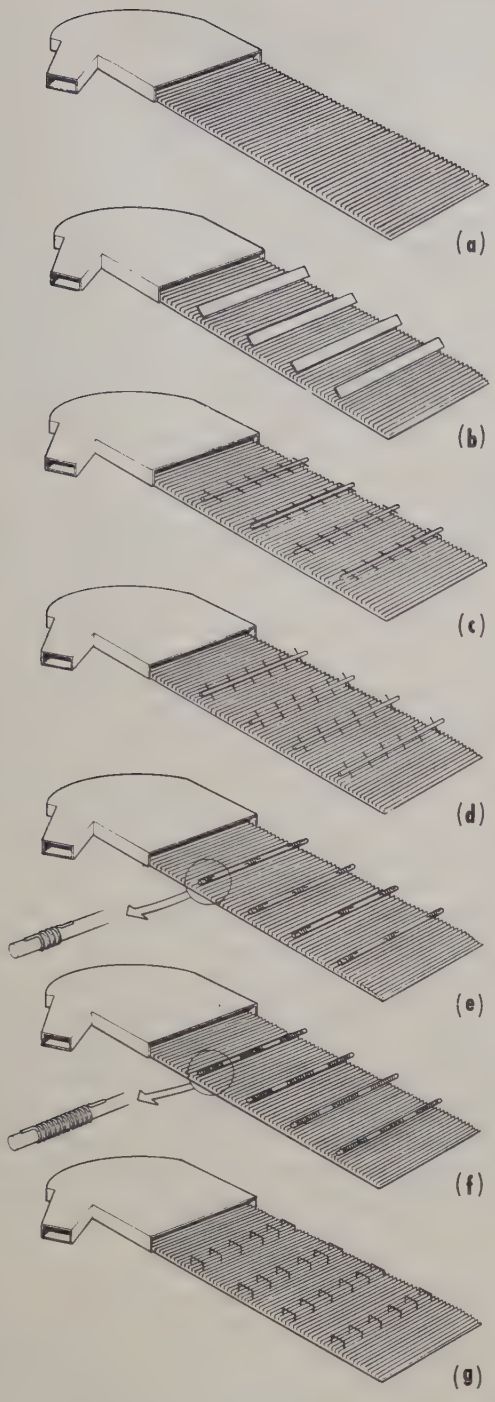

Fig. 1—Representative geometries for parasitic arrays over a corrugated surface.

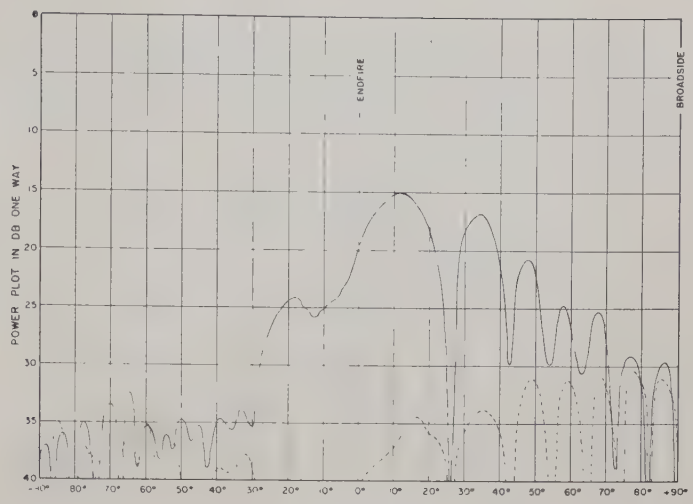

Fig. 2—Reference pattern for an *S*-band corrugated surface, $3\frac{1}{2}\lambda_0$ wide, $7\lambda_0$ long, $\lambda_0/\lambda_g = 1.07$. No parasitic elements.

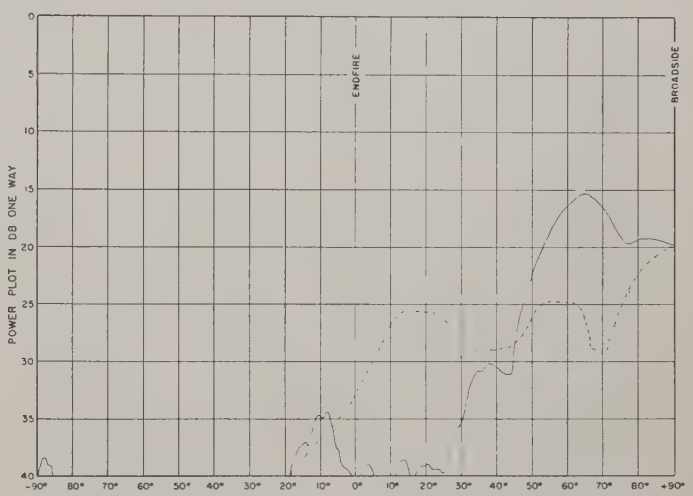

Fig. 3—Parasitic dipoles above the corrugated surface. Four stacks λ_g apart. Six dipoles per stack $\lambda_0/2$ apart. Dipole length λ_0. Array-to-surface spacing $\lambda_g/2$. Dipoles tilted 45 degrees as shown in Fig. 1(d).

and in the *E*-plane, as sketched in Fig. 1(c). The number of stacks, spacing between stacks, dipole length, and distance off surface were all varied. For some positions, considerable energy was thrown into the broadside region, but never in the form of a well-shaped beam. The endfire lobe was not appreciably reduced. No recognizable pattern trends due to parameter variations were noticed.

In the second series, the axes of the stacks were kept parallel to, and equidistant from, the corrugated surface, but the dipoles were rotated, giving arrangements typified by Fig. 1(d). Dipole lengths of $\lambda_0/2$, λ_0, and $2\lambda_0$ were used. The number of stacks, spacing between stacks, and array-to-surface distance were varied. Stacks were rotated in both directions and at different, as well as the same angles. The best result is shown in Fig. 3. The setting was fairly critical. The tilting of different stacks at different angles did not reveal anything startling.

A third series was an extension of the second in which the various stacks were placed at different heights above the surface. No significant improvements were observed.

It was recognized that the dipoles, in their more favorable positions, were not coupling purely to one component of the electric field. This meant that the coupling was more critical and less predictable. In an effort to avoid this, the dipoles were placed in the transverse position and loop-excited, as shown in the sketch of Fig. 1(e). The loops were several turns tightly wound on a $\frac{1}{2}$ inch-diameter lucite rod, the dipoles being λ_0 in length. It is

believed that essentially pure coupling to the H-field was achieved, but the amount of coupling was so small that the principal pattern was hardly affected. The cross-polarized field was everywhere more than 20 db below the principal beam.

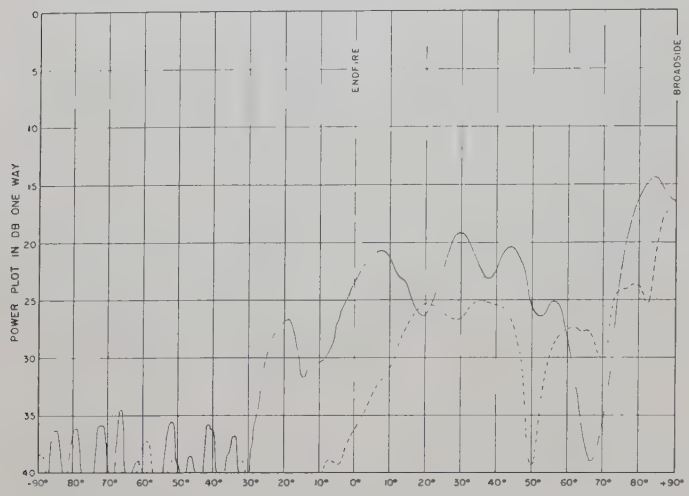

Fig. 4—Parasitic wickets above the corrugated surface. Four stacks λ_g apart. Six wickets per stack $\lambda_0/2$ apart. Wickets $\lambda_0/2$ long and on surface.

Continuing the efforts to obtain magnetic coupling, the loop-fed dipoles were replaced by loops alone. Multiturn loops of various diameters and lengths were arranged in stacks of various sizes and positions, as indicated by Fig. 1(f), but little of interest accrued from this. It was reasoned that perhaps the coupling could be made tighter if the loops were replaced by wickets, as shown in Fig. 1(g). This proved to be the case, and a representative pattern is given in Fig. 4. It appeared possible to throw a good share of the energy broadside and even cause a reverse endfire beam. Though only one pattern is shown, a great variety of geometries were used. Stack spacings, number of stacks, wicket heights and lengths were all adjusted over reasonable ranges.

The fact that it had been proved possible to divert a share of the energy to broadside with both dipoles and wickets was a stimulus to try to improve on the effect. A study of Figs. 3 and 4 indicates that the parasitic excitation was not proper enough to yield an appropriate beamwidth and side-lobe level for the size of aperture being used. One factor which could have been contributing to the poor pattern was the need to have the stacks λ_g apart, which meant they were almost λ_0, apart, since for the corrugated surface used $\lambda_0/\lambda_g = 1.07$. To correct this, a grounded-dielectric slab ($\lambda_0/\lambda_g = 2$) was substituted for the corrugated surface and the wicket experiments repeated. Once again, it proved possible to get a broadside beam, but the pattern was no closer to optimum than before.

To summarize, a course study of parasitic arrays fed by trapped waves was undertaken during which over 150 patterns were recorded. This study revealed that power can be coupled to the parasites and radiated broadside. This effect was noted chiefly with tilted dipoles and with wickets. Moderate adjustments in the coupling parameters caused radical changes in the patterns. This is not surprising when one realizes that the parasites are being excited by an open one-wire transmission line. Consequently, every coupling causes creation of higher-order modes which cannot be damped out and the wave structure along the trapping medium becomes radiative and extremely complicated. The interrelations between the control parameters consequently become complex and it seems reasonable to assume that the proper balance of these parameters to achieve a desired pattern is most critical. The significance of the present study is that it has proved possible to alter the pattern substantially by the use of parasites. Predictable control must await a more refined experimental apparatus, one which will permit fine adjustment of frequency, degree of trapping, array spacing, and coupling dimensions.

Tropospheric Refraction Near Hawaii*

GROTE REBER†

PRIOR to undertaking radio astronomy experiments atop Haleakala volcano on the island of Maui in Hawaii it was decided to investigate the stability of the lower atmospheric bending over the sea using meteorological data.

The first set of data consisted of airplane observations taken at Honolulu during the years 1936 through 1942 about 5 or 6 A.M., using hair hygrometers. This data was on a summary basis, giving daily information at levels of 0.006, 0.5, 1.0, 1.5, 2.0, 2.5, 3, 4 and sometimes 5 kilometers. Data at 10 and 18 km as provided by radiosondes during 1945 were attached thereto. The index of refraction was computed from the relation[1]

$$(n - 1) \times 10^{-6} = 79p/T + 3.79 \times 10^5 e/T^2. \quad (1)$$

One hundred representative days were sampled for both January and July. The incremental bending was computed for each of the above ten levels and a constant of 0.44 milliradians was added to allow for the bending above 18 km. Mount Haleakala has an altitude of 3.066 km, so a suitable interpolation was made for this level. The results are given in Tables I and II for a ray arriving at 0 degrees elevation. In the limit of a great number of observations the sum of the medians should equal the median of the sums if the deviations are small and random. The closeness with which 100 observations approach this limit gives confidence as to the internal consistency of all the data and their interpretation. The sum of the scatter will exceed the scatter of the sums because the variations in the bending of the different layers will partially compensate one another on any given day. If all n levels had equal ranges of scatter and the scatter was random and independent, then the total scatter would be the sum of the individual scatter divided by $(n)^{1/2}$. To a reasonable approximation this is true. Thus the 100 days are a significant sample. As might be expected the positive deviations exceed the negative, except the 90 per cent values within the level 1,000 to 3,066 meters. This is the level containing the trade wind inversion and hence the reverse asymmetry of the scatter. When the ray arrives at 1.42 degrees elevation the results are shown in Tables III, and IV (next page). The bending is less, particularly in the lower layers and the scatter is much less. Also the sum of the scatter is markedly less than the scatter of the sums divided by $(n)^{1/2}$.

TABLE I

JANUARY, 0.00 DEGREE ELEVATION, 6 A.M., HONOLULU

Level	Median	Scatter range: 50 per cent of values		Scatter range: 90 per cent of values	
		−	+	−	+
	Bending in Milliradians				
0– 500	4.42	0.90	1.75	2.70	3.20
500–1,000	1.63	0.23	0.49	0.76	1.61
1,000–3,066	5.11	0.44	0.47	1.49	1.05
3,066–Top	4.67	0.15	0.33	0.28	0.72
Sums	15.83	1.72	3.04	5.23	6.58
0–Top	16.23	1.10	1.47	2.73	3.86

TABLE II

JULY, 0.00 DEGREE ELEVATION, 6 A.M., HONOLULU

Level	Median	Scatter range: 50 per cent of values		Scatter range: 90 per cent of values	
		−	+	−	+
	Bending in milliradians				
0– 500	4.66	0.91	1.00	1.96	3.29
500–1,000	1.90	0.34	0.27	0.88	1.30
1,000–3,066	5.17	0.40	0.38	1.30	1.27
3,066–Top	4.94	0.22	0.25	0.49	0.70
Sums	16.67	1.87	1.90	4.63	6.56
0–Top	16.92	0.98	0.70	2.30	2.99

TABLE III

JANUARY, 1.42 DEGREE ELEVATION, 6 A.M., HONOLULU

Level	Median	Scatter range: 50 per cent of values		Scatter range: 90 per cent of values	
		−	+	−	+
	Bending in milliradians				
0– 500	0.89	0.15	0.24	0.51	0.48
500–1,000	0.74	0.10	0.20	0.32	0.83
1,000–3,066	3.16	0.27	0.25	0.91	0.52
3,066–Top	3.98	0.10	0.26	0.22	0.64
Sums	8.77	0.62	0.95	1.96	2.47
0–Top	8.89	0.25	0.31	0.67	0.60

A second set of data consisted of 60 days of radiosonde observations taken about 4:30 A.M. during December, 1946 and January, 1947, using electric hygrometers. All significant levels were included. These varied from 14 to 29 with an average of about 24 each day. This was as much fine structure as the observations would provide and much finer than the end results warranted. At pressures above 950 mb the data was arbitrarily divided

* Original manuscript received by the PGAP, December 10, 1954; revised manuscript received, March 17, 1955. This study is part of a general investigation of radio astronomy supported by the Research Corporation.

† Hobart, Tasmania, Australia.

[1] M. Schulkin, "Average radio-ray refraction in the lower atmosphere," PROC. IRE, vol. 40, pp. 554–561; May, 1952.

TABLE IV

JULY, 1.42 DEGREE ELEVATION, 6 A.M., HONOLULU

Level	Median	Scatter range: 50 per cent of values		Scatter range: 90 per cent of values	
		−	+	−	+
	Bending in milliradians				
0– 500	0.93	0.15	0.16	0.35	0.48
500–1,000	0.86	0.14	0.11	0.36	0.50
1,000–3,066	3.23	0.27	0.13	0.72	0.50
3,066–Top	4.16	0.14	0.21	0.32	0.48
Sums	9.18	0.70	0.61	1.75	1.96
0–Top	9.19	0.19	0.20	0.43	0.63

TABLE V

DECEMBER, 1946, AND JANUARY, 1947, 0.00 DEGREE ELEVATION, 4:30 A.M., HONOLULU

Level	Median	Scatter range: 50 per cent of values		Scatter range: 90 per cent of values	
		−	+	−	+
	Bending in milliradians				
0– 200	2.91	0.93	0.72	2.00	4.95
200– 500	1.91	0.34	0.56	0.78	1.07
500–1,000	1.86	0.24	0.29	0.61	0.56
1,000–3,066	4.69	0.35	0.38	0.83	1.28
3,066–Top	4.57	0.32	0.42	0.60	0.70
Sums	15.94	2.18	2.37	4.82	8.56
0–Top	16.18	1.30	0.95	2.41	3.99

TABLE VI

DECEMBER, 1946, AND JANUARY, 1947, 0.00 DEGREE ELEVATION, 4:30 A.M., HONOLULU

Level	Median	Scatter range: 50 per cent of values		Scatter range: 90 per cent of values	
		−	+	−	+
	Bending in milliradians				
0– 200	2.91	0.93	0.72	2.00	4.95
200– 500	1.91	0.34	0.56	0.78	1.07
500–1,000	1.86	0.24	0.29	0.61	0.56
Sums	6.68	1.51	1.57	3.39	6.58
0–1,000	6.69	1.01	0.76	2.24	3.83

TABLE VII

JANUARY AND FEBRUARY, 1952 AND 1953, 0.00 DEGREE ELEVATION, 4:30 A.M., *Union*

Level	Median	Scatter range: 50 per cent of values		Scatter range: 90 per cent of values	
		−	+	−	+
	Bending in milliradians				
0– 200	3.14	0.61	0.82	1.27	3.15
200– 500	1.84	0.30	0.32	0.69	0.99
500–1,000	1.85	0.26	0.26	0.56	2.59
Sums	6.83	1.17	1.40	2.52	6.73
0–1,000	6.97	1.14	1.42	2.00	4.36

into levels of 20 to 30 mb, mainly because the largest bending and scatter in bending occur near sea level. A revised index of refraction was used,

$$(n - 1) \times 10^{-6} = 77.6p/T + 3.74 \times 10^5 e/T^2. \quad (2)$$

The results are shown in Table V. These are in close agreement with Table I, so the attempt at improved accuracy was not successful. Table VI is a partial breakdown of Table V for comparison with Table VII.

The ray of cosmic static would touch the open sea about 50 to 140 miles from land, and open sea conditions would prevail where most of the bending occurred. Since the first and second sets of data were taken where a land breeze probably existed, these might not be representative of open sea conditions. Consequently a third set of data was computed at a considerably later date. They were taken by radiosonde at 4:30 A.M. from the weather ship *Union* about 600 miles ENE of Maui. One hundred days observations during January and February, 1952 and 1953, were used. Again the data was taken off the daily work sheets. However, only five to eight levels up to slightly over one kilometer altitude were used. Higher altitude data was omitted because the bending in the upper parts of the atmosphere had been sufficiently well-established and at *Union* the trade wind inversion is lower and of greater magnitude than near Hawaii. Electric hygrometers were used and the relation (2) applied. The results are shown in Table VII and are quite close to those of Table VI. However, the sum of scatter is nearly identical with scatter of sums, and not $(n)^{1/2}$ as great. Thus there is little compensating effect between levels. Apparently over open sea a wet or dry state exists quite uniformly from sea level up to at least one kilometer with little stratification.

A ray arriving at 0 degrees elevation will have a bending in summer about four per cent greater than in winter. The scatter in winter will be about one and a third times as large as in summer. When the elevation angle of the ray is increased to 1.42 degrees, the bending is about 55 per cent and the scatter about one fifth of the corresponding values for a ray with an elevation of 0 degrees. When it was possible to assess the tropospheric bending, it has always been well within the scatter range of 90 per cent of the values and usually within the range of half of the values deduced above. Positive bending is downward toward the earth. Small negative or upward bendings were frequently encountered. Only on January 31st, 1952, at *Union* was the positive bending greater than the curvature of the earth such that a duct was formed.

Effect of Arbitrary Phase Errors on the Gain and Beamwidth Characteristics of Radiation Pattern*

D. K. CHENG†

Summary—**Simple expressions have been obtained for predicting the maximum loss in antenna gain when the peak value of the aperture phase deviation is known. It is not necessary to know the exact amplitude or phase distribution function as long as the phase errors are relatively small; and the same expressions may be used for both rectangular and circular aperture cases. Relations have also been established such that the maximum change in the main-lobe beamwidth can be predicted from the knowledge of the amplitude distribution function and the peak phase deviation.**

Introduction

IT IS KNOWN that for a given amplitude illumination function, a uniform phase distribution over the aperture plane of a microwave antenna reflector gives a maximum gain. A uniform phase distribution requires an exact parabolic surface in addition to a correct primary feed. Any deviation from the exact parabolic surface will introduce phase errors, which in turn will cause a reduction in gain. Unfortunately phase errors are often quite arbitrary and it is in general not possible to insert them under integral signs, weight them properly with the amplitude function, and perform integrations. Ruze[1] has investigated the effect of random phase errors on the radiation pattern as a statistical problem and obtained approximate formulas for the reduction in gain. However, as a statistical problem, only the average behavior of a large number or an ensemble of seemingly identical antennas and the probability distribution of the members of the ensemble about an average radiation pattern can be discussed; the individual patterns will differ from the system-average pattern. By a least-square analysis, Spencer[2] obtained an approximate expression for the fractional loss in gain due to small phase errors. In order to estimate the loss quantitatively it would be necessary to determine the plane least-square solution of the wavefront from a complete knowledge of the amplitude illumination function and the phase-error function over the aperture. The integration process involved is in general very difficult to carry out.

In practice, it is desirable to be able to predict the *maximum* effect on the gain, main-lobe beamwidth, etc., if the peak phase error is given for an *individual* antenna, even when the exact phase distribution is not known or too complicated for analysis. This paper presents a simplified approach with which the maximum loss in gain and the maximum change in beamwidth due to small arbitrary phase errors can be estimated.

Phase-Error Effect on Antenna Gain

Consider the case of a rectangular aperture with separable, symmetrical field distribution. The maximum value of gain function, or simply gain, can be written as

$$G = \frac{2\pi A}{\lambda^2} \frac{\left| \int_{-1}^{1} f(x)dx \right|^2}{\int_{-1}^{1} |f(x)|^2 dx}, \tag{1}$$

in which all notations are conventional. The aperture-field distribution function $f(x)$ is in general

$$f(x) = F(x)\epsilon^{j\phi(x)}, \tag{2}$$

where $F(x)$ is the amplitude illumination function and $\phi(x)$ represents the phase function. It is implied in (1) that the phase error is small and that maximum radiation occurs along the axis of the reflector. $\phi(x)$ may vary in an unknown manner across the aperture but it is assumed that the maximum deviation from an average value is known or can be estimated:

$$|\Delta\phi(x)| = |\phi(x) - \overline{\phi(x)}| \leqq m, \qquad -1 \leqq x \leqq 1. \tag{3}$$

In (3), $\overline{\phi(x)}$ is the average value; it will have no effect on the gain since the term $\epsilon^{j\overline{\phi(x)}}$ can be taken out from under the integral sign. Only the phase deviation $\Delta\phi(x)$ from this average value is of importance. Substituting (2) in (1), one has

$$G = \frac{2\pi A}{\lambda^2} \frac{\left| \int_{-1}^{1} F(x)\epsilon^{j\Delta\phi(x)}dx \right|^2}{\int_{-1}^{1} |F(x)|^2 dx}. \tag{4}$$

When there is no phase error, the maximum gain is

$$G_0 = \frac{2\pi A}{\lambda^2} \frac{\left| \int_{-1}^{1} F(x)dx \right|^2}{\int_{-1}^{1} |F(x)|^2 dx}. \tag{5}$$

Hence, for $F(x) \geqq 0$,

$$\frac{G}{G_0} = \frac{\text{gain with phase error}}{\text{gain without phase error}} = \frac{\left| \int_{-1}^{1} F(x)\epsilon^{j\Delta\phi(x)}dx \right|^2}{\left| \int_{-1}^{1} F(x)dx \right|^2} \tag{6}$$

* Original manuscript received by the PGAP, February 18, 1955; revised manuscript received, April 14, 1955.

† Electrical Engrg. Dept., Syracuse University, Syracuse, N. Y.

[1] J. Ruze, "Effect of Aperture Distribution Errors on the Radiation Pattern," Antenna Lab. Memo., AF Cambridge Res. Center; January 22, 1952.

[2] R. C. Spencer, "A Least Square Analysis of the Effect of Phase Errors on Antenna Gain," Rep. No. E5025, AF Cambridge Res. Center; January, 1949.

Examining the numerator of (6) for small $\Delta\phi(x)$ values, i.e., when

$$\epsilon^{j\Delta\phi(x)} \cong 1 - \tfrac{1}{2}[\Delta\phi(x)]^2 + j\Delta\phi(x), \tag{7}$$

which holds for $(\Delta\phi)^3/3! \ll \Delta\phi$, or $\Delta\phi \ll \sqrt{6} = 2.45 = \pi/1.28$,

$$\left| \int_{-1}^{1} F(x)\epsilon^{j\Delta\phi(x)}dx \right|^2 \cong \left\{ \int_{-1}^{1} F(x)\left[1 - \frac{(\Delta\phi)^2}{2}\right]dx \right\}^2 + \left\{ \int_{-1}^{1} F(x)\Delta\phi dx \right\}^2. \tag{8}$$

The first term on the right-hand side of (8) is

$$\left\{ \int_{-1}^{1} F(x)[1 - (\Delta\phi)^2/2]dx \right\}^2 = \left\{ \int_{-1}^{1} F(x)dx - (1/2)[\Delta\phi(\xi)]^2 \int_{-1}^{1} F(x)dx \right\}^2 \geqq \left(1 - \frac{m^2}{2}\right)^2 \left| \int_{-1}^{1} F(x)dx \right|^2. \tag{9}$$

Eq. (9) is the result of the application of the mean-value theorem [$\Delta\phi(x)$ is continuous and $F(x)$ is positive within the range of integration; $-1 \leqq \xi \leqq +1$] and relation (3). The second term on the right-hand side of (8) is

$$\left\{ \int_{-1}^{1} F(x)\Delta\phi dx \right\}^2 \geqq 0. \tag{10}$$

Substituting (9) and (10) in (8), and then back into (6), one obtains

$$\frac{G}{G_0} \geqq \left(1 - \frac{m^2}{2}\right)^2. \tag{11}$$

Eq. (11) is a useful relation because it sets the lower bound for the gain when the maximum phase deviation m is known; it is independent of the amplitude illumination function $F(x)$ and the exact variation of $\Delta\phi(x)$. From (11), one also readily obtains the maximum fractional reduction in gain

$$\frac{\Delta G}{G_0} = 1 - \frac{G}{G_0} \leqq m^2\left(1 - \frac{m^2}{4}\right). \tag{12}$$

It can be shown that for reflectors with circular aperture and symmetrical field distribution, (6) will be changed to the following:

$$\frac{G}{G_0} = \frac{\left| \int_0^1 F(\rho)\epsilon^{j\Delta\phi(\rho)}\rho d\rho \right|^2}{\left| \int_0^1 F(\rho)\rho d\rho \right|^2}. \tag{13}$$

Provided (7) is satisfied for small phase deviations, the derivation procedure is entirely similar, and one also obtains (11) and (12) as the result.

As an example, if $m = \pi/16 = 0.1964$ (corresponding to $\lambda/32$ in terms of wavelength λ), the *minimum* G/G_0 is 0.9618 which corresponds to a *maximum* reduction in gain of 0.169 db. The *maximum* fractional reduction in gain from (12) is 0.0382 or 3.82 per cent.

When the phase distribution function is such that the maximum radiation does not occur along the axis of the aperture, for instance, if $\phi(x)$ is not an even function of x in the rectangular aperture case, then the gain formula as given by (6) does not give the maximum gain ratio, but the lower bound as given by (11) still holds and is on the safe side.

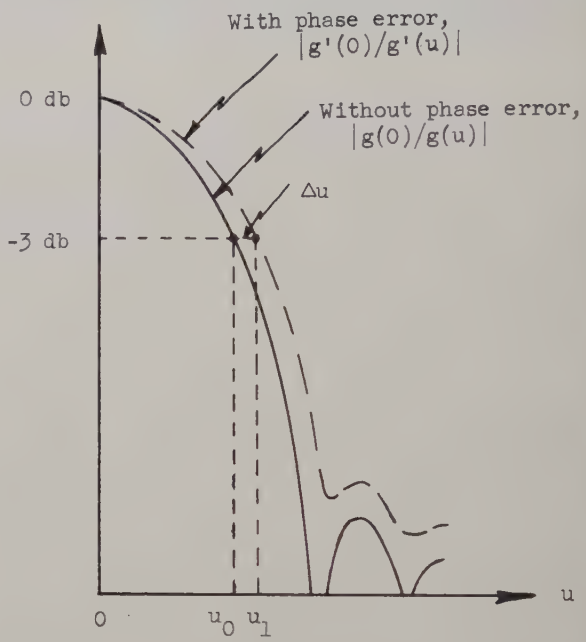

Fig. 1—Normalized radiation patterns. $u = (\pi D/\lambda)\sin\theta$

Phase-Error Effect on Beamwidth

When the phase error is small, an estimate on the maximum change in the main-lobe beamwidth of the radiation pattern can also be obtained. Consider this time the case of a circular aperture. It is necessary to assume here that both the amplitude and the phase distribution functions in the aperture plane are circularly symmetrical. In Fig. 1 are plotted two normalized radiation patterns, one without phase error $|g(0)/g(u)|$ and one with phase error $|g'(0)/g'(u)|$, where

$$g(u) = \int_0^1 F(\rho)J_0(u\rho)\rho d\rho \tag{14}$$

$$g'(u) = \int_0^1 F(\rho)J_0(u\rho)\rho\epsilon^{j\Delta\phi(\rho)}d\rho. \tag{15}$$

The condition for equal normalized radiation level is

$$\left| \frac{g'(0)}{g'(u_1)} \right| = \left| \frac{g(0)}{g(u_0)} \right|, \tag{16}$$

which would be equal to $10^{3/20}$ at 3 db down. It is noted that for $u \leqq 2.405 = \pi/1.3$, the integrand in (14) is always greater than or equal to zero and the following inequality holds:

$$| g'(u) | \leqq g(u). \tag{17}$$

When the small phase error condition as indicated in (7) is satisfied (with x changed to ρ in this case), one may go through the same reasoning that led to (11) and get the relationship

$$| g'(u) | \geqq \left(1 - \frac{m^2}{2}\right) g(u). \tag{18}$$

Combining (16), (17) and (18), one obtains

$$g(u_1) \geqq | g'(u_1) | \geqq \left(1 - \frac{m^2}{2}\right) g(u_0). \tag{19}$$

For small phase errors, the change in beamwidth is small and it is convenient to write

$$u_1 = u_0 + \Delta u, \qquad \Delta u \ll 1. \tag{20}$$

Substitution of (14), (15) and (20) in (19) yields the following result:

$$\Delta u \leqq \frac{m^2}{2} \frac{\int_0^1 F(\rho) J_0(u_0\rho)\rho d\rho}{\int_0^1 F(\rho) J_1(u_0\rho)\rho^2 d\rho} = \frac{m^2}{2}\left[\frac{g(u)}{-\frac{d}{du} g(u)}\right]_{u_0}. \tag{21}$$

Eq. (21) furnishes an upper bound in the change in half-beamwidth for a given maximum phase error; it is dependent upon the amplitude illumination function $F(\rho)$.

For the case of a rectangular aperture, the following expression is obtained by a similar procedure (for $u \leqq \pi/2$):

$$\Delta u \leqq \frac{m^2}{2} \frac{\int_0^1 F(x) \cos(u_0 x) dx}{\int_0^1 F(x)\, x \sin(u_0 x) dx} = \frac{m^2}{2}\left[\frac{g(u)}{-\frac{d}{du} g(u)}\right]_{u_0}. \tag{22}$$

It is seen that (22) is entirely similar to (21). Results listed in Table I are for the simplest case of uniform amplitude illumination function. The maximum change in beamwidth for other typical amplitude illumination functions can similarly be computed; there is no need to know the exact phase deviation curve. Eqs. (21) and (22) do not give useful information for very small u_0-values but are very helpful in estimating changes in 3-db beamwidth. Moreover, it can be proved that when u_0 is small compared with unity, Δu is always smaller than u_0.

TABLE I

MAXIMUM 3-DB BEAMWIDTH CHANGES FOR UNIFORM AMPLITUDE FUNCTION

		Rectangular aperture	Circular aperture
Amplitude function		$F(x) = 1$	$F(\rho) = 1$
Half 3-db beamwidth (no phase error), u_0		0.45π	0.51π
$m = 0.1$	Δu	$\leqq 0.00918$	$\leqq 0.011$
	$\Delta u/u_0$	$\leqq 0.65$ per cent	$\leqq 0.68$ per cent
$m = 0.2$	Δu	$\leqq 0.0367$	$\leqq 0.044$
	$\Delta u/u_0$	$\leqq 2.6$ per cent	$\leqq 2.8$ per cent

CONCLUSION

It has been shown that for small phase errors, simple expressions (11) or (12) can be used to compute the maximum possible loss in antenna gain when the peak values of the phase deviation is known. It is not necessary to know the exact amplitude or phase distribution function in the aperture; and the same expressions apply to both rectangular and circular aperture cases. Similarly, (21) and (22) can be used to compute the maximum possible change in half 3-db beamwidth, which is dependent upon the amplitude illumination and is different for the rectangular and circular aperture cases.

ACKNOWLEDGMENT

The author wishes to acknowledge the valuable assistance of Pranas Grusauskas in the final preparation of this paper.

Abstracts of Papers From the IRE-URSI Symposium Held May 2–5, 1955—Washington D. C.

The International Geophysical Year—J. Kaplan, *University of California*—The progress of plans for U. S. participation in the International Geophysical Year will be reviewed. The proposed program will be briefly described under the following fields: aurora and airglow, cosmic rays, geomagnetism, glaciology, ionospheric physics, meteorology, seismology and gravity, solar activity, latitude and longitude, oceanography, and rocket exploration of the upper atmosphere. The major geographical regions in which the U. S. will operate are (1) arctic and sub-arctic, (2) middle latitudes of the northern and southern hemispheres (including the United States, Central America, South America, and adjacent parts of the Atlantic and Pacific Oceans), (3) the equatorial Pacific, and (4) the antarctic and sub-antarctic.

Wave Coupling by Warped Normal Modes—A. G. Fox, *Bell Telephone Laboratories*—It has been shown by J. S. Cook that wave power may be transferred from one to another of two coupled waveguides through a variation of their phase constants. It is now clear that this is but one example of a new principle of coupling which is here called "normal mode warping." Wave power inserted at one end of a coupled waveguide system may be made to appear at the other end with any desired power distribution by gradual warping of the normal mode field patterns along the coupler. In general, both variation of the coupling coefficient and phase constants are required. Much wider bands are theoretically possible than with any other distributed type of coupler. This principle may be applied to dielectric waveguides, birefringent media, and waveguides containing ferrite, to obtain both reciprocal and nonreciprocal couplers.

Investigations of Angular Scattering and Multipath Properties of Tropospheric Propagation of Short Radio Waves Beyond the Horizon*—J. H. Chisholm, P. A. Portmann, J. T. deBettencourt, and J. F. Roche, *Massachusetts Institute of Technology*—Experimental investigations of uhf and shf propagation over paths well beyond the horizon have been conducted over the period March, 1953 to March, 1955, in order to explore the potential capacity of tropospheric scattering for useful communications over paths 150–200 miles in length. Analysis of measurements of signal levels obtained over a 164-mile path utilizing a high powered uhf transmitter with a directive antenna system and a variety of directive-receiving antenna systems is described, together with the results of several early observations of narrow and broad band frequency modulation studies conducted in cooperation with Major E. H. Armstrong.

A concurrent propagation research program at 3,670 mc, utilizing large highly directive 28-foot diameter paraboloidal antennas, capable of rotation in azimuth and elevation, was conducted in order to explore the angular scattering of these cm radio waves by the troposphere over a 188-mile path. Results of measurements of the signal level received for simultaneous positioning of the narrow beams of the transmitting and receiving antennas at 0.1 degree angular increments in azimuth and elevation are described. Analysis of 3,000 hours of signal level measurements have been made for a study of hourly, diurnal, and seasonal variations of signal levels, together with a comparison of signal levels received over the experimental path utilizing a variety of combinations of 5-foot and 28-foot diameter paraboloidal transmitting and receiving antennas. The results of photographic recording of short pulses transmitted over a variety of antenna combinations and signal level conditions have been obtained in a study of multipath properties of the troposphere. Joint experimental studies of modulation utilizing a 5,050 mc cw system were conducted with the Bell Telephone Laboratories.

* The research in this document was supported jointly by the Army, Navy, and Air Force under contract with the Mass. Inst. Tech

The Effect of Tides and Electric Currents in the Upper Atmosphere on the Ionospheric Characteristics in Equatorial Regions—G. J. Gassmann, *Air Force Cambridge Research Center*—In the different successive attempts to bring atmospheric tides, electric current systems in the upper atmosphere, and anomalies of the ionosphere into causal connection, some additional effects were still disregarded. In the example of solar tides, elementary considerations lead to the conception of a corresponding current system which fits the experimental data of atmospheric pressure as well as both magnetic and ionospheric measurements. The current system is considered to establish its own impedance path especially in equatorial regions by forming a thin belt around 100-km altitude. In equatorial zones the prevailing effect of atmospheric tides on the *F*-region is caused indirectly through their current belt by electro-magnetic induction causing another weaker current system and consequently upward or downward drift of ionized matter. Several world-wide distributions of ionospheric characteristics are discussed, and original airborne ionospheric measurements are presented.

Absorption of Galactic Radio Waves at 21 CM Wavelength—J. P. Hagen, *Naval Research Laboratory*—The detection of the absorption of the continuous radiation from a radio source by neutral hydrogen is directly affected by the strength of the signal from the source as seen in the receiver. In all cases the strong radio sources are smaller in angular diameter than the effective beam widths of presently used antennas. The 50-foot antenna at NRL has a beamwidth at this wavelength of nearly one degree and produces a signal in the receiver from a radio source of at least four times that of any other antenna used in this work. Since in general the hydrogen subtends angles larger than the beamwidth, the hydrogen signals are independent of antenna size. This latter statement is not true, however, when the signals from individual hydrogen clouds are considered.

The receiver used in this work is similar to that used at Harvard but differs from that used in every other installation. In the NRL receiver two bands of information are constantly received. The separation of the bands is fixed, but the frequency to which they are tuned may be changed. In this way profiles are obtained by tuning the signal band through the frequency region where hydrogen emission exists. The signal band accepts a frequency band of 5 kc as compared with 15 to 50 kc of other equipments. The comparison band is 2 mc wide and is displaced in frequency so far from the signal band that hydrogen emission does not normally enter.

The signal band thus contains power from the hydrogen and also from the continuous radiation of the background, whereas the comparison band contains power from the background alone. The difference of the two yields the hydrogen profile modified by any absorption of the background, as shown by Lilley in a later paper.

It is from measurements of this sort made on a radio source on the region immediately surrounding the source that information concerning the absorption of the source radiation by the hydrogen is obtained. Of the known radio sources in this wavelength region there are five or six where meaningful measurements can be made with present equipment. For the other sources either the signal from the source is too small in relation to the uncertainty of the measurement or the source has not yet been observed in the survey.

The direction of the radio source Cygnus A is a few degrees out of the galactic plane, and the hydrogen profile shows a large contribution from the near arm but very little from the far arm. Absorption by hydrogen in the near arm is measured, but any effect in the far arm is too small to be observed. It is to be noted that our profile for this region bears little resemblance to that published by Williams and Davies (*Nature*, vol. 173, p. 1182; 1954) who show a relatively large contribution from the far arm. Our measurements place the source outside the near arm and do not deny the possibility that it is an extra-galactic object.

There is a clear case of absorption in the case of the radio source Taurus A, which is located near the region of the anti-center where little Doppler shift is expected and the hydrogen cannot be located in distance through a frequency shift. The profile for this region shows a large peak near the local standard of rest with some additional emission indicating a lesser amount of hydrogen approaching. The hydrogen in the main peak causes absorption and hence is located between the sun and the source, whereas there is an indication of no absorption on the approach side of the peak. This approaching hydrogen must then be beyond Taurus A.

Any absorption effects in Orion will be small due to the low antenna temperature of the Orion source. Profiles taken on and around the source show very steep gradients in this region. It can be reported that if there is absorption in this region the effect is too small to be seen in the uncertainty of the gradient.

In the direction of Cassiopeia strong absorption is found in the peaks of the profile corresponding to both the near and the far arm. The profiles are seen in detail and indicate the presence of three small dense clouds lying directly between the source and the receiver. One of the clouds is in the near arm and the other two in the far arm. If this interpretation is correct, then the source must be in or beyond the far arm, or at a distance of at least 3,000 parsecs.

Jupiter as a Radio Source—B. F. Burke and K. L. Franklin, *Department of Terrestrial Magnetism, Carnegie Institution of Washington, Washington, D. C.* Observations with a highly directional antenna at 22 mc were made during the first quarter of 1955 along strips of constant declination near the Crab Nebula. Nine out of thirty-one records showed an intermittent, strong source of radio noise

located approximately two hours east of the Crab Nebula. The apparent *Right Ascension* of the source moved slowly westward about twenty minutes *of time* over the three-month period. The motion, which indicated it was not a galactic object, corresponded to the normal geocentric motion of the planet Jupiter. No other planets fit the observed data. The emission was characterized by intense noise bursts of short duration, reaching a peak intensity greater than that of the Crab Nebula, and at times greater than that of any radio source in the sky. The duration of each burst is of the order of half a second. There is evidence that the intensity drops by a factor of at least 150 between 22.2 and 38.7 mc, although the bursts are still strong at 27 mc. Furthermore, there is poor or no correlation between occurrence of the phenomenon and the central meridian of Jupiter's disk, nor is there correlation with solar activity.

The mechanism responsible for the noise generation is not understood. It is tempting to ascribe the phenomenon to atmospheric disturbances similar to thunderstorms, although the observed intensity and frequency spectrum are very different from terrestrial storms. Meteorological studies of Jupiter's atmosphere have been made,* but the electrical properties are not well known.

Gradmeter—M. Graham, *Brookhaven National Laboratory*—The accurate measurement of a magnetic field gradient is required in the testing of magnets for a new accelerator under development at Brookhaven National Laboratory. An instrument was built which vibrates a search coil in the magnetic field and vibrates a reference coil on the same shaft in a reference magnet. The voltages induced in the two coils are compared in a modified bridge circuit whose null is set by a self-balancing arrangement which also runs a recorder pen. The entire device produces graphs of normalized gradient vs position.

A Method for Measurement of a Two-Terminal Impedance—B. Salzberg and K. W. Bewig, *Naval Research Laboratory*—A simple method has been devised for measuring the real and quadrature components of a two-terminal impedance. It requires only a source, a vacuum-tube voltmeter, and a calibrated adjustable resistance or reactance. The latter may consist merely of several resistors or capacitors whose values have been accurately determined. One terminal of both the source and the voltmeter is grounded so that the method, unlike the well-known three-voltmeter method, is useful even at radio frequencies. Moreover, the impedance to be measured also may have one terminal grounded, or it may be entirely above ground. The unknown impedance Z is connected in series with the known adjustable resistance or reactance z and with the source. The voltmeter is used to observe the source voltage V_1 and the voltage drop V_2 across the grounded impedance, which may be either Z or z. Voltmeter readings are taken for several values of z, and the observations are arranged in such a way that, when plotted, a straight line is obtained. (It will be shown that for any two-terminal impedance whatever the observations can always be cast in a form which will lead to a straight-line plot). The real and quadrature components of Z are then determined from the slope and intercept of this straight line.

Measurement of Signal Generator Modulation Factor—H. S. Ingraham, Jr., *Radio Corporation of America*—This paper is devoted to three objectives: (1) a brief review of techniques presently being used to monitor modulation factor in signal generators, (2) a limited discussion of the more common techniques used for precision measurement and calibration of modulation factor, and (3) a more detailed presentation of precision techniques developed at RCA.

By far the great majority of signal generators indicate modulation factor by one method, which consists of measuring the audio signal level derived from the modulator carrier at a particular rf level, usually the "set level" point. Variation in and difficulties with this method will be discussed briefly.

Several precision or semi-precision techniques exist for measurement of modulation factor. Probably the most familiar of these is the trapezoid pattern presented on an oscilloscope. This method has its limits of application and inherent difficulties, as do others of a similar nature. A short discussion of these methods is included.

Several new techniques of measurement have been devised at RCA, and these are discussed at some length. They include a peak-reading voltmeter technique applicable up to about 700 mc, a power measurement technique for use at uhf and microwave frequencies, a spectrum analyzer technique, and a completely new comparison technique to precision laboratory calibration and factory monitoring. Applications of these techniques to signal generator calibration and monitoring are discussed.

A Recording Amplitude Distribution Analyzer—H. D. Hern and I. H. Gerks, *Collins Radio Company*—A new instrument is described whose principal function is that of yielding a continuous record of the median level of a fluctuating signal which is exceeded an arbitrary percentage of the time. An important feature is that the necessity of photographing counters at regular intervals and drawing distribution curves, required with previous instruments of this general type, is eliminated. As the signal level varies, schemes are employed to derive, record, and automatically adjust the threshold level so as to allow the signal to exceed the threshold level some arbitrary percentage of the time. Typical operating data are included.

An Automatic Record Chart Analyzer—H. Ahrens, *Navy Electronics Laboratory*—The Automatic Record Chart Analyzer (ARCA) has been developed to facilitate the reduction of radio field-strength data recorded on plain paper charts by graphic recorders. It is an electronic equipment which automatically samples the data on the record chart and inserts any required calibration curve. The corrected data are presented in the form of a width-modulated pulse, at the rate of sixty samples per second. This part of the analyzer is believed to be of most interest and is described in this paper. The subsequent determination of specific data characteristics, such as average signal level, accumulative amplitude distribution, and power spectra, is accomplished by means of conventional equipment and will not be discussed.

Use of the ARCA for the reduction of radio fading and scattering data has proved quite satisfactory. For the ideal case, any given chart data level is reproduced at the output, in terms of pulse width, with 1 per cent of full-scale accuracy. In practice, the accuracy is a function of the condition of the record, the character of the recorded data signal, the type of calibration curve required, and the nature of the analysis to be performed.

A Probability Computer for Noise Measurement—J. D. Wells and A. W. Sullivan, *University of Florida*—The first amplitude probability distribution function of a noise envelope is measured with the equipment described in this paper. Accuracy on the order of 1 per cent is obtained for each measured point, and the entire distribution may be determined over a dynamic range of 100 db with good accuracy when several points are measured simultaneously. The unit is designed to operate from the intermediate frequency signal of a communications receiver. A complete noise meter is discussed which employs the probability computer and is used principally in the study of atmospheric noise.

Propagational and Jamming Advantage of Compressed Signals—H. S. Marsh—A paper on Bandwidth Reduction at the recent Boulder NBS Symposium aroused some controversy in using Shannon's Trading theorem to show that the transformation illustrated apparently permitted "trading bandwidth for power, without increasing power." This phrase apparently liberates high deviational entropies.

The Trading Theorem is examined more closely herein. Using the previous illustration of mapping facsimile, it appears that, to maintain an original satisfactory s/n value, transmitted power increases of the order of the 0.75 power of the bandwidth reduction ratio would be necessary. This is found to be incorrect.

Roughly, a 2:1 compression might require a few per cent power increase. A 10:1 compression, simply feasible with current military equipment, indicates about a 3:1 power increase, while a 100:1 compression, if feasible, would require only around 9:1 power increase.

A propagational survey of Communication in the Presence of Nature shows that even this is unnecessary. Using standard military Carrier-shift equipment, and applying Crosby's "FM Advantage Factor" for the reduced keying rate, shows that the improved deviation ratio more than balances the initial s/n degradation, both for maximum and average keyspeeds. The multipath advantage gained is clear profit.

For confirmation, simulated test results are shown. Dots representing original maximum keyspeed first, followed by longer, variable-level signals duplicating the transformed compressional signals, are subjected to various conditions of filtering, noise and tone injection, and delayed path echo simulation.

Degree of variance in accuracy of reception of the received durational signals, or degree of power increase necessary to maintain original duration measurement accuracy, with varying levels of noise or distortion introduced, is used to illustrate correspondence with theoretical results.

Summary of Refractive Index Fluctuation and Profile Measurements over Southeastern Colorado in August 1954—C. M. Crain, *University of Texas*, and C. A. Hines, *Wright Air Development Center*—This paper presents the summary of refractive index measurements made during August, 1954 from near ground level to an altitude of 20,000 feet over Southeastern Colorado. The measurements were made by the Propagation Unit of the Wright Air Development Center, using two models of the University-of-Texas-type refractometer mounted in a B-17 aircraft. One of these refractometers was arranged to measure profiles, and the other was especially built for measuring small fluctuations about the mean value of index of refraction. A brief description of the sensitive-scale refractometer, an instrument which can resolve rms index of refraction variations of the order of a hundredth N unit, is presented. Spectral density, rms, autocorrelation, and boundary sharpness analyses of the sensitive scale refractometer data are presented. A comparison between the characteristics of the index-of-refraction fluctuations obtained in August, 1954 and February, 1954, over the same area is made.

Propagation Measurement at 4.3 MM Wavelength—A. W. Straiton and C. W. Tolbert, *University of Texas*—Propagation measurements using a wavelength of 4.3 mm are described. These included 3.5- and 7-mile tests on a line-of-sight path overland and 7.25-mile measurement in a low-level surface duct along the Gulf of Mexico.

The overland data were taken on a number of days, and a graph is drawn showing the attenuation loss as a function of the moisture content of the atmosphere.

* U. S. AF Cambridge Res. Center, "The Study of Planetary Atmospheres," Preliminary Reports 1–9, Final Report, 1952.

The overwater data were also taken using wavelengths of 8.6 mm and 3.2 cm on 7.25 mile and longer paths and the attenuation of the three wavelengths compared.

Meteorological data taken simultaneously with the overwater data indicated a low-level irregular surface duct to be present almost all of the time.

Refraction Effects by Atmospheric Inhomogeneities—M. S. Wong, *Wright Air Development Center*—Ground-to-air propagation over land and sea shows occurrences of deep field-intensity fadings more closely spaced than accountable by smooth-earth reflections. Radio holes may also occur ground-to-air, in addition to their well-explored occurrences air-to-air.

Possible atmospheric conditions under which these phenomena occur are tentatively shown by ray tracing. The relevant conditions range from layers to small-size inhomogeneities —the layers extending a few hundred feet thick and up to hundreds of miles in distance, the small inhomogeneities of the order of 10 feet vertically and a few hundred feet horizontally. On a time-static (snap-shot) view, ray tracing gives spatial variations of densities, arrival angles, and path differences of rays in multipath transmission. These ray-theoretic results are useful preliminaries for needed wave-theoretic solutions.

Direct Ray—Line-of-Sight Propagation Phenomena—R. B. Muchmore and A. D. Wheelon, *Ramo-Wooldridge Corporation*—The effect of turbulence in the atmosphere on the phase stability and angular direction of arrival of radio waves is investigated. On the basis of a phenomenological model of the atmosphere, expressions for rms phase jitter are derived. The mean-square phase noise for a simple exponential correlation of the dielectric constant is

$$\overline{\alpha^2} = \frac{8\pi^2\,\overline{\Delta N^2}\cdot 10^{-12}\,l_0 L}{\lambda^2},$$

where $\overline{\Delta N^2}$ is the mean square index of refraction variation in N units l_0 is the scale length, L the path length, and λ the wavelength.

In addition to the phase noise on a single path, the correlations in phase between two parallel paths and also two paths with one endpoint in common are calculated. The angular deviations in angle of arrival are found and the correlations in these for the same sorts of paths as above. The probability densities in phase and angle of arrival are given.

Scattered Field—Line-of-Sight Propagation Phenomena—A.D. Wheelon and R. B. Muchmore, *Ramo-Wooldridge Corporation*—In the previous paper, the phase deviations experienced in line-of-sight propagation were investigated using a simple geometric, optics ray picture. The effect on the received phase of energy scattered into the receiver by off-axis turbulence clusters and raindrops is studied here. Using the scattering cross section of Booker and Gordon, the amount of off-axis energy scattered into the receiver is found and its angular distribution deduced. The rms phase error is sensibly independent of antenna beamwidth and is given approximately by

$$\langle\alpha^2\rangle = \frac{\pi^2}{2}\,\overline{\Delta N^2}\,10^{-12}\,\frac{L^2}{\lambda l_0},$$

where the symbols have their previous meaning. For paths of several miles and high frequencies, the direct wave result of the previous paper dominates over this scattered effect, which becomes important only for longer transmission paths.

The phase error for propagation through a region of rainfall is then calculated as a function of the rainfall rate. A Doppler scintillation spectrum for received phase due to relative drop motion is inferred from backscatter measurements.

Multipath Signal Distortion in Scatter Propagation—O. J. Jacomini, *General Electric Company*—A signal propagating through the atmosphere beyond the horizon by scatter means will traverse a large number of different paths. In general, these multiple paths will be changing with time. In this paper, the distortion of signals passing through this medium is investigated. The effect of the atmosphere is shown to be analogous to a filter which has a random time-varying impulse response. An equation for the autocorrelation function of a signal propagated through this medium is obtained. For a moderately wide receiver bandwidth, this result reduces to the product of the autocorrelation function of the transmitted signal and a function of the atmosphere which might be described as its autocorrelation function. An equation is also obtained for the ensemble average of a signal which is detected in a linear detector. For a wide-band receiver, this equation reduces to the square root of the convolution of the square of the input signal and a function of the atmosphere. This function is essentially the square of the ensemble average of the impulse response of the atmosphere.

Phenomenological Vector Model of Reflection of Microwaves From the Ocean Surface*—C. I. Beard, I. Katz, and L. M. Spetner, *Johns Hopkins University*—A model of one-way transmission of microwave electromagnetic signals over the ocean surface is developed from experimental observations and theoretical considerations. The received signal is described as a vector sum of a constant direct signal, a coherent reflected signal whose amplitude and phase are fixed by geometry, and a fluctuating reflected component of random amplitude and phase. The Rayleigh criterion $h\psi/\lambda$ is here suggested as a *quantitative* measure of water-surface roughness. ψ is the grazing angle, h the rms surface fluctuation and λ the wavelength of the radio signal. Experimental evidence is given to verify the theoretical relationship given by Ament and others for the normalized coherent term,

$$C/rD = \exp\,[-8(\pi h\psi/\lambda)^2],$$

where C is the coherent component, r the smooth sea reflection coefficient, and D the direct ray. The fluctuating term may be represented as

$$\sigma/rD = 0.33\{1 - \exp\,[-64(\pi h\psi/\lambda)^2]\}^{\frac{1}{2}}.$$

Forecasting Radio Propagation Conditions—A. G. McNish, *National Bureau of Standards*—An experiment was performed to ascertain the reliability of methods for forecasting the quality (Q-figures) of radio propagation conditions for paths traversing the North Atlantic Ocean by prediction formulas. The experiments were confined to forecasting for the first quarter of the Greenwich day which experience has shown is the most difficult to predict. Data used in the predictions were confined entirely to what was available two hours prior to the forecast interval. Because radio propagation conditions usually change little from day to day, fairly good predictions were possible using a linear regression equation involving Q-figures for the 52-hour interval preceding forecast time. However, this method failed to predict the onset of disturbance beginning during the forecast interval. To remedy this defect the prediction obtained by linear regression was corrected by applying a nonlinear term, based on the departure from normal of the vertical intensity of the earth's magnetic field as observed at the Cheltenham Magnetic Observatory (Maryland) during the five hours preceding forecast time. The forecast values of the Q-figures to obtained agreed with the final reported values as well as or better than the forecasts issued on an operational basis for the trial period, which was January 4-December 31, 1953. Since the operational forecasts are based on many more data than were employed in the trial forecasts, the possibility that the data used in operational forecasts may overdetermine the forecasts is recognized. Such conditions may be present in other types of predictions, such as meteorological forecasts.

* This work is suported by U. S. Navy Bureau of Ordnance under Contract NOrd 7386.

A Study of the Relative Merits of Horizontally and Vertically Polarized Skywave Signals Near the Gyromagnetic Frequency—C. S. Wright, *A. D. Ring and Associates*—This paper is an interpretation of the magneto-ionic theory to determine the effects of polarization of the exciting wave on skywave propagation at frequencies near the geomagnetic frequency. The Booker development of the theory is used as a basis for the interpretation. The comparison is made by studying the projection of the electric vector of the exciting plane wave on the polarization ellipses at the entrance of the reflecting layer. The traditional magneto-ionic co-ordinate system is converted into a more usable sperical co-ordinate system. This conversion is described in five equations. These equations are in a form to facilitate the use of the magneto-ionic theory for practical propagation problems. Simplifying assumptions are made on the magneto-ionic theory for the geomagnetic frequency. The simplified theory is then converted into the new co-ordinate system, and calculations are made for various propagation conditions which represent the relative merits of vertical and horizontal excited antennas. Several curves are given which graphically depict this relation, and a method for estimating the relation under more general conditions is suggested.

Ionospheric Layer Heights—L. A. Manning, *Stanford University*—One of the simplest methods for finding true height is that of Booker and Seaton. By assuming the layer of parabolic form, they showed that the true height of the layer maximum is equal to the virtual height at 83.4 per cent of the critical frequency. An extension of their analysis is given to include the effect of the earth's magnetic field.

For geomagnetic latitudes north of 45 degrees the longitudinal approximation of the magneto-ionic equations applies with very slight error. It then is possible to get analytic expressions for the virtual height of reflection from a parabolic layer. It is found that at these latitudes use of the Booker-Seaton analysis yields less error if applied to the extraordinary rather than the ordinary trace. Curves are produced showing the error in neglecting the magnetic field, and also the scaling frequency that gives the true height without error. The method may be of especial usefulness in the International Geophysical Year.

The Effect of Atmospheric Noise on a Manual Radiotelegraph System—R. F. Brown, *University of Florida*—The effect of atmospheric noise on a manual radiotelegraph system is evaluated in terms of statistical parameters of the interfering noise. Problems which arise and precautions which must be taken when human operators are a part of the system are discussed, and the techniques and equipment used in the experiment are described.

A study of the correlation between measured noise parameters and the interference effect of the noise on the system is made, and empirical relationships between the noise parameters and the letter error are derived. An expression for system reliability as a function of received signal strength and measured noise parameters is derived, and it is shown that this expression can be used for the prediction of system performance in the presence of atmospheric noise.

The Effect of Atmospheric Noise on a Frequency-Shift Radioteletype System.—S. P.

Hersperger, Jr., *University of Florida*—The effect of atmospheric noise on a frequency-shift radioteletype system is evaluated in terms of the statistical parameters of the interfering noise. An analytical approach is discussed, and the techniques and equipment used in the experimental evaluation of this effect are described in detail.

A study of the correlation between the measured noise and the system reliability is made. Empirical expressions relating the noise parameters and the expected letter error are derived from the results of this study. The system reliability is expressed as a function of measurable noise parameters, and it is shown that this expression can be used as a basis for predicting the performance of the system in the presence of atmospheric noise.

Lightning Discharge Atmospheric Interference in Aircraft Communications—M. M. Newman, *Lightning and Transients Research Institute*—The lightning discharge channel characteristics are among the most important factors in determining the nature of atmospherics affecting aircraft radio communications. The channel resistivities, surge impedances, and propagation velocities involve nonlinear variations which lead to complex stepped currents. Equivalent electrical circuits were developed for the channel which checked very well both in experiments and calculations taking into account nonlinear variation of the channel resistance.

Typical oscillographic records of lighting channel circuits and resultant radiated atmospheric wave shapes are presented. Frequency resolution of interference effects on a specially built up simplified panoramic interference analyzer indicate time variations of interference bursts to be expected at various communication frequencies of importance in considering communication reliability, and possible methods of improvement, under thunderstorm conditions.

Whistling Atmospherics Observed at Washington, D. C.—H. E. Dinger, *Naval Research Laboratory*—The majority of whistling atmospherics observed at Washington, D. C., during the past year, were of the type that follows the dispersion law discussed by Storey in his theory on their mode of propagation. Storey mentioned several types that were not explained by his theory. Additional types have been observed, on infrequent occasions at the Naval Research Laboratory that do not fit the theory in its present form. Spectrographic analysis has been made of examples obtained on tape recordings.

During one day of considerable activity, a number of otherwise normal whistlers took on an additional characteristic consisting of one or more rising tones which preceded and blended with the descending tone. On another occasion, each descending whistler associated with a lighting stroke was followed by two descending whistlers, of less dispersion, regularly spaced within each train when compared with other trains. On one occasion only, a reversing tone of the kind discussed by Burton and Boardman was heard.

Some additional evidence has been obtained that the "dawn chorus" has definite correlation with the aurora. Bright aurora was observed in the Washington area on the evening of January 17, 1955. On January 18, 19, and 20, excellent examples of the "dawn chorus" were observed. Neither phenomenon had been noticed during any of the observation periods for over two months previous to this date.

R. A. Helliwell, *Stanford University*, discussing observations made on the USS ATKA on her recent voyage to Antarctica.

M. G. Morgan, *Dartmouth College*, discussing records obtained at Dartmouth College and their correlation with records from Knob Lake, Quebec, Washington, D. C., and Gainesville.

Other contributions.

A Method of Wavelength Measurement for the Microwave and Millimeter Wave Regions—W. W. Balwanz, *Naval Research Laboratory*—The usual methods of determining frequency by wavelength measurements are not readily adapted for use in the millimeter region, i.e. between 4 and 0.1 mm. A survey of conventional methods, including standing waves in free space, slotted waveguide sections, resonant cavities, echelette gratings, Newton's rings, Michilson's interferometer and Fresnel interference patterns was made. Although each of these methods is theoretically usable, practical limitations on scaling, the control of illumination patterns, the separation of modes of excitation, the sensitivity of detectors, or the required precision of alignment make their application difficult, if not impractical. In some earlier work it was observed that an intermediate medium moved along the center line between a source and receptor antenna modified the output of the receptor antenna as a function of the position of the intermediate medium. A plot of this output vs the position of the interfering medium shows the variation to be periodic in half-wavelengths of the electromagnetic signal. This interference phenomenon has been investigated both experimentally and theoretically as a possible method of measuring wavelength, particularly for the millimeter region.

A Self-Balancing DC Bolometer Bridge—G. F. Engen, *National Bureau of Standards*—A self-balancing dc bridge, for use in bolometric power measurements, has been developed at the National Bureau of Standards, Boulder, Colo. This instrument combines the self-balancing convenience of ac bridges, and the accuracy of a high quality, manually operated, dc bridge. In addition, measurements may be made with a speed which greatly relaxes the stability requirements of the power source and measuring system. A preliminary evaluation of the errors attending this device, while incomplete, indicates an expected accuracy in excess of 0.5 per cent in the 1–10 mw range.

The self-balancing feature is achieved through use of a modified, commercially available, dc amplifier of excellent stability, with a current gain of approximately 50 db. This amplifier is connected in such a way that the bridge unbalance signal is amplified to produce the dc bridge power.

The problem of measuring the retracted dc power in the bolometer element is simplified, and an improvement in accuracy is achieved through use of a differential ammeter circuit, employing a constant current generator of high stability.

Antenna Pattern Measurements by Aircraft—H. Brueckmann, *Coles Signal Laboratory*—An improved method for measuring the space radiation pattern of large antennas, by means of an aircraft which was developed by the Signal Corps Engineering Laboratories, is described. A small battery-operated signal source using a dipole antenna is suspended horizontally or vertically, depending upon desired polarization, from an aircraft by means of a nylon string, representing a well-defined reference antenna. The aircraft is assigned to fly circles about the antenna under test at prescribed altitudes using a precision altimeter. The received signal at the terminals of the antenna under test is recorded. The elevation and azimuth angle of the aircraft as seen from the antenna under test is also recorded automatically by using standard tracking equipment for meteorological ballons on the ground, with the associated radiosonde-transmitter mounted on the aircraft. The signal strength and the position recordings are co-ordinated by means of an events marker. Details of the method, the equipment, sources of error, limitations, and advantages are discussed.

Standing-Wave Line for UHF Measurements of High Dielectric-Constant Materials—E. M. Williams, *Carnegie Institute of Technology*, and J. H. Foster, *Erie Resistor Corporation*—Samples of high-k ceramics are formed as rectangular parallelopipeds, silvered on two opposite sides. The silvered sides function as the conductors of a parallel plate transmission line. This line is excited with standing waves which are measured by a movable probe in a suitable shielded enclosure. The use of the sample itself as a standing-wave line eliminates many errors caused in other systems by the extremely low impedances involved.

Scattering Measurements Using A 10 CM Parallel-Plate Region—J. E. Keys and A. W. Adey, *Defense Research Board Canada*)—A 10 cm parallel-plate region, similar to those reported by Row of Cruft Laboratory and El-Kharadly of Imperial College, has been developed and its accuracy assessed from the results of scattering measurements on metal cylinders as a standard problem. It has been applied to measuring the scattering properties of dielectric and metal-dielectric cylinders.

The equipment is being employed to measure the reflection and transmission coefficients of isolated wire grids of different wire spacings and materials, and the reflection coefficient of grids backed by lossy dielectric sheets.

A New Direct-Reading Frequency-Measuring System Utilizing a Frequency Synthesizer—R. C. Hess, *Federal Telephone and Radio Company*—A system is described for measuring frequencies directly and with great accuracy over an unusually wide band. Use is made of a frequency synthesizer to generate one single arbitrarily-variable reference frequency of high accuracy and stability. This frequency is varied until a zero-beat is ob tained with the unknown, at which time the unknown frequency can be read directly. This method is usable from 20 cps to 30 mc directly and by means of harmonics up to 600 mc. The operation of the frequency synthesizer and its control by the master quartz oscillator will be described in detail. This paper describes work done by the firm of Rhode and Schwarz, Germany.

Studies in Noise by the Liouville Theorem—G. Held, *University of Washington*—For purposes of understanding the basic limit to which the noise figure of microwave amplifiers may be reduced, the statistical nature of electron flow should be studied. In particular, a more fundamental approach than the single-value velocity theory is needed in the potential minimum problem.

A logical starting point is the Liouville equation. Different attempts have been made to apply the equation to these kinds of problems under special situations.

In the present paper a general approach to the solution of the equation is outlined. A general solution to the differential equation is formulated. It is shown how this solution is transformed into an integral equation for the disturbance in charge distribution as a result of the introduction of a disturbance at some point in the beam. Solutions to some special cases of the integral equation have been worked out, and an approximation procedure for other cases is indicated.

It is also shown how the Liouville equation can be applied to study of modulation of beams and in general the flow of electron beams in electromagnetic fields.

On the Radar Measurement of Angle-of-Arrival in the Presence of Interference From Many Plane Waves—H. R. Brewer and R. D. Wetherington, *Georgia Institute of Technology*—A comparison is made of various antenna configurations for the measurement of the angle-of-arrival of a single plane wave in the presence of interference from many plane waves whose relative phases and angles-of-arrival are random. The average and rms errors are calculated as a function of parameters re-

lated to the characterization of the interference and to the receiving systems considered. In the comparison the over-all physical dimensions of the receiving aperture are held fixed. The receiving systems are idealized, and no consideration is given to internal noise and component imperfections.

Long Distance VHF Fields—F. H. Northover, *Memorial University of Newfoundland*—Reliable propagation of vhf and microwaves from high-power transmitters to distances of several hundred miles beyond optical range has been demonstrated by an ever increasing number of experiments during the past ten years. The fields that have been observed have consistently been many times greater than the field strengths predicted by the "effective radius' theory. The present paper appears in two parts. In Part I the theory that the phenomenon can be explained solely in terms of "partial internal reflection" from elementary layers of a dielectric distribution where the rate of decrease of (μ-1) with height is everywhere continuous and of the same order of magnitude as in a "standard" atmosphere is carefully examined and found to be untenable.

In Part II, the case where the distribution contains "sharp layers" (i.e. local regions where μ-1 changes relatively rapidly with height), is also examined, but it is found that even this hypothesis is not adequate to explain the phenomenon.

It is concluded that the effect in question is probably due to scattering of the electromagnetic waves from atmospheric turbulence.

Measurement of Atmospheric Attenuation at Millimeter Wavelengths—A. B. Crawford and D. C. Hogg, *Bell Telephone Laboratories, Inc.*—A frequency-modulation radar technique especially suited to measurement of atmospheric attenuation at millimeter wavelengths is described. This two-way transmission method employs a single klystron, a single antenna, and a set of spaced corner reflectors whose relative reflecting properties are known. Since the method does not depend on measurements of absolute antenna gains and power levels, absorption data can be obtained more readily and probably with more accuracy than by the usual two-way transmission methods.

Application of the method is demonstrated by measurements in the 5- to 6-millimeter wave band.

Obstacle Gain in the Diffraction Region—K. A. Norton and P. L. Rice, *National Bureau of Standards*—Radio wave propagation over actual terrain usually does not correspond closely either to diffraction over a smooth spherical earth or, at the other extreme, to diffraction over a knife edge. In this report a device is described for predicting diffracted fields under a great variety of terrain conditions.

A smooth-earth model is constructed which maintains the distance and the angular distance between antennas constant. An effective earth's radius factor is determined which fits the terrain conditions better than the usual four-thirds factor; ordinarily, this new factor is less than four-thirds. With distance and angular distance constant, standard smooth-earth diffraction theory is extremely sensitive to changes in effective earth's radius, and a small decrease in this radius increases the expected diffracted field by many decibels.

This new method of calculation agrees on the average remarkably well with observations over more than a hundred vhf and uhf propagation paths.

A Study of Fading Rate in long Distance Tropospyeric Wave Propagation—A. P. Barsis, *National Bureau of Standards*—Long-distance tropospheric propagation measurements have been analyzed in order to obtain data on fading rate. The measurements were performed on frequencies in the 100, 200, and 1,000-mc ranges, over distances of 225 and 400 miles, and with transmitting antennas located at various elevations above the surrounding terrain. Fading rate has been defined as the number of times per minute the signal trace crosses its median value in a positive direction.

The fading rates obtained show a diurnal trend with high values at midday and in the afternoon, corresponding to the absence of atmospheric stratification or similar phenomena. Low values of fading rate were obtained at night and in the morning hours, and can usually be explained by the presence of superrefraction. The measured rates range from less than one fade per minute (100 mc, morning) to thirty and more fades per minute (1,046 mc, afternoon). Average hourly fading rates of various frequencies are well correlated over the diurnal period; however, the ratio of fading rates generally does not equal the frequency ratio. A qualitative analysis is made of these ratios as a function of antenna beamwidth. Results of the measurements are interpreted by using the model suggested by Rice.*

Obstacle Gain Measurements Over Pikes Peak at 60 to 1,046 MC—R. S. Kirby, H. T. Dougherty, and P. L. McQuate, *National Bureau of Standards*—Radio transmission loss measurements made over four propagation paths approximately 100 miles in length show the effect of a large mountain obstacle on vhf and uhf ground-to-ground propagation. Measurements were made at 59.75 mc, 100 mc, 191.75 mc, and 1,046 mc using two portable transmitters and two commercial television stations in the Denver area. Recordings of transmission loss were obtained in the Pueblo-Canon City area at four sites one of which included Pikes Peak in the propagation path. Measurements were made as a function of height while raising the receiving antennas on a 100-foot telescopic mast and by mobile measurements made while driving along a road normal to the path from the transmitters over Pikes Peak.

Measurements made directly over Pikes Peak show well defined lobing associated with four ray-path diffraction theory. Theoretical approximations to the values of transmission loss over Pikes Peak based on Fresnel-Kirchhoff scalar knife-edge diffraction theory predict values of transmission loss and lobe structures which are in good agreement with those observed.

At the other sites, where measurements were obtained without Pikes Peak in the path path the fields were much lower at all frequencies, and large fading ranges were observed. There was also very little tendency to show any consistent lobing.

Mobile measurements made along a route normal to the path over Pikes Peak generally showed the lowest values of transmission loss when propagation was directly over the peak. The observed transmission losses increased on either side of this path.

Circuit Components in Dielectric Image Lines—D. D. King, *Johns Hopkins University*—The symmetry of the dipole mode in a dielectric rod permits the use of an image system. By replacing the lower half of the dielectric and its surrounding field with an image surface, the support problem is eliminated. The resulting image provides structural convenience and also has very low loss provided the wave is allowed to occupy a cross section many wavelengths square. In the millimeter region this is readily achieved.

The possibilities of new types of circuit elements in this image system are explored. The combination of optical and waveguide techniques is a characteristic of the resulting components. The properties of several transducers between image line and either rectangular waveguide or a coaxial line are described. Attenuators, a standing-wave detector, and various types of directional couplers for image lines are also discussed.

The Ultra-Bandwidth Finline Coupler—S. D. Robertson, *Bell Telephone Laboratories*—The "finline coupler" is a recently developed microwave circuit element with which it has been possible to assemble hybrid junctions, directional couplers, and polarization-selective couplers capable of operating over bandwidths of at least three-to-one in frequency. Constructional details and experimental results are given.

Phase Shift by Periodic Loading of Waveguide and its Application to a Broadband Circular Polarization—A. J. Simmons, *Naval Research Laboratory*—A rectangular or square waveguide may be loaded periodically by thin capacitive or inductive irises in order to produce phase delay or phase advance respectively. The amount of phase shift may be calculated with accuracy by making use of available theoretical values of iris susceptance and of transmission line theory. The phase shifting sections may be designed for low vswr over a considerable bandwidth.

When a square waveguide capable of supporting two fundamental modes is loaded periodically, the irises act inductively for one mode and capacitively for the other, thus introducing a differential phase shift. This differential phase shift may be made equal to 90 degrees, in order to convert linear to circular polarization. Furthermore such a device may be made by proper choice of parameters, to yield near-circular polarization over a bandwidth of 1.65:1 because the variation in phase delay for one mode and phase advance for the other tend to compensate each other as the frequency is varied.

Several of these circular polarizers have been built and tested at X-band and the measured results of ellipticity and vswr as well as broadband performance check with theoretical values quite closely.

A Combination Crystal Switch Circuit—F. S. Coale, *Sperry Gyroscope Company*—A crystal circuit is used in which switching is accomplished by varying the ouptut on a crystal. A Smith Chart plot shows that the impedance of a crystal, plus its mount, changes from inductive to capacitive as the bias is varied from positive to negative. The resistance of the crystal also varies from a lower to a higher value. These particular characteristics of a crystal are utilized in the switching operation.

The maximum attenuation frequency of a high-pass, series M derived filter varies with a change of the parallel inductance or the parallel capacitance. If either the inductance or the capacitance is varied the upper cutoff is changed from its original cutoff value to a different cutoff point. This particular characteristic of the high-pass M derived filter is used in the switching operation.

The crystal is placed across the parallel capacitance. The impedance therefore, across the parallel LC circuit is a result of the impedance of the LC circuit plus the impedance of the crystal mount. Since the impedance of the crystal mount varies with a change in bias by varying the bias, the total impedance of the filter is changed. As a result, the attenuation vs frequency characteristics are varied. In the switch developed and tested, two M derived filters were placed in series to attain higher attenuation in the maximum attenuation position. The operating parameters of the switch are as follows: frequency, between 500 and 1,000 mc; bandwidth, 20 mc; dynamic switching, greater than 55 db; average insertion loss, 2 db; switching time, less than 1 msec; and bias voltage, between -0.6 v and $+0.6$ v.

The circuit is also used as a detector by

* S. O. Rice, "Radio field strength statistical fluctuations beyond the horizon," PROC. IRE, vol. 41, pp. 274–281; February, 1953.

utilizing the rectified output. This unit finds application in radar jamming problems, as well as a low power modulator for rf signals.

E-Plane Forked Hybrid-T Junction—W. K. Kahan, *Wheeler Laboratories, Inc.*—A novel rearrangement of the waveguides of a microwave hydrid-*T* junction has been investigated. This junction is formed by the intersection of four rectangular waveguides, two of which (conventionally *E*- and *H*-arms) are mutually perpendicular, cross-polarized, and have their centerlines in one symmetry plane of the junction; the remaining two waveguide arms are formed by symmetric *E*-plane bifurcation of the *E*-arm waveguide extended. This hybrid-*T* possesses special advantages with regard to match and pulse power capacity.

A special test fixture was constructed of 1.122×0.497-inch rectangular waveguide. Experimental design work was carried out over a 12 per cent range of frequencies from 8.5 to 9.6 kmc. The *H*-arm reflection was reduced to 2.6 db swr by simple shaping of the bifurcating element. Addition of conventional matching elements resulted in maximum reflections, within the above band, of 0.8 db and 0.6 db swr in the *H*- and *E*-arms respectively.

The ultimate limitation on the *E*-arm power capacity, as fixed by the intensified electric field at the leading (rounded) edge of the center partition, was computed to be 2 db below uniform waveguide. Experimental corroboration has been obtained.

Applications of the Turnstile Junction—M. A. Meyer and H. B. Goldberg, *Laboratory for Electronics*—The Turnstile Junction is a six-terminal pair microwave network, consisting of four rectangular arms and one circular arm which is excited in two orthogonal TE1,1 modes. The characteristics of this network are such that they lend themselves to some very useful applications in the field of microwave networks. From a consideration of the field division properties and the symmetry conditions of the network, the use of the Junction for the following applications is discussed.

The Junction can be utilized as a cw duplexer with better than 50 db duplexing action, while at the same time generating polarizations of any degree of ellipticity from circular to linear polarization. This cw duplexing is accomplished without any inherent duplexing loss.

The Junction can be set up for transmitting linear polarization and receiving either linear or cross-linear polarizations, while still maintaining the duplexing properties of the junction.

The Junction can be adjusted to transmit circular polarization with the receiver arm made to accept circular polarization of the same or opposite rotation from the transmitted signal.

The Junction can be used to measure the degree of ellipticity of a wave by making use of the property that an elliptical wave is made up of two circular waves, one clockwise and the other counterclockwise.

Among the other uses discussed is the application of the turnstile as a four-way, symmetrical power divider.

Sweep Frequency Pulse Measurements of Ionospheric Propagation over a 2,400 KM Path—V. Agy and P. G. Sulzer, *National Bureau of Standards*—The oblique incidence experiment between Sterling, Va., and St. Louis, Mo., reported earlier (URSI, Spring 1952) has been extended to the longer path (2,370 km) between Sterling and Boulder, and regular measurements have been made over this path for somewhat more than a year.

As in the case of the shorter path, maximum usable frequencies for the longer path determined by application of the N. Smith transmission curves to vertical incidence records made at the midpoint of the path usually agree rather well with those determined directly from the oblique incidence records. However, large differences do occur at times, and the oblique incidence records are in general much more complex than those made over the shorter path.

During the daylight hours, the "classical" muf (the frequency at which the upper and lower rays meet) is not usually the maximum frequency received. This muf extension, or "tail," may occasionally reach frequencies 10 per cent above the classical muf. Measurements of relative field strength in this range of frequencies have been made. Several scatter mechanisms have been suggested to account for the tail. These are discussed.

The Role of Ionospheric Forward Scatter in Oblique Incidence MUF—D. K. Bailey, *National Bureau of Standards*—By using the results of the vhf forward scatter program it is possible to make certain estimates of the role played by forward scatter in hf oblique incidence propagation. In particular it appears that high-power long-distance hf communication circuits using directive antennas will be able to operate successfully on frequencies some ten per cent or more above the classical muf. An examination of observational records from the oblique-incidence hf program suggests that much useful observational material bearing on the general subject may already be available. Some discussion of what to look for and what to measure in connection with this program will be made, and a possible direct method of measuring the fine structure constant of the scattering stratum will be described. Some comments on the implication of these results for muf prediction will be offered.

Theory of the Distribution of Meteor Trail Lengths*—V. R. Eshleman, *Stanford University*—The lengths of the columns of ionization formed by meteors are determined from the theory of the interaction between meteoric particles and atmospheric molecules. The factors controlling meteor trail length include the mass of the meteoric particle, its geocentric velocity, and the zenith angle of the meteor radiant. The distribution of meteor trail lengths is computed from the experimentally-deduced mass distribution of sporadic meteors. An average value for the particle velocity is used in this determination, and it is assumed that the meteor radiants are uniformly distributed over the celestial hemisphere.

The theoretical distribution of meteor trail lengths is compared with the results of an experimental radar investigation of trail lengths.† Theory and experiment are found to be in good agreement. Also, the theory indicates that while the length along which a given trail could produce a detectable radar echo is dependent upon the sensitivity of the radar system, the distribution of such lengths for sporadic meteors should be independent of system sensitivity.

Forward Scatter from Meteor Trails—E. L. Vogan, P. A. Forsyth and C. O. Hines, *Defence Research Board (Canada)*—For the past two years, the Radio Physics Laboratory of the Defence Research Board of Canada has been recording forward scattered signals from meteor trails over several different paths in Canada. The measurements have been made at various frequencies in the range 30 mc to 50 mc. The characteristics of individual meteor signals are illustrated by typical examples. The variation in meteor signal rate, diurnally and during periods of known showers, are described. It would appear that such measurements will prove useful in the study of meteors.

The Role of Meteoric Ionization in Extended-Range VHF Propagation‡—V. R. Eshleman, L. A. Manning, A. M. Peterson, O. G. Villard, Jr., *Stanford University*—It is known that some form of scattering in the *E*-region supports extended-range vhf radio propagation. This scattering has variously been ascribed to (1) partial reflections from horizontally-stratified ionization layers, (2) scattering from "blobs" of ionization created by turbulence, or (3) overlapping reflections from meteor ionization trails. However, the true nature of the scattering has not yet been demonstrated adequately. The available evidence is reviewed, together with some theoretical and experimental results recently obtained at Stanford University. It is pointed out that the antenna systems presently in use represent the worst possible arrangement for obtaining strong transmission via meteors. These antennas highly favor partial reflections from horizontally-stratified layers in the *E*-region, and favor to a lesser degree scattering from "blobs" of ionization which may be created by isotropic turbulence. Nevertheless, the received signal has many characteristics which can be explained by assuming that the propagation takes place primarily by scattering from numerous ionization trails. It is concluded that meteoric ionization plays a dominant role in existing extended-range vhf propagation, and that the meteoric component of the signal would be considerably increased by redesign of the antennas.

Long Range Meteoric Echoes Via *F*-Layer Reflections—W. A. Whitcraft, Jr., *Raytheon Manufacturing Company*, and J. T. deBettencourt, *Massachusetts Institute of Technology*—This note reports hf observations of meteoric backscatter echoes at ranges greatly exceeding radio line-of-sight. The observations were part of a program of measurements on backscatter using COZI equipment.

Examples are given of more recent observations at South Dartmouth, Mass., in November, 1954, on 12 and 17 mc, using improved equipment. Short duration echoes are observed in advance at ranges shorter than those of the ground backscatter. No such meteoric echoes are observed when the ground backscatter disappears. The meteoric echo ranges move with time of day just as the range to the ground backscatter moves. A plausible explanation for the observed meteoric echo ranges exceeding 1,000 miles is that they are due to backscatter from the trail, ionospherically propagated to and fro via the *F*-region, just as the ground backscatter. Other possible ionospheric modes are discussed.

The Contribution of Meteors to Long-Range Backscatter—P. B. Gallagher and A. M. Peterson, *Stanford University*—Theoretical investigations have indicated that meteor echoes should be detectable by radar at ranges as great as 3,000 km even though meteor ionization trails are produced at heights near 100 km. The propagation path involved is from the radar site obliquely to the *F*-layer and back down to the *E*-region, where the meteor trails are formed. Echoes of this type have been detected at Stanford University using high-power pulse transmissions at a frequency of 23.1 mc. These long-range echoes exhibit the characteristic time durations, echo shapes, and Doppler shifts which are found for the short-range, line-of-sight reflections from meteors. Detection rates up to several per minute have been observed over these long paths. Meteor echoes of this type lend further support to the conclusion that for the most part long distance backscatter echoes result from scattering at the earth's surface. The meteor echoes are found to precede the leading edge of the ground scattered echo by amounts ranging up to 500 km.

The Use of Sweep-Frequency Backscatter Data for Determining Vertical and Oblique-Incidence Ionosphere Characteristics—R. Silberstein, *National Bureau of Standards*—It is

* This work was supported by the AF Cambridge Res. Center, Air Res. and Dev. Command.

† L. A. Manning, O. G. Villard, Jr., and A. M. Peterson, "The length of ionized meteor trails," *Trans. AGU*, vol. 34, pp. 16–21; February, 1953.

‡ This work was supported jointly by the U. S. Navy (Office of Naval Research), the U. S. Army Signal Corps, and the U. S. Air Force.

possible to use sweep-frequency backscatter data for obtaining monthly median values of x-kilometer maximum usable frequencies at control points in a circle of radius one-half this distance. Diurnal graphs are shown for a 2,370-km path comparing the classical muf as deduced from experimental backscatter data with the same muf as deduced from midpoint vertical-incidence data and from actual oblique-incidence characteristics. For the two cases shown, the median muf deduced from backscatter was about 2 per cent higher than that deduced from oblique-incidence records, while that deduced from vertical-incidence data was about 2 per cent lower.

Possible causes of anomalous echoes are discussed as are characteristics of some unusual records. A strong, sporadic morning-hour echo apparently associated with the E-layer is described.

Characteristics of High Frequency Discharges from Severe Storms—H. L. Jones, *Oklahoma Agricultural and Mechanical College*—The tornado research project at Oklahoma A & M College is in general concerned with the study of sferics originating from thunderstorms. Particular emphasis has been placed on the study of the severe storms that are accompanied by tornadoes and hail.

It has been found that the sferics associated with severe storms experienced in the great plains area have a characteristic high-frequency component. The frequencies involved in this component are especially pronounced in a band from 125 to 250 kc.

A new high-frequency direction finder has been completed that is designed to respond to the high-frequency component. The response of this new direction finder is compared to that of the low-frequency direction finder. It is believed that the hfdf will make it possible to obtain considerable new information pertinent to storms within a two hundred mile range of the laboratory. It is particularly valuable for the study of thunderstorms in the immediate vicinity of the station.

Included in this report is a preliminary discussion of the high-frequency waveforms. The important characteristics of these waveforms include the frequency, the duration, and the rate of arrival. It may be possible to correlate the variations of these characteristics with storm intensities.

Atmospheric Noise Characteristics—A. W. Sullivan, *University of Florida*—The statistica distribution of noise amplitudes has been investigated in both the pre-detection and post-detection cases. A good approximation to the distribution at the output of linear amplitude detector is found in the logarithmic-normal distribution. This distribution is discussed, and the relative merits of average and root-mean-square noise measurements are treated.

Preliminary results of the study of the effects of pre-detection bandwidth on noise amplitudes are presented.

A Statistical Model of Atmospheric Noise—J. M. Barney, *Convair Corporation*—A general statistical model of the first and second probability density functions of the output envelope of an amplitude-modulated receiver, shock-excited by atmospheric noise, is developed. This model is used to obtain explicit expressions for two particular time pulses, exponential and triangular. The resulting integral equations are not amenable to the ordinary methods of the calculus, and various methods of evaluating the equations are investigated.

One discrete solution is obtained which, although different from the continuous distribution of atmospheric noise as measured in the laboratory, gives a good approximation for small values of the variable. Another, obtained by a series expansion of the integral equation, offers considerable promise for a continuous type of solution.

The Measurement of Recurrent Impulsive Noise—A. Eckersley and D. B. Geselowitz, *University of Pennsylvania*—Radio interference meters are required to measure impulsive noise. This paper is concerned with the interpretation of readings obtained on such meters.

Readings are, in general, dependent on: (1) The spectral intensity and repetition rate of the impulses; (2) The selectivity, gain and linearity characteristics of the meter; and (3) The detector circuits of the meter.

The concept of an impulse and the expression of spectral intensity in appropriate units are discussed first. Next the response of an idealized narrow-band meter with average, root-mean-square, quasi-peak, or peak detectors is treated. An important parameter is the effective bandwidth. A brief discussion of this bandwidth and its measurement is included.

Finally, precautions involved in applying the idealized relationships to practical situations are discussed.

A Probability Computer for Noise Measurement—J. D. Wells and A. W. Sullivan, *University of Florida*—The first amplitude probability distribution function of a noise envelope is measured with the equipment described in this paper. Accuracy on the order of 1 per cent is obtained for each measured point, and the entire distribution may be determined over a dynamic range of 100 db with good accuracy when several points are measured simultaneously. The unit is designed to operate from the intermediate frequency signal of a communications receiver. A complete noise meter is discussed which employs the probability computer and is used principally in the study of atmospheric noise.

Microwave Traveling-Wave Tube Millimicrosecond Pulse Generators—A. C. Beck and G. D. Mandeville, *Bell Telephone Laboratories*—For some time short pulse techniques have played a useful part in the microwave art. In order to obtain better resolution, equipment for generating and viewing microwave pulses about six millimicroseconds long was developed and described previously. The regenerative pulse generator in that equipment was rather complex and difficult to build and adjust. A much simpler generator of pulses with about the same time duration is now being used. It produces short pulses by properly gating a conventional microwave signal source with a traveling-wave amplifier having suitable transient voltages applied to both its helix and its beam-forming electrode. It is easier to construct and operate, requires fewer components, and gives a more stable output. It can be used at any frequency where a signal source and a traveling-wave amplifier are available. The pulse frequency can be set anywhere within the amplifier bandwidth. The power output is determined by amplifier saturation.

Both generators are described and compared. Equipment for receiving, displaying, and measuring the pulses is also briefly discussed. Pulse shapes and resolution are shown by means of oscilloscope photographs.

The Regeneration of Binary Microwave Pulses—O. E. DeLange, *Bell Telephone Laboratories*—The chief advantage of binary pulse systems resides in the possibility of regenerating such pulses at intervals along the transmission route to prevent the accumulation of distortions due to noise, bandwidth limitations, and other disturbing effects. A very important part of any such transmission system is the regenerative repeater employed. This paper reports the results of experiments performed to determine the possibilities of such a repeater operating in the microwave frequency range.

With maximum economy in mind, a simple device was developed for producing partial regeneration directly at microwave frequencies. To determine the capabilities of such a regenerator, one of them was included in a circulating test loop in which pulse groups were passed through the device a large number of times. Results indicate that even in the presence of serious noise and bandwidth limitations pulses can be regenerated many times without noticeable deterioration.

It was found that for "errorless" transmission through a long chain of such repeaters the required signal-to-noise ratio is approximately 5 db higher than the theoretical value for an ideal system. Part of this difference is attributable to the fact that only partial regeneration was employed and part to other imperfections in the system.

Investigation of VHF Non-Optical Propagation, Sardinia—Minorca—J. M. Clara, *Compañía Telefónica Nacional de España*, and A. Antinori, *Ministro delle Poste e delle Telecomunicazioni* (Rome, Italy)—An experimental link has been set up between Minorca and Sardinia in the Mediterranean Sea, a distance of 240 miles. Either 240 mc or 300 mc may be used for transmission with either horizontal or vertical polarization. The transmitter output is 1 kw and 10-m diameter paraboloids are used. A particular feature of the tests is that the transmitter is modulated by an accurately controlled tone, and at the receiving terminal the carrier and the two nearest sidebands are received on individual narrow-band receivers, so that differential fading and time delay can be measured over a band of 240 kc. From these data it is hoped to be able to predict the transmission bandwidth that might be practicable for a communication link.

900 MC PTM Over-the-Horizon Radio Link—F. J. Altman, R. E. Gray, A. G. Kandoian, W. Sichak, *Federal Telecommunication Laboratories*—A two-way link in the 890–940 mc band has been established between Nutley, N. J., and Southampton, N. Y. (91 miles), to determine the applicability of over-the-horizon propagation to commercial radio links. Pulse-time modulation, capable of handling 23 or 46 telephone channels, with a radio bandwidth of about 1 mc, is used. The transmitter has a peak power of 1 kw; the receiver noise figure is less than 9 db. To permit diplexing the transmitter and receiver on one antenna with a modest amount of filtering, a dual polarization horn is used to feed a 28-foot diameter paraboloid.

Data on the median received signal, fading, and effect of airplane reflections will be given.

A Method for the Accurate Measurement of the Noise Temperature Ratio of Microwave Mixer Crystals*—R. E. Davis and R. C. Dearle, *University of Western Ontario*—The noise temperature ratio, t of a mixer crystal can be determined most conveniently by measuring an intermediate ratio, the Y-factor (measured at the output of the IF amplifier) which is itself a joint function of t, the IF conductance g_1' of the crystal, and the amplifier noise parameters. It is known that if the output noise power of the amplifier is made independent of g_1' for $t=1$, a very simple relation exists for Y, t, g_1'. The Robert's line network is commonly used as a matching device to satisfy the above condition, but it will be shown here that sources of error exist which were not previously apparent, and that these errors may be eliminated to a good order of precision by the use of cathode lead inductance in the amplifier. Once these errors are eliminated, the crystal conductance may be determined simply and accurately, leading to a precise determination of t with little loss in the simplicity of measurement.

Data on the Temperature Dependence of X-Band Fluorescent Lamp Noise Sources—W. W. Mumford and R. L. Schafersman, *Bell Telephone Laboratories*—This paper is concerned primarily with the performance of fluorescent lamps as microwave noise sources at 9,000 mc. In particular it deals with the tem-

* This work was sponsored by the Defence Research Board of Canada under contract DRB, X-33.

perature dependence of the excess noise ratio of an 8w lamp running at a lamp current of 150 ma in a 10-degree *E*-plane holder. It was found that (1) the bulb temperature is much higher than that with a lamp current of 75 ma encountered in the 90-degree *H*-plane circuit investigated previously at 4,000 mc, hence the temperature coefficient of excess noise vs waveguide temperature obtained in the 4,000-mc circuit does not apply; (2) anomalous and unreproducible inversions in the temperature coefficient at these higher bulb temperatures have been observed; (3) these anomalies can be avoided by operating the bulb at lower temperatures, 40 degrees C. to 50 degrees C., where the lamps appear to be just as uniform and stable and probably just as noisy as they are at 4,000 mc.

Noise Measurements in the UHF Range*—E. Maxwell and B. J. Leon, *Massachusetts Institute of Technology*—Comparative noise figure measurements in the 400 mc frequency range have been made using commercial noise diode sources, thermal noise sources and fluorescent lamps as noise generators. The thermal sources were of two kinds, a high temperature source at about 1,000 degrees K and a low temperature source at 4 degrees K. Measurements made with noise diodes yielded results about 1.0 db higher than those made with the thermal noise sources, from which it is inferred that the diodes are not satisfactory primary standards of noise in this frequency range. The effective noise temperature of a standard 6w fluorescent tube (coupled to a helical line) was determined to be approximately 12,000 degrees K by comparing its noise output with that of the hot thermal source. This is consistent with the figure of 11,400 degrees K reported by Mumford† at 4,000 mc.

Methods of Determining Long-Wave Reflection Coefficients for a Specific Ionospheric Model‡—J. D. Wolf and J. J. Gibbons, *Pennsylvania State University*—The purpose of this paper is twofold. The first objective is to test the applicability of an iterative process due to Bailey§ to the problem of computing the 75-kc ionospheric reflection coefficient for a specific model. The details of two applications using different first approximations are presented.

The second part of the paper deals with the computation, by numerical integration, of the 75-kc reflection coefficient for the same ionospheric model. A comparison is then made of the values obtained from the iterative process and those obtained by numerical integration, and the results discussed.

The Amplitude and Phase Variations of 150 KC Signals Reflected from the *E*-Layer—‖ R. E. Jones and R. W. Parkinson, *Pennsylvania State University*—In the first part of the paper the statistical properties of the periods of fading and of oscillation in phase of the main *E*-layer reflection at 150 kc are compared and discussed. The distributions of daytime fading periods and of daytime and nighttime phase periods are seen to be similar while the nighttime fading is distinctly different. This is interpreted in terms of earlier work on the diffraction of downcoming plane waves by a phase-amplitude screen.

Secondly, a study is made of the fading properties of the nighttime main *E*-layer reflection and the nighttime backscatter attributed to magneto-ionic coupling at a level below the normal reflection height. It has been noted that the coupling echo often exhibits two fading periods simultaneously which are superposed but which can easily be distinguished. The shorter periods have a distribution similar to that of the main reflection. The apparent existence of two different mechanisms giving rise to fast and slow fading may be attributed to diffracting layers at two levels. However, an alternate explanation in terms of two differen effects from one screen is proposed.

A Low Frequency Long Range Propagation Problem*—J. Shmoys, *New York University*—With the variation of electron density and collision frequency assumed exponential, the propagation constants of the first few modes of propagation of low frequency radio waves have been calculated. A simple relation between group velocity and angle of arrival has been derived. The validity of this analysis in the case of vertically polarized waves will be discussed. Similarities and differences between ray and wave treatment of the problem will be pointed out.

A Study of Recent VLF Oblique Incidence Propagation Data—J. L. Heritage and S. Weisbrod, *Navy Electronics Laboratory*—New oblique-incidence vlf signal strength data is analyzed for information about the propagation mechanism. Field strength recordings made on fixed-distance paths and on variable-distance aircraft runs are used to study the separate influence of phase interference between propagation modes and of absorption on the field observed at different distances from the transmitter. The variable distance aircraft data is analyzed by comparing the position and relative amplitude of observed signal maxima and minima with amplitude vs distance curves calculated from a simplified ray picture of the transmission path. Discrepancies between the two indicate the probable way that reflection height, phase change on reflection, and reflection coefficient vary with incidence angle. Longer distance aircraft runs give useful figures of path attenuation in db per 1,000 km. Fixed point recordings are analyzed for onset of sunrise and sunset dips and for diurnal and seasonal path attenuation.

Study of LF Propagation Path Characteristics in the Alaskan Area—J. E. Bickel, *Navy Electronics Laboratory*—Using a ray model, analysis is made of field intensity recordings of 135-kc signal over 1,500 km paths in the Alaskan area to determine propagation path characteristics. From recordings of field intensity variations during the night changes in height of reflection and average reflection coefficients for the various sky-wave modes are obtained. A figure for daytime reflection coefficient is obtained by observing day-to-day variations of the signal intensity over a several weeks' period. These figures agree with results of other workers.

Analysis of the shape of the sunrise and sunset dips allows interpretation of the dynamic processes responsible for them. They are explained on the basis of interference between ground and sky waves. A figure for rate of change of ionospheric height and rate of change of sky-wave absorption is obtained.

Comparison of data taken simultaneously in two different paths is made.

Heights of Irregularities Giving Rise to Fading of 150-KC Waves†—R. B. Banerji, *Pennsylvania State University*—Evidences are quoted which show that the fading of 150-kc pulsed waves is due to random absorption rather than random scattering in the ionosphere. On the basis of this, a statistical theory has been worked out for the relationship between the phase and amplitude of a wave which has encountered random absorption on its downward passage. The predicted behaviors show excellent agreement with experiment, and yield a method for estimating the collisional frequency at the region where the absorption is taking place. Experimental results pertaining to 150 kc waves at State College are described and discussed.

The method has possibilities for supplementing wind measurement results to provide information regarding the heights of winds.

High Resolution Radio Astronomy at 13.5 Meters—K. L. Franklin and B. F. Burke, *Carnegie Institution of Washington*—The large Carnegie "Mills Cross" at Seneca, Md., has been completed, and a survey of radio sources and background brightness distribution is in progress. The antenna and associated equipment will be described, and results of the first observations will be discussed. The instrument is designed to operate at a wavelength of 13.5 m, and has a beamwidth of approximately 1.5 degrees. The principal known sources have been observed, and in addition, several weaker sources have been seen. During the day, ionospherically propagated signals usually interfere, although occasional daytime operation has been possible. During the night, very little difficulty is experienced with interference.

Absorption Effects in the Spectra of Radio Stars Produced by Interstellar Hydrogen—A. E. Lilley, *Naval Research Laboratory*—Observations show that 21-cm hydrogen line profiles for directions which contain radio stars are very unusual in shape and amplitude. When one obtains a 21-cm profile for the exact direction which contains a radio star, the profile is considerably distorted compared to the profiles obtained for directions immediately adjacent to the radio star. The effect is due to the absorption of continuum radiation from the radio star by interstellar hydrogen which lies between the observer and the radio source.

If the radio star lies in the center of the antenna reception beam, the absorption is effective only over the small cone subtended by the radio star, whereas the emission contribution originates over the entire cone subtended by the antenna reception beam. With the 50-foot NRL antenna and radio stars such as Cassiopeia A and Taurus A, the cone subtended by the radio star is quite small compared to the reception cone of the antenna. This provides a unique increase in the effective angular resolution in the absorption observations.

By obtaining hydrogen line profiles for selected positions very close to the radio star, one can readily determine the "expected" 21-cm profile for the direction of the radio star. The expected profile is the profile that would have been obtained in the absence of the radio star, and is taken as the mean of the profiles obtained from the adjacent comparison positions. The comparison profiles show only minor differences, and their mean is an acceptable measure of the "expected" profile. If we call this expected profile $\overline{\Delta T(\nu)}$, then it can be shown that the profile obtained when the radio star is in the antenna beam is given by:

$$\Delta T^1(\nu) = \overline{\Delta T(\nu)} - T_A(1-e^{-\tau(\nu)}) - \left[T_K(1-e^{-\tau_2(\nu)})e^{-\tau_1(\nu)}(1-e^{-\tau\sigma})\right]\frac{\Omega_\sigma}{\Omega_B},$$

where T_A is the apparent antenna temperature of the radio star, $\tau_1(\nu)$ and $\tau_2(\nu)$ are HI optical depths within the small cone subtended by the radio star, $\tau_1(\nu)$ the optical depth to the radio

* The research in this document was supported jointly by the Army, Navy and Air Force under contract with the Mass. Inst. Tech.

† W. W. Mumford, E.S.T.J., 28, 608, 1949.

‡ The research reported in this paper has been sponsored in part by the Geophysics Research Directorate of the AF Cambridge Res. Center, Air Res. and Dev. Command, under Contracts AF19(122)-44 and AF19(604)-1304.

§ V. A. Bailey, *Phys. Rev.*, vol. 96, pp 865–868; November 15, 1954. URSI-IRE-AGU Joint Meeting, Washington, May 5, 1954.

‖ The research reported in this paper has been sponsored by the Geophysics Research Directorate of the AF Cambridge Res. Center, Air Res. and Dev. Command, under Contracts AF19(122)-44 and AF19(604)-1304.

* The research reported in this paper was done at the Inst. Math. Sci., New York Univ., and has been made possible through support and sponsorship extended by the U. S. Air Force, AF Cambridge Res. Center, under Contract No. AF19(122)-42.

† The research reported in this paper has been sponsored by the Geophysics Research Directorate of the AF Cambridge Res. Center, Air Res. and Dev. Command, under Contracts AF19(122)-44 and AF19(604)-1304.

star and $\tau_2(\nu)$ the optical depth from the radio star to the most distant limit of HI. T_K is the temperature which defines the population distribution over the hydrogen hyperfine levels, $\tau\sigma$ is the continuum optical depth of the radio star, and Ω_σ/Ω_B is the ratio of the solid angles subtended by the radio star and the antenna beam. For an antenna only 50 feet in diameter, Ω_σ/Ω_B is of the order of 10^{-2} or less, and the last term in the equation above may be safely neglected. This enables one to determine the approximate HI optical depth from the observer to the radio star along the small cone subtended by the radio star:

$$\tau_1(\nu) \cong -\ln\left(1 - \frac{\Delta T(\nu) - \Delta T^1(\nu)}{T_A}\right).$$

The observations* obtained for Cassiopeia A show three sharp maxima in the HI optical depth suggesting HI cloud structure. One peak is near the local standard of rest in radial velocity, and two peaks occupy the radial velocity range of the second spiral arm near galactic longitude 80 degrees. Van de Hulst, Muller and Oort† place this second arm at a distance of approximately 3 kiloparsecs, which becomes the minimum distance to the Cassiopeia radio star. If a different model of galactic rotation were assumed, the computed distance to the second arm would be adjusted, but the minimum distance of the radio source remains that of the second arm, whatever its "true" distance.

It is interesting that for radio stars and interstellar hydrogen clouds, the effect is very similar to optical interstellar absorption lines in stellar spectra.

Recent 21-CM Absorption Measurements in the Direction of the Galactic Center—E. F. McClain, *Naval Research Laboratory*—The absorption by interstellar neutral hydrogen of continuum radiation from a discrete radio source permits one to assign relative distance positions to the source and the hydrogen along the line of sight. Using this effect, it is possible to determine whether the hydrogen lies in front of or behind the radio source.

This technique has been applied to that portion of the sky containing Radio Source IAU 17S2A (NRL No. 5, Sagittarius A, BSS 68). This source has been suggested as being associated with the galactic center. Measurements indicate that hydrogen exists on both the near and far sides of this radio source, and of particular interest is the fact that the far hydrogen has a velocity of approach with respect to the local standard of about 15 km/sec. If this hydrogen is indeed beyond the galactic center, then there is a radial velocity of approach between hydrogen on the far side of the galaxy and the local standard of rest.

21 CM Studies of Interstellar Clouds in Intermediate Galactic Latitudes—R. S. Lawrence, *National Bureau of Standards*—Using the Agassiz Station radio telescope, an attempt has been made to demonstrate the relationship between optical interstellar absorption lines and 21-cm observations. Six stars, not in the vicinity of the galactic plane, were selected from a list of stars which were found by Dr. G. Münch at Mt. Wilson and Palomar Observatories to exhibit complex absorption spectra. In the directions of four of these stars a weak hydrogen line appears. In each case, the radial velocity of the hydrogen line corresponds closely to some component of the optical spectrum. A detailed study of the variations in this line over the area of the sky containing two of these stars reveals a cloudlike structure. These observations are presented, and a comparison is made with the results from the optical spectra.

* Hagen, Lilley and McClain, Naval Res. Lab. Rep. No. 4448, Washington, D. C.; 1954.

† Van de Hulst, Muller and Oort, *BAN*, vol. 12, No. 452; 1954.

Extension of Radio Source Spectra to a Wavelength of 3 CM—F. T. Haddock and T. P. McCullough, *Naval Research Laboratory*—Last July a survey was undertaken at a wavelength of 3.15 cm (9,500 mc) of discrete radio sources, or radio "stars," principally those recently detected* at a wavelength of 9.4 cm using the same 50-foot diameter paraboloidal reflector. The antenna pencil beam had a width of about 9 minutes of arc. A chopper-type radiometer with a one-second time constant was used.

Seven sources were detected—the Orion Nebula and two other bright hydrogen emission nebulae, the three brightest sources known at meter wavelengths,† and a source recently suggested‡ as the nucleus of our galaxy. These are the seven brightest sources observed at 9.4 cm. This is also the first radio detection of galactic or extra-galactic radiation at a wavelength shorter than 9.4 cm.

The radiation intensity of the Orion Nebula measured at 3.15 cm appears to be consistent with the thermal model of this source derived from the 9.4-cm measurements.*

These observations show that at a wavelength of 3 cm the average value of flux from the three hydrogen emission nebulae (Orion, Omega, and NCG 6357) is just greater than the average value of flux from the three brightest sources known at longer wavelengths (Cassiopeia A, Cygnus A, and Taurus A). This appears to be the wavelength at which the brightest radio sources switch from the peculiar nonthermal sources so dominant at longer wavelengths over to the well-known hydrogen emission nebulae radiating thermally at shorter wavelengths.

Theoretical Determinations of Sporadic Meteor Rate and Radiants*—V. R. Eshleman, *Stanford University*—The number (rate) and orientation (radiant) of ionized meteor trails formed in the upper atmosphere are determined theoretically, using two different models for the distribution of meteor orbits about the sun.

In the first model, it is assumed that the meteors have random heliocentric directions, and that they all have the same heliocentric velocity. With this model, the number of meteor trails formed within the horizon of an earth-bound observer is expected to be maximum at 0600 local time and minimum at 1800. Seasonally, the rate is maximum at the autumnal equinox and minimum at the vernal equinox. The amount of the daily variation in rate decreases with the latitude of the observer, while the amount of the seasonal variation increases with latitude. The distribution of meteor radiants for this distribution of orbits is such that most of the meteor echoes detected with an omni-directional radar system located north of the tropic of Cancer will arrive from the west at 0000, from the north at 0600, from the east at 1200, and from the south at 1800 local time.

In the second model, it is assumed that the meteor orbits are in the ecliptic plane, and, within this plane, they have random heliocentric directions and the same heliocentric velocities. For this model, the time of occurrence of the morning maximum of meteor rate varies with season, being after 0600 at the summer solstice and before 0600 at the winter solstice. At the autumnal equinox, the maximum is at 0600, but at the vernal equinox, the morning maximum splits into two maxima which occur before and after 0600.

The results of the theoretical rate and radiant determinations are compared with preliminary experimental results.

* F. T. Haddock, C. H. Mayer, and R. M. Sloanaker, *Astrophys. Jour.*, vol. 119, p. 456; 1954, and *Nature*, vol. 174, p. 176; 1954.

† W. Baade and R. Minkowski, *Astrophys. Jour.*, vol. 119, pp. 206 and 215; 1954.

‡ R. X. McGee and J. G. Bolton, *Nature*, vol. 173, p. 985; 1954 and J. P. Hagen and E. F. McClain, *Astrophys. Jour.*, vol. 120, p. 368; 1954.

§ This work was supported by the AF Cambridge Res. Center, Air Res. and Dev. Command.

The High Frequency Behavior of Certain Artificial Dielectrics—W. S. Ament, *Naval Research Laboratory*—We consider dielectrics formed by randomly dispersing metallic or high-dielectric spheres of radius r throughout a lossless, low-dielectric fluid. At low frequencies, where the fluid's propagation constant, k, is small compared with $1/r$, the Clausius-Mossotti laws describe the dielectric constant, ϵ', and permeability, μ', of the composite medium. When $kr = 0(1)$, ϵ' and μ' become meaningless to the degree that quadrupole scattering is significant. A meaningful propagation constant k' can still be computed through a self-consistent formulation, with the aid of addition formulas for the spherical-wave functions. The excitations of one sphere are sums of excitations from scattering by all other spheres; the sums are replaced by volume integrals over the space outside a "sphere of exclusion" of radius $\bar{r}$. The resulting k' deviates from the Clausius-Mossotti approximation by real terms in $(kr)^2$ and $(k\bar{r})^2$, and by imaginary terms in $(kr)^3$ and $(k\bar{r}^3)$; the loss terms are related to Rayleigh scattering.

On the Determination of the Electrical Properties of a Medium from the Reflection Coefficient*—I. Kay, *New York University*—Given a lossless medium or transmission line in which the electrical properties vary in a single direction, the propagation of waves through the medium can often be described by the differential equation

$$\frac{d^2u(k, x)}{dx^2} + [k^2 - V(x)]u(k, x) = 0,$$

where $u(k, x)$ represents the complex wave amplitude, x the distance in the direction of the variation, and k is the wave number. The description of the medium's variable electrical properties is contained in the function $V(x)$, which we assume to vanish for x less than a certain constant $-\delta$; $V(x)$ is also assumed to die out sufficiently rapidly as $x \to +\infty$ so that $\int_{-\infty}^{\infty} |V(x)|\,dx < \infty$. Then an incident wave from the left of the form e^{ikx} will give rise to a wave $u(k, x)$ which has the behavior $e^{ikx} + b(k)e^{-ikx}$ as $x \to -\infty$ and $a(k)e^{ikx}$ as $x \to +\infty$. The functions $b(k)$ and $a(k)$ are the reflection and transmission coefficients, respectively, associated with the medium described by $V(x)$. If the reflection coefficient $b(k)$ is known, one can determine the function $V(x)$ by means of a procedure developed by Gelfand and Levitan and applied to similar problems in quantum mechanics by Yost and Kohn.

In addition to the problem of determining the electrical properties of a medium by observing the reflection coefficient experimentally, in principle the method can be directed toward the problem of synthesizing such a medium given certain prescribed reflection characteristics beforehand. Sufficient conditions, needed to solve the latter problem, for a function $b(k)$ to be a reflection coefficient have been obtained.

The case of the more general differential equation,

$$\frac{d^2u(k, x)}{dx^2} + [k^2\mu(x) + V(x)]u(k, x) = 0,$$

including the case where $V(x) \equiv 0$, can also be handled by considering changes of dependent and independent variables which transform the equation into one of the first type. However, the solution in this case will not be unique unless further restrictions are prescribed.

Pseudo-Resonance Between Parallel Plates—B. G. King, I. Tatsuguchi, E. H. Scheibe,

* The research reported in this article was done at the Inst. Mathe. Sci., New York Univ., and has been made possible through support and sponsorship extended by the U. S. Air Force, AF Cambridge Res. Center, under Contract No. AF19(122)-42.

University of Wisconsin, and G. Goubau, *Signal Corps Engineering Laboratories*—A response very much like a resonance was found to occur between two parallel metal plates having a diameter and mutual spacing of many wavelengths. Since such a system has no natural frequencies like an LC circuit or a cavity and the resonance is not brought about by the excitation of a natural frequency, the phenomena may be termed "pseudo-resonance." The response curve of this pseudo-resonance differs considerably from a normal resonance curve particularly in that it is unsymmetric. A measure of the sharpness of the resonance may be obtained by ignoring the dissymmetry at the response curve and finding the apparent Q from the 3 db points. Using this technique, apparent Q's as high as 60,000 have been obtained when the diameter of the plates was 60 wavelengths and their distance 100 wavelengths. The effect is explained, and some experimental and theoretical studies are discussed.

A Geodesic Analog of the Luneberg Lens*—A. H. Schaufelberger and L. F. Culbreth, *Georgia Institute of Technology*—A geodesic analog of the Luneberg lens has been designed and fabricated in which the entire feed system is contained within the lens proper and in which the focal line is off the lens periphery. This arrangement results in simplification of the feed system and permits location of the focal point of the feed horn on the focal line of the lens, thereby eliminating phase errors due to noncoincidence of these foci. The surface of the lens is composed essentially of a central Rinehart-Parker surface and toroidal lip sections consisting of an output lip curved outward and an input lip curved inward. The procedure for deriving this surface is discussed and far-field patterns are exhibited.

A Three-Dimensional Microwave Luneberg Lens—M. C. Volk, *Emerson & Cuming, Inc.*, and G. D. M. Peeler, *Naval Research Laboratory*—A three-dimensional microwave Luneberg lens has been constructed and tested. At 9,375 mc, the radiation pattern of the lens has a beam width of 4.2 degrees; sidelobe level is down 18 db. The lens is 18 inches in outside diameter. It is composed of a central molded spherical core of dielectric constant 2.0 and nine concentric molded spherical shells of dielectric constant 1.9, and $1.8 \cdots 1.1$. Accuracy of each dielectric constant is within ± 0.02. Air at dielectric constant 1.0 is the theoretical outer shell of the lens. The material of construction of the lens is modified polystyrene, specially formulated and molded in each instance to a bulk density corresponding to the desired dielectric constant. Over-all dissipation factor of the lens material is less than 0.0002.

Luneberg Lenses Utilizing Void-Dielectric Materials—W. G. Scott, K. S. Kelleher, and E. G. Kelso, *Melpar, Inc*—This paper describes a technique utilizing variation in the size and spacing of spherical voids in a base dielectric to obtain the required index-of-refraction variation in a Luneberg lens.

The utility of such a void-dielectric medium was first demonstrated by the successful design of a parallel plate, two-dimensional lens. A one-inch thick flat disk composed of concentric annular rings of three different base dielectric materials having dielectric constants from the center outward of 2.0, 1.63 and 1.25, respectively, was sandwiched between two parallel, flat, metal plates. The number and spacing of the holes machined in the dielectric materials was obtained by referred methods.† Data taken over an 8-to-1 frequency range demonstrated the utility of spherical voids and provided a basis for the construction of a spherical lens.

The spherical lens consisted of seventeen disks similar to the one disk of the two-dimensional model. These disks, of different radii, were stacked symmetrically on either side of the central disk so as to approximate a sphere. The desired index variation in each disk was obtained from the expression $n^2 = 2 - R^2 - Z^2$ where R is the normalized radius coordinate in the disk and Z is the axial distance from the center of the sphere to the center of the disk. Data taken over a 7-to-1 frequency band proved the lens to be a useful broadband focusing objective for signals of arbitrary polarization.

Simultaneous Scatter-Sounding Observations of Sporadic-*E* Clouds at Two Separated Locations*—O. G. Villard, Jr., A. M. Peterson, and R. L. Leadabrand, *Stanford University*—Sporadic-E clouds seen on fixed-frequency PPI-display scatter sounders are generally of limited size and are most usually confined to a particular location. In an effort to learn whether a given sporadic-E cloud presents the same appearance when viewed by sounders at different locations, a portable sounding station has been operated at Spokane, Wash., for the purpose of checking data taken at Stanford University. The field unit is substantially identical to one of the home transmitters, and both operate on a common frequency of 17.31 mc with slightly differing PRF's.

Results indicate that sporadic-E patches do have approximately the same appearance when viewed from separate locations, and confirm that these patches are in many instances highly localized. Use of a common radio frequency for the sounders permits comparison of one-way propagation with backscatter indications, since directly propagated pulses from one transmitter register as moving dots on the PPI screen of the other. From these records some deductions concerning the size of the individual sporadic-E cloudlets are made.

Some Regularities in Sporadic-*E* Obtained from Vertical Incidence Data—E. K. Smith, *National Bureau of Standards*—Sporadic-E critical frequency data scaled from ionosphere sounder records must be analyzed with extreme caution. Some trends, however, appear strong enough to overshadow other variations. Where these receive support from adjacent stations, or over many cycles at one station, it is felt they may be accepted with some degree of confidence.

With 1952 data a good, if indirect, correlation may be obtained between sporadic-E of critical frequency greater than 5 mc and Auroral Percentage Frequency Days as given by Vestine. The sporadic-E measure used is the product of the night-to-day ratio and the nighttime incidence. This correlation holds for E_s stations in the zone of greater than 15 per cent auroras. The temperature latitude seasonal effect is found to increase markedly with latitude to this crossover zone. The stations on the magnetic equator are, of course, a separate group.

Some light may also be shed on the character of sporadic-E at a given station by comparing the distributions of sporadic-E incidence on the five magnetically-disturbed days of each month to those five quiet. Analyses of data from six stations indicate more sporadic-E capable of supporting any given frequency occurs on disturbed days than on quiet days at the auroral zone maximum for all frequencies. Three temperate latitude stations show more sporadic-E on quiet days for frequencies up to 10 mc. Two low-latitude stations exhibit no discernible magnetic effect. These results suggest that whereas auroral zone E_s is predominately associated with a disturbed ionosphere, temperate latitude E_s occurs more frequently with a quiet ionosphere, one that is perhaps more conducive to stratification or laminar flow in the E-region.

An Improved Method for Determining Predicted Sky-Wave Maximum Usable Frequencies Using Sporadic-*E* Prediction Charts—S. M. Ostrow, *National Bureau of Standards*—A new method, based on the combination of the independent probabilities of propagation of a given frequency by E_s and regular layers, is presented for use of the E_s charts of the CRPL Basic Radio Propagation Predictions. Equations and nomograms are given for computation of the expected percentage of time of occurrence of propagation of a given frequency for given E_s and regular layer median maximum usable frequencies. An example is also presented of a set of curves that simplifies the application of this method to a common type of communications problem.

Auroral Echoes Observed North of the Auroral Zone on 51.9 MC—R. B. Dyce, *Cornell University*—During November, 1954, a simple radar system, designed for observation of auroral echoes at 51.9 mc, was operated at Pt. Barrow, Alaska. This location is north of the accepted maximum of the auroral zone, and therefore most of the visible aurora is seen to the south of the observing station. The radar used a continuously-rotating antenna to see with equal sensitivity in all directions, but more than 90 per cent of the echoes were obtained from directions north of east and west. Echoes were obtained only from 500 to 1,100 km. These effects are explained by the theory of Moore as enlarged by Booker, Gartlein, and Nichols, requiring near-perpendicularity of radio-ray paths to the lines of the earth's magnetic field.

During visible aurora, propagation at 51.7 mc was investigated over an 800-km path from College to Barrow, across the auroral zone. Bursts of signal due to meteor ionization were readily observed. Propagation associated with aurora was almost nonexistent, even with visible aurora at the mid-path. If the theory of auroral echoes of Harang and Landmark were true, auroral propagation should have been readily detected.

Aurora Borealis Studied Using VHF Radio Echoes*—K. L. Bowles, *Geophysical Institute of the University of Alaska* and *Cornell University*—Two experiments recently performed by the author are described. In the first a 100 mc radar set with good horizontal antenna beamwidth was used in Alaska. Simultaneous photographs of the visible aurora and the PPI pattern were taken. In many cases direct comparison may be made between the two. Echoes were received from both homogeneous and rayed auroral forms. A suggested accounting is made for similar visible forms which do not correlate with echoes.

In the second experiment rf spectrograms were made of cw echoes from aurora at several carrier frequencies (between 25 and 150 mc) and locations. A-scope presentation of pulsed echoes was available at the same time for comparison with the spectra. Final analysis has been made from tape recordings of the two types of information. Whenever possible visual aurora was correlated with the radio echoes. The results show that the auroral echoes are generally Doppler shifted several hundred cycles relative to the transmitted frequency. They are also broadened over a band of several hundred cycles width. Both quantities depend upon carrier frequency and location of the station in the geomagnetic field. Homogeneous

* This work was sponsored by the Signal Corps Engrg. Labs., Ft. Monmouth, N.J., under Contract DA-36-039-sc-42707.

† W. O. Puro and K. S. Kelleher, "Isotropic variable index media," 1954 IRE Convention Record, Part 1, "Antennas and Propagation," pp. 76–78.

* This work was supported jointly by the U. S. Navy (Office of Naval Research), the U. S. Army Signal Corps, and the U. S. Air Force.

* This work has been supported by research contracts of the U. S. Signal Corps and Air Force with the Geophysical Inst., College, Alaska, and with Cornell University, Ithaca, N.Y.

auroral forms produce upwards Doppler shifts (approaching motion) while rayed forms produce downwards shifts (receding motion).

The results are taken as support for the suggestion of earlier Cornell work that the radio echoes arise from thin columns of ionization aligned with the lines of force of the earth's magnetic field. The motions implied by the Doppler shifts are downwards in homogeneous forms but upwards in rayed forms in the visible aurora. With accounting taken for geometry, velocities along the columns of the order of 6 km are implied.

Brightness Distribution of the Sun at 207 MC—J. W. Firor, *Carnegie Institution of Washington*—Measurements made of the quiet sun with a variable spacing interferometer and with several fixed-spacing interferometers operating at 207 mc lead to a brightness distribution of the sun. The measurements include determinations of the phase as well as the amplitude of the interferometer trace. In deriving the distribution from the experimental results it is assumed that the sun has either circular or elliptical symmetry. The resulting distribution shows marked limb brightening and is in good agreement with the unpublished results of Reinhart and with the distribution predicted by Smerd.

The 1944 Occulation of M1 by the Solar Corona—B. F. Burke, J. W. Firor, and H. L. Helfer, *Carnegie Institution of Washington*—The occulation of the crab nebula by the solar corona in June, 1954, was observed at radio frequencies of 207, 3,817, and 22.2 mc. Interferometric techniques were used, which confirmed the apparent source enlargement first observed by Machin and Smith. The effect was marked at the lower frequencies, although the corona seemed somewhat less extensive than for previous years. Little, if any, source broadening was observed at 207 mc.

Polarization of Solar Radio Bursts—T. Hatanaka, *Cornell University* and *University of Tokyo*—While working at Cornell University during 1952–53, it was found that solar radio bursts were almost linearly polarized when the source was very close to the limb of the sun's disk. The need for a new type of polarimeter which gives at least four independent pieces of information about the polarization simultaneously was discussed. A radio polarimeter has since been built at the Tokyo Astronomical Observatory, University of Tokyo. With a pair of crossed dipoles attached at the focus of 10-meter paraboloid of equatorial mounting and suitable combinations of retardations, it gives six components of polarization, two circulars and four linears, almost simultaneously by electronic switching. One set of observations is obtained in 1/200 second.

A preliminary analysis of the observations made during December, 1954, and January, 1955, reveals the following points on the polarization of the so-called "polarized bursts": (1) the radiation is a mixture of two components—one is elliptically polarized and the other random; (2) the ellipticity varies from nearly 100 per cent to 10 per cent, and the variation from day-to-day is similar to that of the ellipticity of a circle put tangentially on the sun's surface at the position of the source and viewed from the earth; (3) the degree of polarization, or the fraction of the elliptically polarized component, is 80 or 90 per cent on most days, but sometimes drops below 50 per cent and even down to 10 per cent. This variation is not correlated with the position of the source on the sun's disk; and (4) the tilt angle of the ellipse is almost constant during the observing time in a day, but is different on different days. It is pointed out that the direction of the polarization ellipse is rotated by some amount because of the Faraday effect in the earth's ionosphere. The observing frequency is 200 mc, both at Cornell and Tokyo.

Solar Flares and Atmospheric Noise—E. I. King, *University of Florida*—In this paper, the effects of solar flares on low-frequency atmospheric noise are examined. Relations between the rise of noise, and the area of the flare, its intensity, location on the sun, and time of day are studied. Noise levels preceding flares are also examined to determine whether there are any phenomena which may be used for the prediction of high-frequency fade-outs.

Flares are eruptions at the surface of the sun, in which flaming hydrogen shoots out with high velocities, and reaches great elevations. They emit ultra-violet radiation and sub-atomic particles, both of which cause various phenomena at the earth. These include the aurora borealis, terrestrial magnetic storms, sudden fade-outs of short-wave radio communications, and increased propagation of low-frequency atmospheric noise. Other investigators have observed an increase of the noise preceding a flare by about one hour. If this effect were to be generally apparent, it might be used as a basis for the prediction of fade-outs on the higher frequencies. Information of this nature would be quite valuable.

The Influence of Noise in Radio Reception—S. Matt and O. J. Jacomini, *General Electric Company*—This paper presents a portion of the available data on the external and internal noise sources which influence the reception of radio signals at frequencies between 50 and 3,000 mc. The sources of noise which are considered are man-made, atmospheric, cosmic, solar, thermal, and receiver noise. The effects of these noise sources are combined to form curves of the average effective noise figure for current and future receivers.

The present data indicates that the optimum operating frequency of the receiver with respect to external and internal noise is in the region of 300 to 500 mc. The effective noise figure at the optimum frequency which can now be attained is approximately 1.5.

In addition, the influence of discrete radio sources such as Cassiopeia and Cygnus A on the region of the optimum frequency is considered.

Effect of Arbitrary Phase Errors on Antenna Gain—D. K. Cheng, *Syracuse University*—Previous investigations on the effect of arbitrary phase errors on the gain of microwave antennas fell into two categories, (1) as a least-square problem, an approximate expression for the fractional reduction in gain was obtained; and (2) as a statistical problem, the probability distribution of the members of an ensemble about an average radiation pattern was derived. The first method necessitates the determination of the plane least-square solution of the wavefront from a complete knowledge of the amplitude-illumination function and the phase-error function over the antenna aperture, which is in general a quite involved process, while the second approach gives only the average behavior of an ensemble; the individual antennas will differ from the system average.

This paper presents a simplified approach with which the maximum loss in antenna gain due to arbitrary phase errors can be readily estimated. It provides a lower bound for the gain of an antenna with an arbitrary distribution of phase errors for which the maximum phase error is known; it is not necessary to know the exact phase-error function. The result is independent of the amplitude-illumination function. It is also shown that the same result applies to antennas with a rectangular aperture as well as to those with a circular aperture.

Systematic Errors Caused by the Scanning of Antenna Arrays*—L. A. Kurtz and R. S. Elliott, *Hughes Research and Development Laboratories*—If it is assumed that the mutual coupling between elements in an antenna array is the same for all elements for a given interelement phase shift, but is a function of phase shift, a useful equivalent circuit representation of the entire system is possible. The equivalent circuit consists of a main transmission line periodically loaded by branch transmission lines which are terminated by identical impedances. The impedances represent the radiating elements and are functions of phase shift. If the array is scanned by placing phase shifters in the branch lines, these phase shifters can be mathematically treated as variable lengths of branch transmission lines.

The problem thus is reduced to circuit theory. Expressions for the radiating currents as functions of phase shift and equivalent element impedances are readily deduced. From these an expression for the radiation pattern follows. This expression is seen to be an infinite series, each term of which represents a pattern having a main beam and sidelobes. These beams have relative angular positions corresponding to multiples of the interelement phase shift and relative magnitudes dependent upon the impedances of the radiators. The first term of the series corresponds to the desired radiation pattern and hence the remainder of the series can be defined as the systematic error.

The excursions in the value of the equivalent element impedance control the magnitude of this systematic error. Reducing mutual coupling serves to restrict the excursion in equivalent element impedance and hence to restrict pattern deterioration with scan.

A two-dimensional array of edge slots in X-band waveguide has been built with which to verify the theoretical expression for the radiation pattern. By controlling independently the interelement phase shift in one plane of the array and the impedances of individual branch line linear arrays which make up the two-dimensional array, radiation patterns were obtained which were in close agreement with the predicted radiation patterns. The patterns show clearly how the magnitude of systematic error depends on the impedance match of the branch line terminating impedances.

The Asymmetrically Excited Spherical Antenna—R. C. Hansen, *University of Illinois*—A spherical dipole antenna excited so that the resultant pattern is not rotationally symmetric is considered. Inside the sphere is a parallel plate or radial transmission line terminating at the gap. The fields are represented in terms of an assumed distribution of tangential E in the gap.

By eccentrically locating a feed wire across the radial line a wide variety of patterns may be produced. Some patterns have been calculated for a number of antenna diameters and offsets. Still more versatile is the sectoral dielectric loading scheme where the radial line, with central feed wire, is filled with sectors of low loss material whose dielectric constant or permeability may be different for each sector. A synthesis technique is developed for obtaining the dielectric sector constants corresponding to a desired azimuthal pattern. Excellent results have been obtained for a cardioid and a fan beam pattern.

Development of a Skip-Range Antenna*—J. D. Tillman, W. T. Patton,† C. E. Blakely, and F. V. Schultz, *University of Tennessee*—The problem involved here is the development of a shore antenna system to transmit or receive reliably 24 hours each day signals over the range of 40 to 500 miles at all latitudes. The antenna is intended primarily for shore-to-ship applications.

At night this range of distances usually includes a zone in which the ground wave and the sky wave are of the same order of magnitude, resulting in severe fading. If a sufficiently high

* This research has been supported by the Air Force under Contract AF19(122)-458.

* The research reported in this paper has been sponsored by the Bureau of Ships, Department of the Navy.

† Now on active duty with the U. S. Navy.

frequency is used that the sky wave skips this range, the ground wave is so attenuated that reliable communication is not possible because of noise. Some method of reducing interference between ground wave and sky wave is a necessity.

An azimuthally, omnidirectional, circular array of vertical monopoles proved to be best for meeting the difficulties imposed by these conditions. This array can be excited in either of two ways. At night it is so excited that the greatest radiation occurs at about 58 degrees above the horizon and because of a null, no interfering ground wave is radiated. For daytime use the antenna is excited so that maximum radiation occurs along the ground and high-angle radiation, causing interference, is minimized.

The antenna consists of nine vertical monopoles, 0.25 wavelengths high, equally-spaced around the circumference of a circle of 0.383 wavelength radius. A 1,200-mc model was constructed and pattern tests were made using this model. The patterns obtained in all cases showed good agreement with those calculated from the theory.

Extensive calculations were made of the results to be expected from the use of this array. For average ionospheric conditions, a ground path consisting mainly of sea water, and with a 15-kw transmitter, the following distances should be covered at 2.5 mc: daytime, ground-wave phasing: 0 to 710 miles; nighttime, ground phasing: 0 to 270 miles; nighttime, sky-wave phasing: 70 to 750 miles.

Radiation Patterns of Multiple and Distributed Sources—L. W. Lechtreck, *Emerson Electric Manufacturing Company*—The purposes of this report are as follows: (1) to discuss microwave antenna radiation pattern prediction through the use of Fourier transformations; (2) to apply this information to lumped and distributed arrays; and (3) to evaluate the effects of linear and quadratic aperture phase errors on the antenna far field.

A derivation is given of the radiation from (1) a linear array of variable phase point sources, (2) an aperture area describable by separable cartesian integrals, (3) the continuous line source with a linear-phase deviation, and (4) the continuous source with a quadratic phase deviation.

Four graphs are included to show the effects of a square-law phase error on uniform and cosine aperture illuminations. The Fresnel integrals are used, and two methods are reviewed for the Taylor approximation of these patterns resulting from amplitude and phase tapering of the antenna aperture illumination.

The results are applied to three types of antenna geometries, (1) the pyramidal horn antenna, (2) the paraboloidal reflector with a displaced point source (approx), and (3) the Fresnel zone of a plane-phase front antenna.

Note is made of the fact that the spectrum of a linear frequency shift in pulse analysis is identical to the derived Fresnel patterns of antennas.

A Mechanically Simple Foster Scanner—R. C. Honey and E. M. T. Jones, *Stanford Research Institute*—The Foster scanner is a mechanical scanning antenna permitting relatively high scanning rates. It utilizes a rapidly rotating cone located inside a conical rotor to vary periodically the angle of the radiated beam with respect to the fixed exit aperture. In the construction of a conventional Foster scanner, interleaving fingers are used to direct the energy around the parallel-plate transmission line formed by the space between the rotor and the stator. For good electrical performance it is necessary that the clearance between the interleaving fingers be very small. However, the mechanical difficulties of constructing these fingers and maintaining the proper clearances in operation has prohibited the widespread use of the Foster scanner.

The form of the scanner described here does not have this mechanical limitation because it uses a choke groove and solid barrier instead of interleaving fingers to direct the energy around the rotor. This scanner is easy to construct, gives excellent electrical performance, and permits high scanning speeds.

The design of the functions, chokes, and barriers used in the Foster scanner has been carried out in waveguide by making use of the rigorous analogy that exists between parallel-plate transmission lines and waveguides. The unity-coupling-factor T-junction, which couples the parabolic pillbox to the conical transmission line in the scanner, and the choke groove on the rotor were designed from the best available waveguide data on series T-junctions, and then checked experimentally in waveguide. The solid barrier junction for the stator was designed empirically in waveguide.

A scanner using a choke groove and a solid barrier was built to operate at 35,000 mc. The feeding line source is a parabolic pillbox embedded in the rotor and energized through a rotary joint. At the design frequency the scanner sweeps a beam of 1.2 degrees in width to the 3-db points, over a 47-degree angle, with no pattern deterioration. The flyback or switching time takes only 6 per cent of the total sweep time. The scanner behaves equally well over a 10 per cent bandwidth, centered at the design frequency. Still greater frequency changes result in variations in the amplitude of the beam through the scan cycle caused by multiple reflections between the barriers. Gain tests show that the antenna behaves as expected, with no unaccountable losses or other abnormalities in performance.

The rotor of experimental scanner has been dynamically balanced and spun at 1,000 rpm with no measurable deflection. If a reinforced parabolic-pillbox were used as the line source, it is estimated that speeds as high as 3,600 rpm, corresponding to 60 sweeps per second, might be attained. Still higher scan rates could be obtained using a slotted-waveguide line source in the rotor, since the rotor would not need to be partially split to contain the pillbox and would be correspondingly stronger.

INSTITUTIONAL LISTINGS

The IRE Professional Group on Antennas and Propagation is grateful for the assistance given by the firms listed below, and invites application for Institutional Listing from other firms interested in the field of Antennas and Propagation.

ANDREW CORPORATION, 363 E. 75th Street, Chicago 19, Ill.
Development and Production of Antenna and Transmission Line Systems.

COLLINS RADIO COMPANY, Cedar Rapids, Iowa
Fundamental Antenna Design and Propagation Research Related to Development of Airborne and Ground Communication Systems.

DORNE AND MARGOLIN, INC., 30 Sylvester Street, Westbury, L. I., New York
Antenna Research and Development—Radiation Pattern Measuring Services.

THE GABRIEL LABORATORIES, Div. of the Gabriel Co., 135 Crescent Road, Needham Heights 94, Mass.
Research and Development of Antenna Equipment for Government and Industry.

HUGHES AIRCRAFT COMPANY, Culver City, California
Research, Development, Manufacture: Radar Systems, Guided Missiles, Antennas, Radomes, Tubes, Solid State Physics, Computers.

JANSKY & BAILEY, INC., 1339 Wisconsin Ave. N.W., Washington 7, D.C.
Radio & Electronic Engineering; Antenna Research & Propagation Measurements; Systems Design & Evaluation.

RADIO ENGINEERING LABS., INC., 36-40 37th St., Long Island City 1, N. Y.
Complete equipment for communication and propagation test purposes for beyond the horizon UHF communications systems.

WHEELER LABORATORIES, INC., 122 Cutter Mill Road, Great Neck, New York
Consulting Services, Research and Development, Microwave Antennas and Waveguide Components.

The charge for an Institutional Listing is $25.00 per issue or $75.00 for four consecutive issues. Application for listing may be made to the Technical Secretary, The Institute of Radio Engineers, 1 East 79th Street, New York 21, New York